ISBN 978-82-326-5112-2 (printed ver.)
ISBN 978-82-326-5113-9 (electronic ver.)
ISSN 1503-8181 (printed ver.)
ISSN 2703-8084 (electronic ver.)

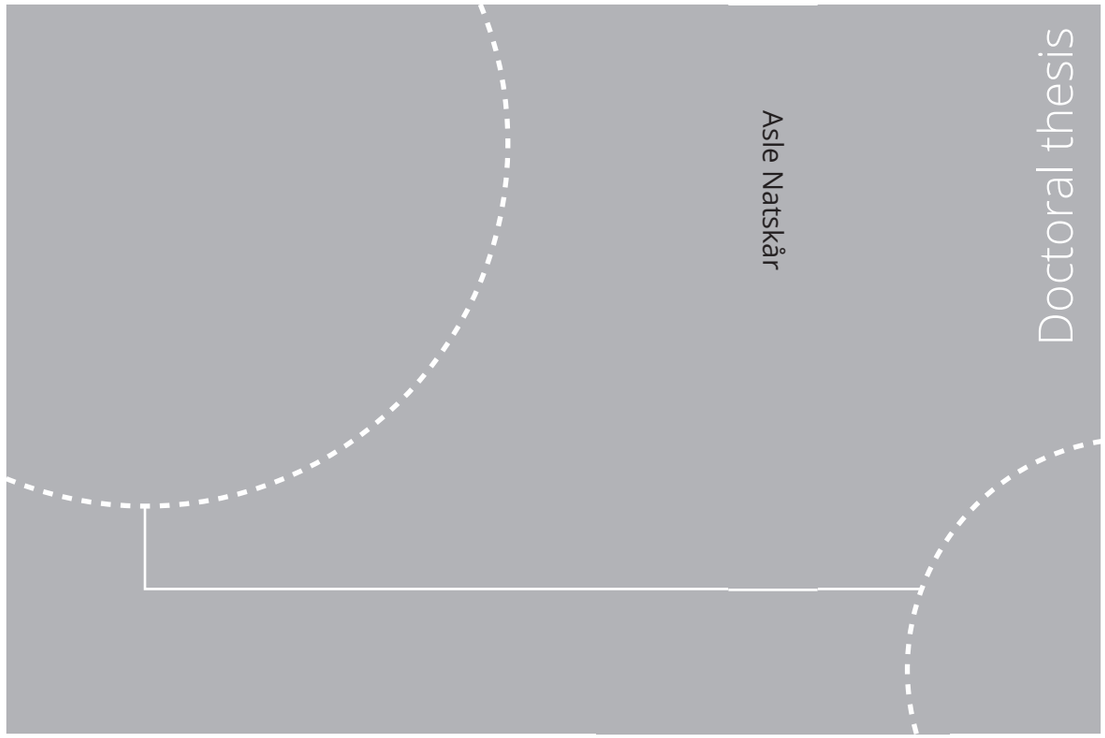

Doctoral theses at NTNU, 2020:383

Asle Natskår

Reliability-based assessment of marine operations with emphasis on sea transport on barges

Doctoral theses at NTNU, 2020:383

NTNU
Norwegian University of
Science and Technology
Thesis for the degree of
Philosophiae Doctor
Faculty of Engineering
Department of Marine Technology

NTNU
Norwegian University of
Science and Technology

NTNU
Norwegian University of
Science and Technology

Asle Natskår

Reliability-based assessment of marine operations with emphasis on sea transport on barges

Thesis for the degree of Philosophiae Doctor

Trondheim, December 2020

Norwegian University of Science and Technology
Faculty of Engineering
Department of Marine Technology

NTNU
Norwegian University of
Science and Technology

NTNU
Norwegian University of Science and Technology

Thesis for the degree of Philosophiae Doctor

Faculty of Engineering
Department of Marine Technology

ISBN 978-82-326-5112-2 (printed ver.)
ISBN 978-82-326-5113-9 (electronic ver.)
ISSN 1503-8181 (printed ver.)
ISSN 2703-8084 (electronic ver.)

Doctoral theses at NTNU, 2020:383

PRINTED IN NORWAY
NO - 1598

NORDIC SWAN ECOLABEL
Printed matter
2041 0731

Printed by Skipnes Kommunikasjon AS

Abstract

This thesis addresses the structural reliability assessment of marine operations related to the transport of large and heavy objects. The base case has been sea transportation by means of a towed barge with an emphasis on seafastening structures, considering both weather-restricted and weather-unrestricted operations. The results are, however, generic in the sense that they are relevant for other marine operations where environmental loading governs. The reliability assessments are related to natural uncertainties and variations. Human and organizational errors are not considered. The focus is on the structural failure of the grillage and seafastening.

While the methods for structural reliability analysis are quite mature, modeling uncertainties in loads and load effects as well as the structural strength are crucial and challenging. Particular efforts are directed towards uncertainty in estimated vessel motions based on numerical and experimental investigations as well as on the uncertainty in wave conditions.

The estimated motion of the transport vessel is input to calculations of the corresponding accelerations and roll/pitch angles that are applied in calculating the load effects in the grillage and seafastening. The motion of a typical transport barge have been studied by model tests. A model of a North Sea barge at a scale of 1:50 was exposed to severe seas in regular and irregular waves. Roll damping tests were also performed. Barge models with sharp and rounded corners were tested. Based on the experiments, a model for roll damping is established. The maximum expected extreme value of the roll angle from the experiments was 22 degrees for a storm duration of three hours. The linear analyses overestimated the maximum roll angle, while the nonlinear analysis compared well.

For most marine operations, environmental loads play an important role in the design of the operation, and there will be a limit on the environmental condition in which the operation can be performed. Weather forecasts provide important information for marine operations with duration up to three days and form the basis for decision making during operations. The uncertainties in weather forecasts of the significant wave height have been studied, especially by shedding light on the approach used in practice to account for forecast uncertainty, where the so-called Alpha factor method is used. This method was implemented in the structural reliability analyses performed in this thesis and was seen to effectively compensate for the uncertainty inherent in the weather forecast. Marine operations lasting more than three days are weather-unrestricted, and the environmental conditions are based on long-term statistical data. Such data have been ap-

plied in structural reliability analyses to study variations through seasons of the year and durations of the operation. While the study of the forecast uncertainty did not reveal an abrupt change in forecast quality for lead times exceeding three days, this limitation was still used in the reliability assessment to be in compliance with current design standards.

The uncertainties in load effects and the resistance of the seafastening structure and the corresponding failure probability are estimated. The structure is assumed to be designed according to current practice, and the results provide an indication of the inherent reliability of the current practice. Moreover, the sensitivity of the reliability to environmental conditions, load effects and resistance variables is investigated.

This thesis may contribute to safer sea transport on barges by providing more knowledge on some effects that influence the structural reliability, e.g., the time of year when transport is executed and the duration of operation. The effect has not been quantified here, but the results can provide a useful reference for future versions of design standards for marine operations.

Preface

This thesis is submitted to the Norwegian University of Science and Technology (NTNU) for partial fulfilment of the requirements for the degree of philosophiae doctor.

This doctoral work has been performed at the Centre for Ships and Ocean Structures (CeSOS), Department of Marine Technology, NTNU, Trondheim, with Professor Torgeir Moan as the main supervisor and Per Øystein Alvær, DNV GL, as the co-supervisor.

This thesis was financially supported by the Research Council of Norway through the Centre for Ships and Ocean Structures (CeSOS), headed by Professor Moan. This support is greatly appreciated.

I was partially supported by a scholarship from the Det Norske Veritas' Education Fund from DNV GL, which is also greatly appreciated.

For the sake of good order, it is mentioned that any opinions expressed in this document are mine, and they should not be construed as reflecting the views of my employer, DNV GL.

Acknowledgments

During my PhD project, I have had the pleasure to meet many highly qualified people at NTNU and Sintef Ocean in addition to my colleagues at DNV GL. Professor Torgeir Moan has been my main supervisor. His knowledge, work capacity and enthusiasm towards engineering technology and science are extraordinary, and I am very grateful for his assistance, guidance and patience. My co-supervisor has been Per Ø. Alvær at DNV GL, the company's main expert within the area of marine operations. He has always been available for discussions and is a great source of inspiration.

In preparing my PhD project, I received support from many DNV GL colleagues. I was inspired by talking to Dr. Knut O. Ronold. My line managers during these years have always supported me. I would in particular mention Gunnhild Laastad, who gave valuable support for initiation of the project.

Thank you to all my professors/lecturers for their excellent lectures and support. I would also like to thank professors Sverre Haver, Trygve Kristiansen, Dag Myrhaug and Sverre Steen, as well as Dr. Amir R. Nejad at NTNU and Dr. Bjørn Abrahamsen and Torfinn Ottesen at Sintef Ocean for their discussions and kind support. Thank you to my fellow PhD students at NTNU/CeSOS for our time together and for good discussions during our courses in reliability and hydrodynamics. During my work in the laboratories, I received assistance from many employees at NTNU and Sintef Ocean. I would especially like to thank Ole Eirik Vinje and Knut Arne Hegstad at NTNU for their substantial support. I would also like to thank Dr. Zhuang Kang from Harbin Engineering University in China and my family members Sigrid Olsen and Arne Natskår who assisted me during the model tests in the MC-lab. Thank you Dr. Arnt Fredriksen and Dr. Giri Rajasekhar Gunnu for help during model testing in the Towing Tank. I would also like to thank Peter Sandvik at Sintef Ocean for assistance with the Simo calculations.

I have had excellent assistance from the administration at NTNU/CeSOS, and the Head of the IT department, Bjørn Tore Bach, which is greatly appreciated. The University library at the Marine Technology Centre and the DNV GL library have provided excellent support, which is also greatly appreciated.

I am very pleased to have professor Jonas Ringsberg (Chalmers University of Technology), professor Ove Tobias Gudmestad (University of Stavanger) and professor Stein Haugen (administrator, NTNU) as the doctoral committee. I am grateful for the editorial comments I have received to

the draft version of the thesis, giving me the opportunity to improve the presentation of my PhD-work.

I would like to thank the Research Council of Norway and the board of the education fund of DNV GL for their financial support.

My dear Sigrid has been extremely patient during the years of my PhD work, for which I am very grateful.

List of Appended Papers

This thesis consists of an introductory part and three papers, which are appended.

Paper 1:
Barge motions
Rolling of a transport barge in irregular seas, a comparison of motion analyses and model tests
Authors: Asle Natskår, Sverre Steen
Published in *Marine Systems & Ocean Technology*, Vol. 8 No. 1, pp. 05-19, June 2013

Paper 2:
Uncertainty in weather forecasts
Uncertainty in forecasted environmental conditions for reliability analyses of marine operations
Authors: Asle Natskår, Torgeir Moan, Per Ø. Alvær
Published in *Ocean Engineering*, Vol. 108, pp. 636-647, 2015

Paper 3:
Reliability analysis
Structural reliability analysis of a seafastening structure for sea transport of heavy objects
Authors: Asle Natskår, Torgeir Moan
Submitted for publication in *Ocean Engineering*

Declaration of Authorship
The papers that serve as the core content of this thesis are coauthored. I was the first author and responsible for initiating the ideas, performing the model tests, analysis and calculations, providing the results and writing the papers. Professor Torgeir Moan has contributed by providing support, corrections and constructive comments to increase the scientific quality of all the publications. Professor Sverre Steen has contributed by providing support, corrections and constructive comments to increase the scientific quality of *Paper 1*. For *Paper 2* and *3*, Per Ø. Alvær has contributed by providing support, corrections and constructive comments, particularly related to practical aspects and towards the DNV GL standards.

Additional paper
The following conference paper related to the model tests has been produced as part of the doctoral work. It is not included in this thesis because the experimental results relevant for Papers 2 and 3 are covered by Paper 1.

Paper 4:
Experimental investigation of barge roll in severe beam seas.
Authors: Asle Natskår, Torgeir Moan
Published in *Proceedings of PRADS 2010, the 11th International Symposium on Practical Design of Ships and other Floating Structures, Rio de Janeiro, Brazil*

Abbreviations and terms

Alpha factor	A factor to account for the uncertainty in the weather forecast. The design environmental condition (the operational limiting criterion) is multiplied by the Alpha factor to obtain the forecasted operational criteria.
Cargo supports	Structural elements with the purpose of supporting the transported object, typically by grillage beams.
FORM	First order reliability method.
Grillage	A structure secured to the deck of a barge or ship, formally designed to support the cargo and distribute the loads between the cargo and the transport vessel.
HAZID	Hazard identification analysis. HAZID is used to identify and evaluate hazards early in the project and may be a useful technique for revealing weaknesses in the design and the preliminary operation procedures.
HAZOP	Hazard and operability study. The application of a structured and systematic review technique to a marine operation, to identify hazards and operability problems, including causes, consequences, safeguards and remedial actions but also issues related to the operability of an activity or operation, including possible improvements, to avoid accidents and incidents and fulfill the zero accident/incident target philosophy and increase safety during the operations.
Hindcast data	Data, e.g., significant wave height and peak or mean zero-crossing wave period, reconstructed based on meteorological data registered by the meteorologist.

HTV — Heavy transport vessel, a vessel that is designed to ballast down to submerge its main deck and to allow self-floating cargo to be on-loaded and off-loaded.

ISO — International organization for standardization.

Lead time — The period from forecast is issued until the time that the forecast is given for.

Load transfer — The operation to transfer the load (i.e. the transported object) from or to a vessel without using cranes, i.e., by ballasting or de-ballasting the vessel. A typical load transfer operation is load-out.

Load-out — Transfer of an object (module, component, etc.) onto a transport vessel, e.g., by horizontal movement or by crane lifting.

Marine operation — Non-routine operation of a limited defined duration related to handling of object(s) and/or vessel(s) in the marine environment during temporary phases. In this context, the marine environment is defined as construction sites, quay areas, inshore/offshore waters or sub-sea.

MWS — Marine warranty surveyor, the independent third party that has been contracted to approve marine operation. The MWS will review the proposed procedures and equipment and, when satisfied that they and the weather forecasts are suitable, issue a Certificate of Approval for each relevant operation. The MWS may also attend during the operation to monitor that the procedures are followed and to agree with any necessary changes.

QRA — Quantitative risk analysis

Seafastening — Structural elements used to secure the transported object from rotations and translations in all directions, as well as uplift at the supports. The term “Seafastening Structure” and “Seafastening System” as used here also includes vertical supports.

SORM — Second order reliability method.

SRA — Structural reliability analysis.

Standard North Sea barge: A flat top barge with a length of 91.4 m, width of 27.4 m and depth of 6.1 m (300 by 90 by 20 feet), with a raked bow and stern.

Vessel Barge, ship, tug, or other vessel involved in marine operation.

Weather-restricted operation: A marine operation with defined restrictions to the characteristic environmental conditions planned to be performed within the period for reliable weather forecasts. The estimated duration is typically not more than 72 hours, and the environmental design criteria are defined by the owner or his representative and confirmed by weather forecasts prior to the start of the operation.

Weather-unrestricted operation: A marine operation with characteristic environmental conditions is estimated according to long-term statistics, normally with an estimated duration of more than 72 hours.

Contents

Chapter 1

Introduction

1.1 Marine operations

1.1.1 Definition

The term Marine Operations includes many activities performed in or at sea. The marine operations considered herein are limited to specially planned, non-routine operations of limited duration related to the load transfer, transport and installation of objects.

1.1.2 History and background

For several decades, complex marine operations have been performed within the offshore oil and gas industry. During the construction of an offshore platform for drilling and petroleum production, several marine operations are performed. Modules to be assembled into topsides for drilling and production platforms are transported from fabrication yards all over the world to assembly sites. Complete topsides and substructures are transported from the assembly sites to the installation locations offshore.

The offshore oil and gas activity started in the Norwegian sector of the North Sea in the late 1960s. Steel jacket structures and reinforced concrete platforms require a large number of marine operations during construction and installation. In Fig. 1.1, the Condeep platform *Statfjord B* is shown moored at the construction site. Examples of marine operation include the transport of topside modules, installing the topside onto the substructure (deck mating) and towing of the complete platform.

The activity in the renewal energy sector is increasing, and this market is expected to grow substantially in the future. For fabrication of large infrastructure projects, e.g., fjord crossings by road bridges, cutting edge

Figure 1.1: The Condeep platform Statfjord B *during construction in Vats, Norway, 1981. Photo: Jon Natskår.*

marine operations will be required. The marine operations performed during construction and installation can utilize the experience obtained from the offshore industry over the last five decades. The demand for marine operations related to the transport of large and heavy structures is therefore predicted to be high in the future.

1.1.3 Sea transport of heavy objects

Heavy transports are often performed by towed barges; an example is shown in Fig. 1.2. Barges are given special attention in this thesis, but the general methodology is similar for other towed objects and for transport on self-

propelled vessels. The part related to forecasting uncertainties is relevant for all marine operations.

The need for special planning may arise, e.g., because the transported object is large and/or heavy, is of high economic value, has a long replacement time or there could be a risk of environmental pollution. Therefore, the consequences of severe damage to, or total loss of, the transported objects are large with regard to economic loss. Most likely, there will also be delays in the project, and the companies involved may experience a loss of reputation. It is therefore necessary to quantify the uncertainties inherent in such operations. Furthermore, there will probably be a requirement for increased cost effectiveness in the future, such as in the offshore wind industry, compared with the traditional oil and gas industry. An optimized safety level in marine operations should therefore be attained.

Figure 1.2: A typical heavy transport; transport of the Peregrino *jacket on the barge* H-542 *towed by the tug* Bylgia *from the Netherlands to Brazil in November 2019 (the picture is taken during an inspection of the barge and cargo; during offshore tow, the tow line is much longer). Photo: Asle Natskår.*

1.2 Assumptions and limitations

Several assumptions have been made for the work performed in this thesis. Some main assumptions and limitations are listed below.

- Roll motion is normally governing for the loading in the grillage and seafastening and has been in focus in this study, and pitching is not studied
- The structural reliability assessment focus on the cargo support structure; the structural capacity of the cargo is not considered
- The forces in the cargo supports are calculated based on dynamic equilibrium of the cargo
- The weather forecasts and the long term statistical data in this thesis are from the Norwegian Sea and the North Sea (however, they are considered to be more generally representative of extratropical conditions)
- The reliability assessments performed in this thesis are related to natural uncertainties and variations
- Human and organizational errors are not considered in detail other than in Sec. 1.3.4, where precautions to reduce the probability of such errors are discussed
- Forward motion of the barge is not included, as the barge is assumed to be towed at low speed or in drift during the governing loading condition

1.3 Risk assessment of marine operations

1.3.1 Risk management

Active risk management is normally considered vital for the successful execution of marine operations and should be an integrated part of planning. The risk management plan should cover risk assessment of the marine operations as well as the various construction phases [55], and human errors should also be analyzed in risk management work; see also Sec. 1.3.4. Risk management should include risk assessment to define relevant loading conditions and accidental load cases [30, 71]. Robust and well-proven equipment, vessels and operational procedures should be used to minimize the

risk of failures or unacceptable delays as much as possible. The principle of ALARP, "As Low As Reasonable Practicable", should be adhered to, meaning that the risk is reduced as much as found practicable during planning and execution, which is also below the formally defined acceptance levels, based on cost-benefit assessments [30, 34].

1.3.2 Risk exposure during marine operations

Marine operations involve many stages and many suboperations where the handled object is exposed to risk. For the marine operations considered herein, see Sec. 1.1.1, the following sub-operations are generally relevant:

- Load-out of the object onto the transportation vessel by lifting with a crane, multiwheel trailers or skidding
- Berthing of the transportation vessel after the load-out (i.e., shift the vessel from the load out position to a temporary position along the quay)
- The loaded vessel moored along the quay during final preparations
- Commencement of the voyage; leaving the quay and maneuvering out of the harbor
- Sea voyage in open water
- Maneuvering into the harbor and berthing of the transport vessel when arriving at the destination, or arrival at an offshore location
- Discharge of the transport vessel, typically by a reversed load-out (load-in) at a yard or by lifting with a crane or by a float-over operation for an offshore installation

Keeping the general risk exposure and the various failure modes in mind, the focus here is on the structural failure of grillage and seafastening.

1.3.3 Categorization of uncertainties

Various categories of uncertainties are used, for example, random errors, systematic errors and gross errors (blunders) [41], human and organizational factors, etc.

The categorization can also be based on the type of uncertainties [96]:

- fundamental or inherent uncertainties; the aleatoric uncertainties

- uncertainties in mechanical or probabilistic models and statistical uncertainties; the epistemic uncertainties
- uncertainties related to human errors that affect the resistance and load effects

An alternative categorization for structural assessment could be 1) normal variability and uncertainty due to inherent variability or lack of data (also to establish analysis models) and 2) human errors, affecting both the loads and the load effects as well as the resistance [98].

The fabrication quality is one of the main design assumptions. Deviations in the fabrication quality contribute to the uncertainties in the structural capacity. Welding of grillage and seafastening is performed on the deck of the transport vessel, and weather sheltering can be challenging.

1.3.4 Effects of human factors

Human errors and omissions may be related to:

- the planning of the operation and choice of equipment
- the fabrication of the object to be handled, grillage and seafastening, etc.
- the execution of the operation

Several studies related to the human and organizational factors in marine operations have been performed, and it is indicated that human errors account for as much as 80-90% of all accidents [83, 88].

During the project phase, e.g., when performing structural design, human errors may lead to under-dimensioned structures [94, 138] that may substantially increase the risk of structural failure.

Other studies illustrate that the probability of personnel making the wrong choice while performing a task, by pushing the wrong buttons, etc., may become very high under unfavorable working conditions with high stress levels [66]. This approach to consider the effect of human errors can be relevant for execution of marine operations related to control panels for ballasting as an example.

Human errors should not be compensated by an additional design factor. Instead, gross errors in marine operations should be eliminated by extensive QA/QC activities (quality assurance and quality control) during design, fabrication and execution as well as utilizing defined safety barriers and redundant equipment and systems. Standard methods for risk reduction

during the planning of marine operations include independent (third party) design verification, Hazids, Hazops, etc. [30]. Operational errors should be eliminated by adequate training of the involved personnel [57] and by safety meetings, toolbox talks and risk assessments [128]. Safety barriers should be applied where possible to prevent one single failure from leading to severe failures [31, 65, 133].

While human factors are not directly included in this thesis, the above mentioned precautions are assumed to have been taken as relevant, substantially reducing the probability of human errors leading to catastrophic failures. Based on this assumption, the structural capacity checks are performed in the ultimate limit state. The corresponding target reliability level is discussed in the following section.

1.3.5 Target reliability level

An acceptable reliability level for marine operations is presently not accurately defined in any design standard. However, muck work has been performed with respect to code calibration to obtain a specific safety level for offshore structures (at the offshore site) [41, 97, 99].

Offshore structures will typically be on location for twenty years or more, and the definition of the reliability level is linked to the annual probability of failure. Marine operations typically last a few days or weeks, and it is then more natural to define a probability of failure per operation, independent of the duration [84]. This approach is applied in this thesis. The target safety level, however, could depend on the possible progressive failure of structural components, i.e., the consequences of a component failure.

Structural reliability analyses (SRA) are used to quantify the probability of failure. While SRA are tools for assessing failure probability, they do not account for human errors. Hence, the probabilities should not be considered as the “true”, or “real”, failure probabilities but rather than as a calibrating tool relating to the generic uncertainties included in the analysis.

Research has also been performed to combine quantitative risk analysis (QRA) with structural reliability analysis for marine operations [124, 125, 142], which is an alternative to SRA. The reliability level will depend on the type of analysis performed to some extent.

1.4 Planning and execution of marine operations

1.4.1 General principle

The marine operations discussed here are based on thorough planning and preparations. The environmental condition, wave-induced load effects, structural integrity, etc., are some key elements in planning such operations. All parts of marine operations need to be described by operational procedures, drawings, etc., collected in an operation manual. The structures and equipment must comply with the relevant requirements in the design standards. A few items related to the planning and execution of marine operations are described below, and a short discussion and a brief review of some previous research are given.

1.4.2 Rules and standards for marine operations

There is a long history of standards and guidelines in marine operations. The first guidelines (to my knowledge) were given as far back as 1958, when Captain William David Noble introduced criteria for tow preparation for the LeTourneau jack-up AMDP-1 to cross the Atlantic Ocean, which was the first drilling platform to do so [24]. Later, the *Noble Denton guidelines* [47] became well known in the industry. The first guidelines from DNV were issued in the late 1970s, and the first design standard was issued in 1985, the *DNV Standard for Insurance Warranty Surveys in Marine Operations*. This standard was replaced by the *DNV Rules for Planning and Execution of Marine Operations* in 1996 [23]. These rules were replaced by an Offshore Standard [26] in 2011. During this period, marine operations could be planned according to the DNV standards or the Noble Denton guidelines.

The ISO standard for Marine Operations was issued in 2009 [72]. Parts of this standard were based on the Noble Denton guidelines, and there were some differences compared with the DNV standards [6].

Following the merger between DNV and GL in 2013, the DNV standard and the Noble Denton guidelines (Noble Denton was owned by GL at the time) were both managed by DNV GL. The standard and guidelines both gave technical requirements and guidance for all types of marine operations, but their structure and detailing of the requirements were quite different [7], and they were combined into one standard [31].

There are also other standards and guidelines available. London Offshore consultants have their own *Guidelines for Marine Operations* [86]. The International Maritime Organization, IMO, issued *Guidelines for safe ocean towing* [70] in 1998. The US Navy issued a towing manual [110]. Ship-

ping and oil and gas companies have issued *Guidelines for Offshore Marine Operations* [48]. The API Recommended Practice for fixed platforms [8] contains a chapter with general requirements for load-out, transportation, and installation. Oil companies may also have their own specification with requirements in addition to the standards and guidelines for the design of marine operations. Some of the large marine operation contractors have company-specific design guidelines.

The main reference standard in this thesis is the current version of the DNV GL standard for marine operations [31][1]. This standard has the most comprehensive method for planning operations, such as accounting for uncertainty in weather forecasts.

1.4.3 Weather-restricted and -unrestricted operations

Marine operations are defined as weather-restricted or weather-unrestricted operations depending on the duration. The separation between these two categories is important, as they are planned differently with respect to environmental conditions. If the duration of the operation is less than 72 hours (96 hours when the contingency time is included) or if the operation can be halted and the handled object brought into a safe condition during the same period, the operation can be defined as weather-restricted. The design environmental criteria are defined in an early phase of the project. The operation may commence when all preparations are finished and the weather forecasts indicate acceptable environmental conditions. The uncertainty in the weather forecasts and how to include this uncertainty in the planning of the operation thus become key issues [108, 107].

Operations with planned durations longer than 72 hours are weather-unrestricted. They are not planned based on environmental conditions that can be confirmed by weather forecasts because the duration of such operations is longer than the duration for which weather forecasts are considered reliable. In the planning of a weather-unrestricted operation, the environmental criteria for the design must be considered according to long-term statistics accounting for the geographical area, the season of the year, and the duration of the operation.

[1]This standard is not freely available, and access requires a subscription. However, the requirements referred to in this thesis are practically the same as those given in the previous DNV offshore standards. Planning related to the duration and requirements for weather-restricted operations (see Sec. 2.2) are covered by DNV-OS-H101 [26], while the barge motion criteria can be found in DNV-OS-H202 [27]. These standards are available for free on the Internet.

1.4.4 Capacity checks and failure modes

For a typical marine operation, numerous design checks are required. Generally, four types of limit states are checked (see Sec. 1.4.7), but the ultimate limit state is the focus here. The structural strength is calculated according to recognized design standards, e.g., Eurocode and Norsok standards [36, 113], and adequate capacity is documented for the relevant limit state by applying the relevant reference levels for the loads and load effects. All vessels, equipment and structures involved in marine operations need to have documented capacity and shown to be adequate for their purpose. The sufficient capacity of the tug (e.g., the bollard pull) and the tow line capacity must be verified. The hydrostatic and dynamic stability of all floating vessels must be documented.

The design checks cover normal uncertainties due to fundamental variability/uncertainty and lack of data. As mentioned in Sec. 1.3.4, human errors are not accounted for in the standard ultimate limit state capacity checks.

1.4.5 Wave-induced loads and load effects

The governing load effects in the cargo supports are typically caused by the wave-induced motions, i.e., accelerations and rolling/pitching, of the transport vessel. Much research, both numerical and experimental, has been performed on wave-induced barge motion, particularly for the rolling of barges. Early research on the rolling of ships was performed by Froude in the 1860s [42]. In the 1960s, research on the rolling of ships and the effect of bilge keels was performed by Tanaka and Kato [80, 140]. In the 1970s, Ikeda et al. studied roll damping of ships with forward motion [68]. A barge research project was also initiated by Noble Denton [37].

The rolling of ships and barges is influenced by roll damping, which can be split into potential damping due to wave generation and viscous damping due to vortex shedding at the bilges. Vortex shedding and the details of the flow at the bilges have been studied by several researchers [49, 50, 12, 33, 126, 67], and studies are still ongoing [40, 51, 52, 101].

Handbooks based on numerical analysis and experiments, giving specific values to be used for typical vessel shapes during rolling, heaving and swaying, are available [81, 144]. More recently, ITTC issued a report giving a method for roll damping estimation that can be used in the absence of experimental data [75]. In addition to studying viscous damping as such, research has been performed on barge motion in waves [14, 18, 135]. Additionally, studies on wave-induced motions based on real transports have

been performed, and full-scale measurements of barge motions have been published [139], as well as model test results [79, 136].

The deformation of the transport barge in head and beam seas will have a limited effect on an object placed on four supports with a static determinate seafastening system, while there is a larger effect of deformations in oblique seas and for the transport of structures on several supports, e.g., a jacket [20]. Then, the relative stiffness of the transported object and the transport barge will influence the support forces.

The statistical distribution chosen to represent the responses for the analysis of sea transport is also important. Research is performed on the statistical distribution of the extreme value of the responses. The standard approach is to assume Rayleigh or Weibull distributed individual maxima. An alternative method was developed by Naess and Gaidai [102]; this method can be used for extreme value statistics of roll motions [45]. Other methods have also been studied [105, 119].

1.4.6 Weather forecasts

The start-up of a marine operation requires forecast confirmation that the environmental criteria are fulfilled, and hence weather forecasts are important input for decision making during the execution of marine operations. The uncertainty in the forecasts must be accounted for in the planning of the operation.

The standard method to account for the forecast uncertainty is to reduce the design criteria by an *Alpha factor* [31]. For example, if the design sea state is $H_{s,design} = 4$ m and $\alpha = 0.75$ (the Alpha factor depends on the duration of the operation), the operation can start when the forecast predicts $H_{s,wf} \leq 3$ m throughout the operation period. The Alpha factors are based on the uncertainty estimated based on a comparison of the measurements and forecasts [87, 146]. Alternative approaches exist, for example, for making criteria for unmanning platforms during storm events [59], where ensemble weather forecasts are utilized.

Weather routing has become more available as technology has progressed. While the traditional approach for weather routing was to avoid certain areas during the winter season, weather routing can now use updated weather forecasts on board as part of the decision-making process [1]. Instead of defining the limit for the execution of marine operations based on the wind speed and significant wave height, the industry seems to be heading towards a response-based approach. For several years, there has been great interest in this approach within the industry, and in 2019, DNV GL initiated a joint industry project (JIP) to further investigate response-based methods. With

the response-based approach, the wave forecasts are not limited to H_s and T_p/T_z, but forecasted 2D wave energy spectra can be utilized (an example of a 2D spectrum is shown in Fig. 3.1). Several wave systems, e.g., wind waves and one or more swell systems, can thereby be included in the numerical models. Until now, this method has mostly been used in addition to the traditional approach and not as a complete decision tool for marine operations [19]. There have also been studies related to the assessment of operational limits and limiting sea states based on the allowable response [54]. Such operational-based methods by means of the on board monitoring of waves and vessel motion are being developed [21]. The response-based approach contains various methods for improving shipping and marine operations in general. The methodologies are expected to be further developed over the coming years. Nevertheless, the traditional approach based on the significant wave height will be used for small projects and by companies without the resources or the need for a response-based system. To quantify the forecast uncertainty, the forecasts should preferably be compared with measured data. However, hindcast data are of high quality and can be used in comparisons instead of measured data [82]. The European Centre for Medium-ranged Weather Forecasts, ECMWF, verifies the forecasts by comparing the measured and forecasted environmental data [9, 147].

In areas and times of year where polar lows can occur, this phenomenon should be included in the forecasts. The period where a reliable forecast of polar lows can be given is short, as polar lows may be predicted for a period of approximately 24 hours [114]. Standard weather forecasts do not include polar lows. Polar lows should be specially considered where relevant [118, 123].

1.4.7 Structural design of the grillage and seafastening

The grillage and seafastening are designed based on the load effects from accelerations and roll/pitch angles given by a motion analysis using a 3D panel model or from simplified motion criteria. The forces should include possible effects of friction. Even if vessel motions used for calculating the load effects for the design of the cargo support system can be calculated by different methods, the safety coefficients, e.g., the load and material factors, applied in the design do not reflect the method for calculating the motions but depend on the design limit state.

The transports are assumed to be planned and executed according to a recognized standard using the load and resistance factor design approach, and the structural capacity can generally be verified for four design limit states:

- ultimate limit state, ULS
- accidental limit state, ALS
- fatigue limit state, FLS
- serviceability limit state, SLS

The ULS covers the normal uncertainty and variability in the loads and resistances, while the ALS is introduced to avoid progressive failure after accidental damage. The accidental limit state is important when there is a risk of the tanks flooding or the load shifting. For heavy cargo, shifting of the load will lead to a total loss, but for smaller cargo, this may be a relevant ALS case. The fatigue limit state is relevant for transports with a long duration, i.e., transports lasting more than a few days, and for structures with poor fatigue properties (high stress concentrations). Fatigue is not considered here. The serviceability limit state is mainly related to deformations and is normally not of main importance for sea transports. The SLS may be important if the transported object has equipment that is sensitive to relative deformations, e.g., large equipment and piping in a process module. The main category is the ultimate limit state, which is relevant for all transports. This category is the focus here.

The method used to calculate the structural strength can affect the overall reliability, e.g., the use of standard capacity formulas versus linear or nonlinear finite element analyses. For example, capacity checks according to Eurocode 3 [36] may serve well for design purposes for plate girders with a relevant geometry, but it is difficult to apply these checks to more complicated fabrications [32].

Even if there are recommendations for the general principles for seafastening [53], different transport vessels, e.g., a barge, a transport ship or a heavy transport vessel, may also have different characteristics, and a vessel-specific design approach may be required. For example, a module placed on grillage beams on a barge, as shown in Fig. 4.1, cannot rely on friction at all because wet steel to steel has very little friction. On the other hand, a large object transported on the deck of a heavy transport vessel is normally set on wooden cribbing, and the positive effect of friction can be included [5].

As a consequence, the probability of failure will to some extent depend on the type of transport and how the load effects are calculated. Hence, the calculated probability of failure could vary from case to case depending on the design method.

1.4.8 Operational procedures

Operational procedures and other relevant information related to organizational and technical items needed during the execution of a marine operation are written in a *Marine Operation Manual*. The operation manual is custom-made for each operation and should include the following, as applicable [31]:

- reference documents
- general arrangements and references to relevant drawings
- permissible load conditions
- organization charts and lines of command
- environmental criteria
- weather forecasts and wave reporting
- specific step-by-step instructions for each phase of the operation
- references to relevant calculations, e.g., environmental loads, mooring arrangements, ballast conditions, stability, tug bollard pull
- permissible draughts, trim, and heel and corresponding ballasting plans
- contingency and emergency response plans
- vessels involved
- tow routes and ports of refuge
- towing arrangements

This information is needed for the crew to know what to to in the normal operation mode and in case of emergencies. For barge transport, this document is called a *Towing manual* and will contain the above listed information as relevant, depending on the type of transported object, geographic area, distance, duration, etc.

1.4.9 Marine warranty surveys

Insurance companies often require that an independent verification of the planned operation and the execution be performed to ensure the required quality in the operations. A Marine warranty surveyor (MWS) is then engaged to verify and approve the marine operation [60]. The MWS will perform their work in accordance with a recognized standard [31, 72] and approve the planning of the operation, which typically include drawings, design calculations and operational procedures. The MWS is normally present during the execution of the operations, confirming that all preparations have been performed, that the forecasted weather conditions are within acceptable limits and that the operational procedures are being followed [46]. These verification activities aim to improve the quality and hence reduce the risk inherent in the operation.

1.5 Aim and scope

The scope of this thesis is shown in Fig. 1.3, where the interconnection between the research topics and papers included in Appendix A is demonstrated. The primary aim of the research is to develop a structural reliability model to quantify the reliability level implicit in current guidelines and possibly calibrate the reliability level. The focus is on assessing the uncertainties of the environmental conditions, wave-induced load effects, and structural capacity and studying the safety level and reliability of the cargo support system for sea transport in the ultimate limit state. The main objectives and scope of the research work in this thesis can be summarized as follows:

- To study the methods for the prediction of wave-induced barge motion and related seafastening forces for cargo on a transport barge in severe seas and compare linear and nonlinear numerical motion analysis results with experimental results
- To investigate the uncertainty inherent in the calculation of the wave-induced load effects
- To investigate the uncertainty in the calculated structural capacity
- To study the uncertainty in forecasted environmental conditions for weather-restricted marine operations

- To quantify the forecast uncertainty of the significant wave height for weather-restricted operations and the statistical environmental data for weather-unrestricted operations
- To develop a reliability model for the structural capacity of the cargo supports
- To perform structural reliability analyses of the support structure and compare the implicit reliability level for various design conditions, e.g., for several forecasted significant wave heights, as a function of the durations of the operation, assuming that the operation occurs in various seasons of the year

1.6 Thesis outline

This thesis is written in the format of several briefly descriptive chapters and appended papers related to the objective of this research. The organization of this thesis is as follows:

Chapter 1:
This chapter provides an introduction, the background, the motivation, a brief review of current guidelines and standards, the historic and current developments in research related to marine operations, the aim and scope, and an outline of the thesis.

Chapter 2:
This chapter addresses the planning of marine operations with a focus on environmental conditions. The important categorization of marine operations into weather-restricted and weather-unrestricted operations is further explained. A brief review of the calculation methods for the design wave heights for unrestricted operations is given. Uncertainties related to the design wave height, e.g., due to uncertainty in the weather forecasts, and uncertainties in the background data are discussed. A simplified method for estimating a design wind speed for a given significant wave height is presented. The main results from Paper 2 are included in this chapter.

Chapter 3:
This chapter elaborates on the key issues related to wave-induced load effects. It contains a description of the regular and irregular wave concepts. The calculation of wave-induced load effects in the frequency and time domains is briefly described. A description of the model tests is given. Nu-

merical and experimental uncertainties are discussed. This chapter contains information from Paper 1.

Chapter 4:
The structural strength in the ultimate limit state, as well as the structural reliability method and the application for the barge transport case, are presented. Capacity checks in the ultimate limit state are discussed, as well as the uncertainties in the structural capacity and load effects. This chapter is partly related to Papers 2 and 3.

Chapter 5:
Conclusions, an overview of the original contributions and recommendations for future research are presented in this chapter.

Appendix A:
Appended papers

Paper 1:
Rolling of a transport barge in irregular seas, a comparison of motion analyses and model tests
Authors: Asle Natskår, Sverre Steen
Published in *Marine Systems & Ocean Technology*, Vol. 8 No. 1, pp. 05-19, June 2013

Paper 2:
Uncertainty in forecasted environmental conditions for reliability analyses of marine operations
Authors: Asle Natskår, Torgeir Moan, Per Ø. Alvær
Published in *Ocean Engineering*, Vol. 108, pp. 636-647, 2015

Paper 3:
Structural reliability analysis of a seafastening structure for sea transport of heavy objects
Authors: Asle Natskår, Torgeir Moan
Submitted for publication in *Ocean Engineering*

Appendix B:
Layout of a typical transport barge.

Appendix C:
Motion analysis of ships and barges.

Appendix D:
Description of the model tests.

Appendix E:
List of previous PhD theses at the Department of Marine Technology.

The work is organized as shown in Fig. 1.3.

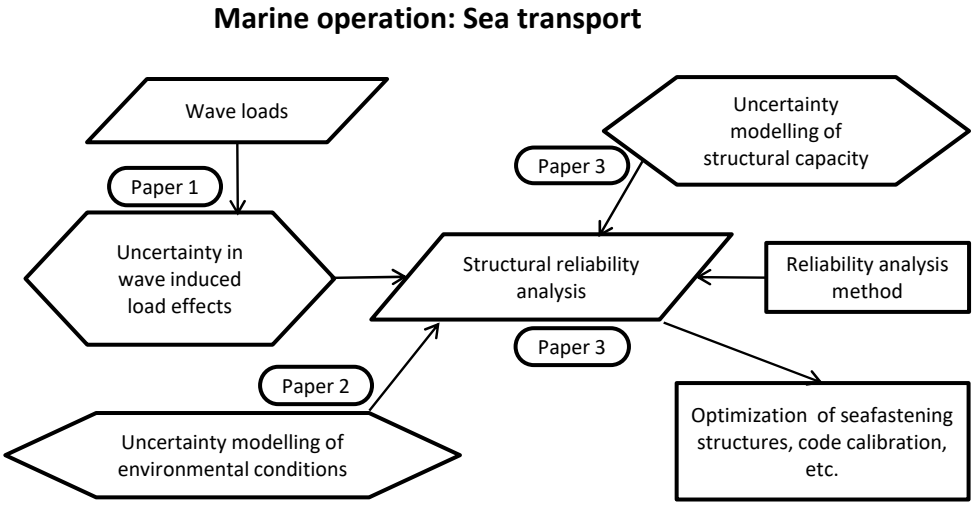

Figure 1.3: Organization of the thesis and its interconnection with Paper 1 [109], Paper 2 [108] and Paper 3 [107]

1.7 Outline of the papers

Paper 1 addresses the sea transport of heavy objects and the motions of a transport barge exposed to wave loading. The aim is to investigate methods for the prediction of barge roll motion and related sea fastening forces by numerical analysis and model tests of a barge in irregular waves. The response from linear and nonlinear numerical analyses is compared with the results of the model tests. It is found that the numerical analyses give slightly conservative results and that the nonlinear time-domain analyses give only

marginally more accurate results than the linear frequency domain method. The results from Paper 1 are used for modeling the uncertainty in the wave-induced load effect.

Paper 2 is concerned with planning marine operations with regard to environmental conditions and operational limits. Operational decisions are based on weather forecasts, and the uncertainty inherent in weather forecasts of significant wave height is studied using data from the Norwegian Sea. The results from Paper 2 form the basis for the uncertainty model of the environmental conditions in the reliability analyses.

Paper 3 addresses the structural capacity of the transport vessel and the cargo and discusses the uncertainty models used in the structural reliability analyses. The bulkheads in the transport vessels are exposed to large vertical local forces from the cargo supports, and when these bulkheads have horizontal stiffeners, the in-plane bulkhead loading acts perpendicular to the stiffeners. The modeling of the uncertainty in such structures is discussed. Furthermore, the paper presents a structural reliability analysis method to accommodate the uncertainties affecting the design checks. The implied probability of structural failure by use of the relevant design standards for marine operations is studied using structural reliability analyses for two categories of marine operations, notably weather-restricted and weather-unrestricted operations. While weather-restricted operations are designed for a chosen limit of the significant wave height, a weather-unrestricted operation cannot rely on forecasts but must be designed using long-term statistical data for the relevant season. The probability of failure is calculated for both categories. The probability of structural failure during weather-restricted barge transport is calculated for various durations and several forecasted significant wave heights. For weather-unrestricted operation, where the environmental loading is given by long-term data, the failure probability is calculated for several operational durations and for execution in various months or seasons.

Chapter 2

Environmental conditions for marine operations

2.1 General

The purpose of the marine operations studied here is to safely transport an asset from one location to another location. Environmental loads are the key input for the design of marine operations and will often define the limits for the actual execution of an operation. Even if the design should aim at making the operation robust, most operations are sensitive to environmental loading, and waiting on weather commonly occurs. During the planning of weather-restricted operations, the environmental design conditions should be optimized to balance the cost related to the size of the transport vessels, tugs, structural steel, equipment, etc., with the cost related to waiting on weather; see also Sec. 2.5.1.

2.2 Planning of marine operations and required environmental data

During marine operations, the handled object is brought from one defined safe condition to another. The marine operation is over when the safe destination has been reached. A key parameter is the duration of the marine operation. To estimate the duration, the time when the handled object is in a safe condition and the operation is finished must be clearly defined. The duration of an operation, called the operation reference period, is defined as follows [31]:

$$T_R = T_{POP} + T_C \tag{2.1}$$

where
T_{POP} is the planned operation period and
T_C is the estimated maximum contingency time.
The estimated maximum contingency time is normally between 50% and 100% of the planned operation period. The total duration is a stochastic variable but is assumed to be deterministic here.

Marine operations are classified as either weather-restricted or weather-unrestricted, depending on the duration of the operation. Weather-restricted operations are based on weather forecasts and are beneficial since the owner, or their representative, may define the environmental criteria to operate in. The operation may commence when the weather forecasts show acceptable conditions. A key issue is then the uncertainty in the weather forecasts and how to deal with that uncertainty during planning of the operation. For weather-restricted operations (i.e., operations of short duration and operations that may be halted within a short notice), the environmental conditions are given by weather forecasts. An ample margin must be set on the forecasted wave height, wind speed, etc., when defining the operational criteria to have a sufficiently low probability of exceeding the design criteria.

For operations with a long duration, weather forecasts do not give reliable information, and the design criteria are instead based on long-term statistical data; the operation is weather-unrestricted. An environmental condition with a low probability of being exceeded is defined based on long-term statistics. The environmental criteria for the two categories of marine operations are treated differently. In the ISO standard for marine operations [72], a planned duration including a contingency (T_R) of 72 hours is the maximum for a weather-restricted operation. In the DNV GL standard [31], the limit is somewhat increased: If T_R is less than or equal to 96 hours and T_{POP} is less than or equal to 72 hours, the operations can be defined as weather-restricted. The operation can also be defined as weather-restricted if the operation can be halted and the handled object can be brought into a safe condition within that time frame. For sea transport, this means that the route needs to be divided into several legs between ports or areas of shelter along the transport route. Each leg is planned as a weather-restricted transport. Operations where T_R is more than 96 hours or T_{POP} is more than 72 hours are by definition weather-unrestricted. The separation between these two categories is important since they will be planned differently with respect to environmental criteria. Two examples are shown in Fig. 2.1. To the left is a transport along the coast of Norway, where shelter can be found and the transport can be divided into several legs, each performed within a weather window. The example on the right-hand side is a transport crossing

the Indian Ocean. Even if there are several islands in that area, they are not considered to provide sufficient shelter or safe haven, and the transport is weather-unrestricted. See also Sec. 2.6.

Figure 2.1: Example of weather-restricted transport with a sheltered stop (left) and weather-unrestricted transport; red lines represent transport routes (maps from www.fn.no)

In areas or seasons where weather forecasts are reliable for a shorter period, a shorter limit for weather-restricted operations must be applied.

2.3 Weather forecasts

Weather forecasts for marine operations are typically operation specific and specially ordered forecasts that include a significant wave height, wave period and wind speed, among other information. The forecast can be given for one specific location or for a given transport route. The forecast is ordered based on an estimated vessel speed, and an updated route is sent to the forecaster during the operations if the actual route deviates from the planned route.

In this thesis, the total sea, i.e., the combination of wind-generated waves and swell, has been studied; see also Sec. 2.5.2. The sea state is modeled by a one-peak wave energy spectrum, as described in Sec. 3.2.

The forecasted significant wave height and the hindcast significant wave height (i.e., "true" H_s) for one year are shown in Fig. 2.2 for a lead time of 48 hours. Fig. 2.3 shows the same comparison for the month of May. It

is evident that not all the peaks in the observed wave heights are captured by the weather forecasts.

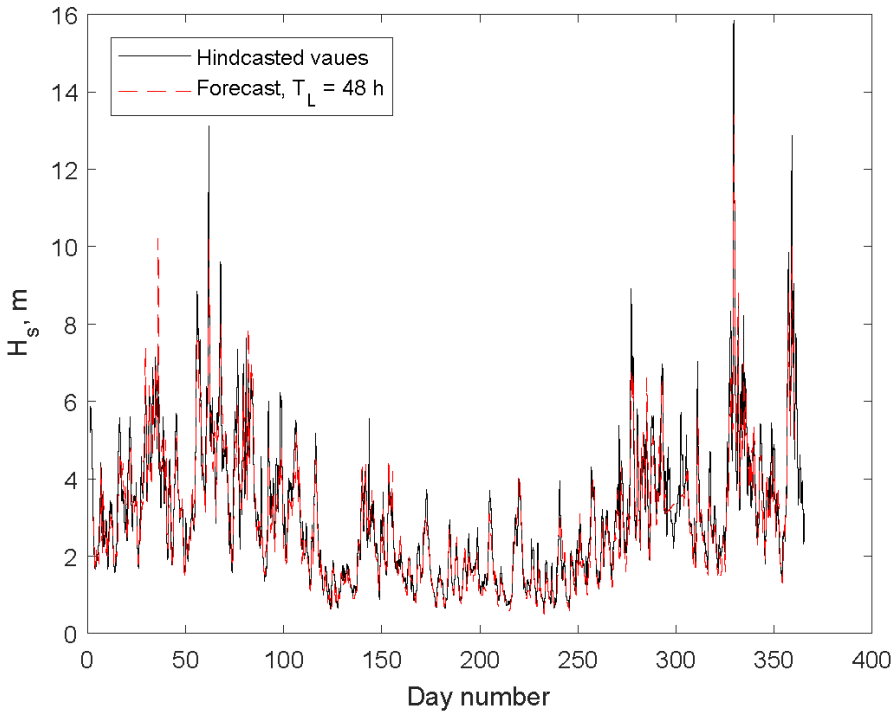

Figure 2.2: Hindcast and forecasted H_s for lead time of 48 hours in 2011, at Location 1 in Fig. 2.6

The correlation between the forecast and hindcast significant wave heights is shown for several lead times in Fig. 2.4. The correlation decreases with increasing lead time. In Fig. 2.5, the wave periods (spectral peak periods, T_p) are similarly shown. The correlation between the forecast and hindcast values is lower for peak periods than for the significant wave height for a lead time less than 72 hours. The peak period appears to be more difficult to forecast than H_s. This is not limited to weather forecasts; the uncertainty in sea state parameters from spectral estimation has been studied by Rodrigues et al. [127]. It was concluded that the use of different methods of spectral estimation did not have a large effect on the variability of, e.g., the significant wave height, but the peak period showed great differences as a function of the spectral method adopted.

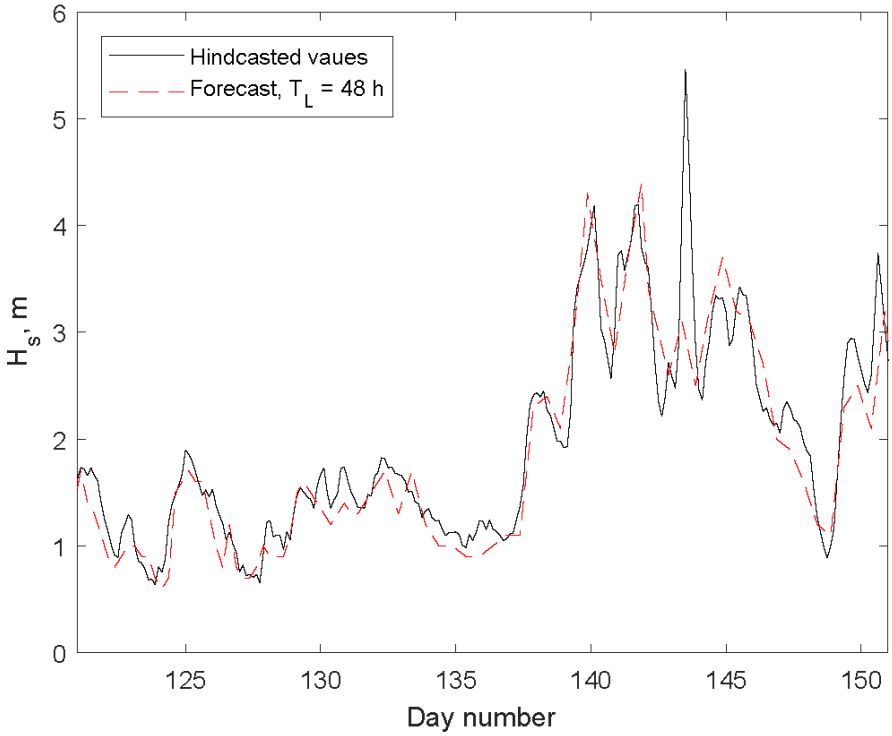

Figure 2.3: Hindcast and forecasted H_s for a lead time of 48 hours at Location 1 in Fig. 2.6 for May 1 to 31. 2011

2.4 Hindcast data

2.4.1 The use of hindcast data

Ideally, measured wave data would have been used for comparison with weather forecasts. However, access to measured data is limited, and hindcast data are used instead. The quality of the hindcast database is high, and hindcast data are extensively used for design work on the Norwegian Continental Shelf [62]. The uncertainty in the forecasted significant wave height is estimated in this thesis by comparing one year of the forecast and hindcast data. The limited duration as well as the uncertainty inherent in the hindcast data may therefore affect the results. The accuracy of the hindcast significant wave height compared to measurements has been studied by Haver [61]. The difference between the hindcast and measured H_s values had a standard deviation of 1.15 m, based on 168 storm events with

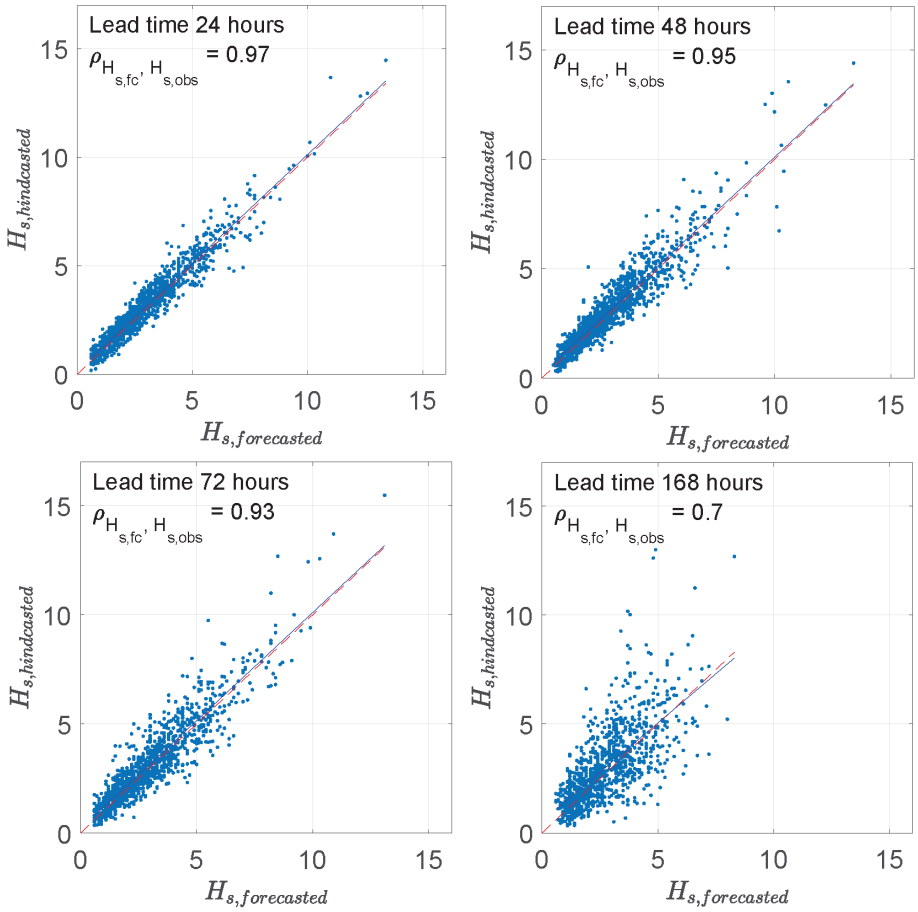

Figure 2.4: Hindcast and forecasted significant wave height

$H_{s,hindcast} \geq 7.5$ m. No clear dependence of the standard deviation on the wave height was observed in that study. However, for weather-restricted operations, the main interest is in lower wave heights, typically H_s of 3-5 m. According to Brooker et al. [13], a scatter index [1] of 10-15% for significant wave heights from the hindcast is representative of modern hindcasts compared with measured values.

A comparison of hindcast data with measurements has also been performed by Bruserud and Haver [15]. They found the hindcast significant

[1]The scatter index (S.I.) is defined as $S.I. = \sigma_m/\mu_{meas}$, where σ_m is the standard deviation of the difference between the measured and modeled values and μ_{meas} is the mean of the measured wave heights used for comparison.

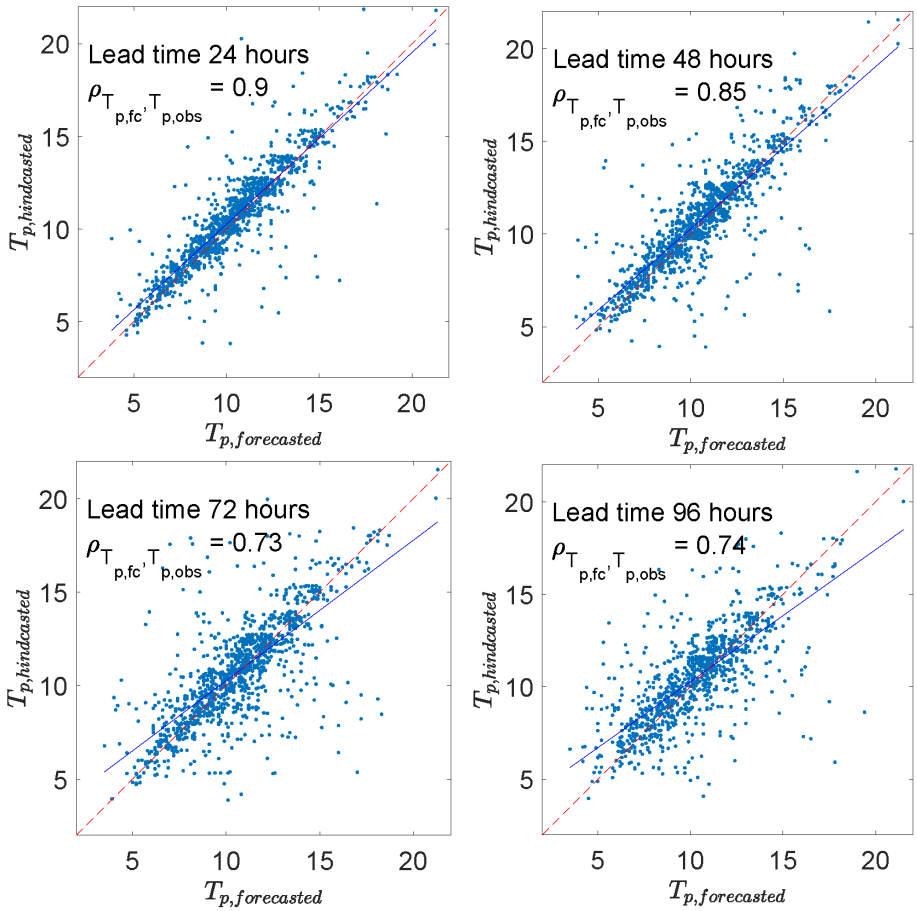

Figure 2.5: Hindcast and forecasted significant wave period

wave height from NORA10 [2, 123] to be slightly conservative compared with the measurements. However, the difference was small, and they did not correct the significant wave height from NORA10.

Haakenstad et al. [58] compared NORA10 data (and a new hindcast model, NORA10EI) for the Norwegian Sea, North Sea and Barents Sea with the measurements. They found that the comparison with the observations was good in general. There seems to be a slight conservatism in the hindcast data, as the presented 99.9th percentile H_s-values are generally slightly higher from NORA10 than from the measurements.

In the abovementioned studies, hindcast values of H_s were compared with the measurements. Wave measurements contain some uncertainty as

well. This was studied by Magnusson [91], comparing measurements from wave rider buoys with radar and laser measurements. There was generally a good fit between the methods, but some deviations were evident, in particular for significant wave heights larger than $8 - 10$ m.

Based on the studies above, it was concluded that the measurements and hindcasts are both suitable for a study of the uncertainty in weather forecasts, and in this thesis, hindcast data were directly used without any corrections. The hindcast data were used as follows:

- Hindcast significant wave heights were compared with weather forecasts to estimate the uncertainty in the forecasted significant wave height (Location 1 in Fig. 2.6)
- The long-term statistical distribution of the significant wave height and the conditional distribution of the wave period were estimated based on the hindcast data (Location 2 in Fig. 2.6)

2.4.2 Long-term distribution from the hindcast data

In the hindcast data, the significant wave height is given every three hours. A three-parameter Weibull distribution can be fitted to the long-term distribution of H_s. The parameters can be estimated according to [17, Sec. 17.6]. The approach is explained in detail in [62]. The probability density function for the Weibull distribution is defined as follows:

$$f_{H_s}(h_s) = \frac{\beta}{\alpha}\left(\frac{h_s-\gamma}{\alpha}\right)^{\beta-1}\exp\left[-\left(\frac{h_s-\gamma}{\alpha}\right)^{\beta}\right] \tag{2.2}$$

where
α is the scale parameter (different from the Alpha factor used elsewhere),
β is the shape parameter and
γ is the location parameter.
To estimate the three parameters, the three lowest moments are used, i.e., the mean value, the variance and the skewness. The mean value is calculated as follows:

$$\mu_{H_s} = \gamma + \alpha\Gamma\left(1+\frac{1}{\beta}\right) \tag{2.3}$$

The variance is calculated as follows:

$$\sigma^2_{H_s} = \alpha^2\left[\Gamma\left(1+\frac{2}{\beta}\right) - \Gamma^2\left(1+\frac{1}{\beta}\right)\right] \tag{2.4}$$

Figure 2.6: Locations where hindcast data are taken from [108, 107] (map from www.fn.no)

The skewness is calculated as follows:

$$\gamma_1 = \frac{\Gamma\left(1+\frac{3}{\beta}\right) - 3\Gamma\left(1+\frac{1}{\beta}\right)\Gamma\left(1+\frac{2}{\beta}\right) + \Gamma^3\left(1+\frac{1}{\beta}\right)}{\left[\Gamma\left(1+\frac{2}{\beta}\right) - \Gamma^2\left(1+\frac{1}{\beta}\right)\right]^{1.5}} \tag{2.5}$$

Γ is the gamma function ($\Gamma(t) = \int_0^\infty x^{t-1}e^{-x}\,\mathrm{d}x$).

The mean, variance and skewness of H_s are calculated directly from the hindcast data (see Eq. (2.8)-(2.10)) and are used to calculate the parameters in the Weibull distribution.

The skewness only depends on the parameter β. Hence, β is calculated from Eq. (2.5). Then, Eq. (2.4) is solved to obtain the parameter α. Finally,

the parameter γ is estimated from Eq. (2.3). The Weibull parameters for Location 2 in Fig. 2.6 are given in Tables 4.4 and 4.5.

2.5 Weather-restricted operations

2.5.1 General

Marine operations, e.g., load-out operations, sea transports and installation of offshore units and equipment, all need to be designed, planned and executed considering environmental loads.

The design environmental criteria for a weather-restricted operation are set in an early phase of the project. A low criterion may lead to extensive waiting on weather, which is expensive. A criterion that is too high will increase the economic cost related to the operation, e.g., due to the increased tug size, mooring arrangements, amount of seafastening, etc. The optimum environmental criteria should be chosen based on an overall assessment.

The operation may commence when the weather forecasts indicate that acceptable environmental conditions are present for the entire operation period. The uncertainty in the weather forecasts and how to include this uncertainty in the planning of the operation thus become key issues. Based on the *design* environmental condition defined in the planning phase ($H_{s,design}$), the corresponding limiting environmental criteria for the *execution* of the operation, i.e., the maximum allowed forecast value, ($H_{s,forecast}$), is defined. $H_{s,forecast}$ is lower than $H_{s,design}$ to account for the uncertainty in the forecasted environmental conditions. The maximum allowed forecasted significant wave height can be determined by the Alpha factor method described in Sec. 1.4.6.

The uncertainty in weather forecasts was studied in Paper 2 [108]. Section 2.5 is an overview of weather-restricted operations, including a summary of that paper.

2.5.2 Forecasted wave height

Wave-induced loads will normally dominate the structural load effects for marine operations where floating vessels are involved. Hence, the significant wave height is of main interest for marine operations. It is therefore vital to have information about the level of accuracy for the forecasted wave height. The forecasts include wind-generated seas, swells and the total sea. In the studies, the significant wave height for the total sea has been used, i.e., $H_{s,total\ sea} = (H^2_{s,wind\ waves} + H^2_{s,swell})^{0.5}$.

The true maximum significant wave height was defined as a stochastic variable depending on the forecasted wave height. Two mathematical models were defined in Paper 2 [108]: an additive and a multiplicative model. In the additive model, the true significant wave height is described as:

$$H_{s,true} = \Delta + H_{s,fc} \tag{2.6}$$

where Δ is a stochastic variable describing the difference between the hindcast and forecasted wave heights. In the multiplicative model, the maximum wave height is expressed as:

$$H_{s,max} = \chi \cdot h_{s,fc,max} \tag{2.7}$$

where χ is a stochastic variable describing the ratio between hindcasted and forecasted wave heights. An unbiased weather forecast leads to $\mu_\Delta = 0$ for the additive model and $\mu_\chi = 1.0$ for the multiplicative model.

By defining the variable as the difference between two wave heights, i.e., the additive mathematical model, large waves will have larger bias than small waves for the same percentage of accuracy. This effect is eliminated if the multiplicative model is used to define the stochastic variable. Based on the comparisons performed in Paper 2, it was concluded that the multiplicative model is preferred for the study in this thesis. Statistical data for χ based on one year of data from the Norwegian Sea are given in Tab. 2.1.

Table 2.1: Numerical values of $\mu_{\ln\chi}$, $\sigma_{\ln\chi}$, μ_χ, σ_χ and COV used to describe the uncertainty in forecasted H_s for the total sea

No. of days	T_R, (h)	$\mu_{ln\chi}$	$\sigma_{ln\chi}$	μ_χ	σ_χ	COV
1	24	0.055	0.112	1.06	0.12	0.11
2	48	0.066	0.119	1.08	0.13	0.12
3	72	0.079	0.134	1.09	0.15	0.13
4	96	0.084	0.153	1.10	0.17	0.15
5	120	0.095	0.176	1.12	0.20	0.18
6	144	0.111	0.204	1.14	0.24	0.21
7	168	0.127	0.224	1.16	0.26	0.23

2.5.3 Statistical parameters

Since χ depends on the forecast period, the mean value and standard deviation are functions of this parameter. The statistical parameters for a realization of the stochastic variable χ are calculated by the standard formulas

using the software package MATLAB [93]. The mean value is calculated as:

$$\mu_\chi \approx M_\chi = \frac{1}{N}\sum_{j=1}^{N}\chi_j \tag{2.8}$$

where N is the number of samples in the realization.
The standard deviation is:

$$\sigma_\chi \approx S_\chi = \sqrt{\frac{1}{N-1}\sum_{j=1}^{N}(\chi_j - M_\chi)^2} \tag{2.9}$$

The skewness is calculated as follows:

$$\gamma_1 = \frac{\frac{1}{N}\sum_{j=1}^{N}(\chi_j - M_\chi)^3}{\left(\frac{1}{N}\sum_{j=1}^{N}(\chi_j - M_\chi)^2\right)^{3/2}} \tag{2.10}$$

The kurtosis is calculated according to the formula:

$$\gamma_2 = \frac{\frac{1}{N}\sum_{j=1}^{N}(\chi_j - M_\chi)^4}{\left(\frac{1}{N}\sum_{j=1}^{N}(\chi_j - M_\chi)^2\right)^{2}} \tag{2.11}$$

The skewness is zero, and the kurtosis is three for the normal distribution.

2.5.4 Wave period conditional upon H_s

Offshore weather forecasts include the wave period. The uncertainty in the forecasted periods can be analyzed similarly to the method for the wave height in Sec. 2.5.2. However, the uncertainty in the forecasted wave periods is larger than for the wave height, and in the current work, the wave period is defined by a statistical distribution conditional upon the wave height. Hence, for a given wave height, the motion response calculations for a floating vessel are performed for a range of wave periods.

The wave period range could be based on environmental statistics from a specific location, or it could be taken from design standards and guidelines.

The mean zero-crossing wave period (T_z) range can, for example, be taken as follows [31, Sec C.3.4]:

$$2.84H_s^{0.5} \leq T_z \leq \max\{5.43H_s^{0.5}, 13\} \tag{2.12}$$

where H_s is given in meters and the unit for T_z is seconds.

The mean zero-crossing periods can be modeled as a lognormal distribution conditional upon the significant wave height [11, 108]; see Eq. (4.13) on page 69. The parameters for the distribution can be found for the North Atlantic and for the Worldwide operation of ships [29] and in Table 4.6 for Location 2 in Fig. 2.6.

2.5.5 Wind speed

The uncertainty in the forecasted wind speed may be quantified by comparing forecasted values with hindcast values, resulting in a statistical description of the deviation, similar to what was done for the wave heights. This is particularly relevant for marine operations performed in sheltered areas where the wind load dominates, e.g., load-out operations where wind loads govern for the mooring of the transport vessel.

For typical sea transport on a large ship or transport barge, the wave load will dominate over the wind load; see Sec. 3.3.7. The uncertainty in the wind load will therefore have a limited effect on the total load in the supports and is not considered further for weather-restricted operations.

2.6 Weather-unrestricted operations

2.6.1 General

Marine operations with a planned duration longer than three days cannot be designed as weather-restricted operations but need to be designed as weather-unrestricted operations; see Sections 1.4.3 and 2.2.

While for a weather-restricted operation, the environmental criteria are based on weather forecasts accounting for the uncertainty, environmental criteria for weather-unrestricted operations are based on long-term environmental statistics. The design criteria are calculated for the relevant geographical area, the season of the year and the duration of the operation. The design wave heights may be calculated based on scatter diagrams [29, 64]. It should be noted that scatter diagrams based on visual observations of the sea may, to some extent, include the effects of heavy weather avoidance (i.e., the largest waves are never observed).

For commercial projects, more accurate data may be purchased, e.g., from Fugro Oceanor. Data from Fugro Oceanor are derived from hindcast models and are calibrated against satellite data and, where available, in situ wave buoy data [43]. A study of a VLCC (very large crude carrier) and a bulk carrier [130] indicated that the use of data from Fugro Oceanor gave approximately 15% larger amidship bending moments than those deduced from the scatter diagrams from DNV GL [29]. Another alternative is the computer program Safetrans [92], which contains an environmental database and can provide wave statistics for a defined transport route for a given start date and transit speed.

In addition, methods from design standards are available for defining design criteria. These methods are briefly described below.

2.6.2 Wave height obtained from the long-term distribution

The long-term distribution of the significant wave height is assumed to follow a three-parameter Weibull distribution:

$$F_{H_s}(h_s) = 1 - \exp\left[-\left(\frac{h_s - \gamma}{\alpha}\right)^{\beta}\right] \tag{2.13}$$

where α, β and γ are the scale, shape and location parameters, respectively. The extreme value distribution is equal to $F_{Hs,max}(h_{s,max}) = [F_{Hs}(h_{s,max})]^n$, where n is the number of sea states. Assuming a storm duration of three hours, set $n = 8d_n$, where d_n is the number of days within the operation period. The design significant wave height can be expressed as follows:

$$H_s = \gamma + \alpha[-\ln(1 - (1 - \zeta)^{1/(8d_n)})]^{1/\beta} \tag{2.14}$$

where ζ is the probability of exceeding the design wave height, typically set equal to 10%. The parameters for the distribution are given in Table 2.1.

Table 2.2: Weibull parameters [29] for the locations shown in Fig. 2.6

Location	Area [29]	α	β	γ
1	4	2.84	1.53	0
2	11	2.19	1.26	0

2.6.3 Wave height based on the ISO standard

According to ISO 19901-6 [72], weather-unrestricted operations may be designed using environmental criteria with return periods estimated as a multiple of the operational duration. A minimum return period equal to 10 times

the duration of the operation should be used. The cumulative probability function is then equal to:

$$F_{Hs}(h) = 1 - \frac{1}{10n_R} \tag{2.15}$$

where $n_R = 8d_n$ is the number of three-hour sea states.

Setting Eq. (2.15) equal to Eq. (2.13) and solving for h yields the significant wave height to be used in design:

$$H_{s,ISO} = \gamma + \alpha \left[\ln(80d_n)\right]^{1/\beta} \tag{2.16}$$

The significant wave height is then practically the same as the wave height from Eq. (2.14) with a 10% exceedance probability. An alternative approach using standard return periods is described in Sec. 2.6.4.

2.6.4 Wave height from standard return period tables

While the above sections describe how to calculate the significant wave height, Table 2.3 shows how the significant wave height to be used in design can be based on a return period depending on the duration of the operation. In the table, the recommended return periods from the ISO and DNV GL standards are given. This approach is not used in this thesis, but examples

Table 2.3: Recommended minimum return periods in the design standards from ISO and DNV GL

	Recommended return periods	
Duration (T_R)	ISO [72]	DNV GL [31]
Up to 3 days	Weather-restricted	1 month
3 days to 1 week	1 year, seasonal	3 months
1 week to 1 month	10 year, seasonal	1 year
1 month to 1 year	100 year, seasonal	10 years
More than 1 year	100 year, all year	100 years

of H_s with a one-year return period are given in Tables 4.4 and 4.5.

2.6.5 Wave period conditional upon H_s

For a weather-unrestricted operation, the wave period is based on statistical data. Since a weather-unrestricted operation cannot be aborted, the full range of periods must be included in the design; see also Sec. 2.5.4. The T_z-range from Eq. (2.12) can be used, or the periods can be taken from

a scatter diagram for the actual location. A statistical distribution for the mean zero-crossing period conditional on the significant wave height is given in Eq. (4.13), and the parameters for the distribution can be found in Table 4.6 for Location 2 in Fig. 2.6. This conditional distribution is applied in the structural reliability analyses.

2.6.6 Wind speed conditional upon H_s

The wind-induced loads act in addition to the wave-induced loads. Even if the wave-induced loads are dominant for large and heavy objects, the wind speed corresponding to the design significant wave height for sea transport may still be needed. The relation between the wave height and the wind speed at a certain location may depend on the wind and wave directions, storm duration, fetch, water depth, etc. A simple method is proposed to estimate the wind speed from a given significant wave height. A formula for calculating the one-minute wind speed 10 m above sea level as a function of a specified significant wave height is presented as follows [108]:

$$V_{one\,minute} \approx 10\sqrt{H_s} \tag{2.17}$$

where H_s is given in m and the unit for the wind speed is m/s. The significant wave height representing the total sea (i.e., both wind-generated waves and swell) is used in the comparison. The one-minute design wind speed is thus approximated as a function of the significant wave height only. The one-minute averaged wind speed is used when the wave load dominates [31]. Similarly, the one-hour wind speed can be approximated as:

$$V_{one\,hour} \approx 8\sqrt{H_s} \tag{2.18}$$

This wind speed is plotted in Fig. 2.7. It is noted that there is a large spread in the wind speed for a given H_s. The significant wave heights in Eq. (2.17) and (2.18) represent the fully developed wind-generated waves. The significant wave height assumed in long-term wave distributions describes the total sea, i.e., it also includes swell. This means that when the wind speed is calculated from Eq. (2.17) and the design significant wave height includes swell, the wind speed will be overestimated. This is also illustrated in Fig. 2.8, where contour lines for the significant wave height and wind speed are shown for several return periods. The simplified wind speed estimate is higher than the wind speed that corresponds to the largest significant wave height for a given return period. For a typical sea transport, where the wave load dominates over the wind load, the wind load could be included to simulate the reaction forces in the grillage and seafastening.

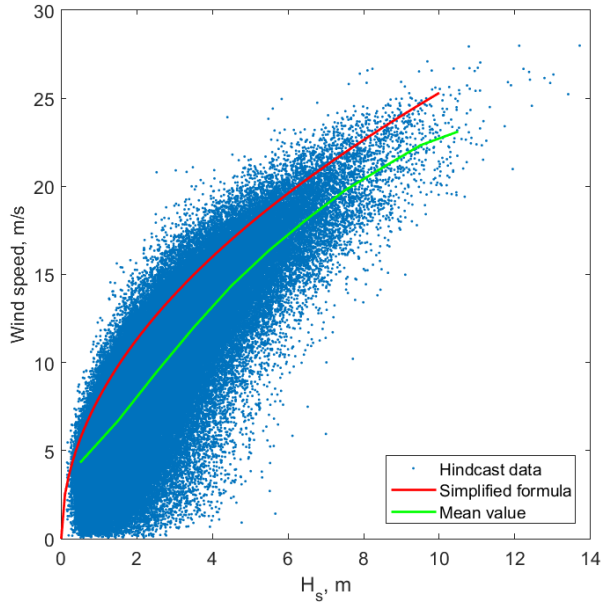

Figure 2.7: Significant wave height of the total sea and one-hour wind speed at Location 2 in Fig. 2.6, the mean value (green line) and the wind speed from Eq. (2.18) *(red line)*

The wind-induced load may then be calculated from the wind speed given in Eq. (2.17). In sheltered water, there will typically be small waves, and the wind load will dominate. Then, the wind load should be calculated for a given probability of occurrence during the operation, or the design wind load should be based on a wind speed with a given return period.

While the above process refers to the design phase, a different approach would have been used in the reliability analyses, where the mean value and standard deviation of the wind speed conditional upon H_s could have been estimated based on the data plotted in Fig. 2.7. In the reliability analyses performed in this thesis, wind-induced loads are very small compared with wave-induced loads (see also Sec. 3.3.7), and wind-induced loads are not included in the analyses.

2.6.7 Seasonal environmental conditions

The majority of marine operations are performed during the summer, and the use of seasonal data may therefore be favorable. Data are often divided into four seasons or monthly data. Seasonal data are analyzed in the same

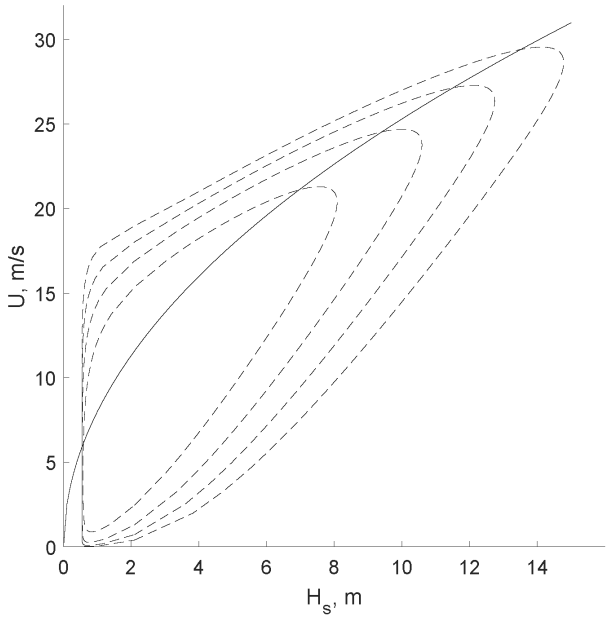

Figure 2.8: Contour lines for the significant wave height and mean wind speed (one hour average) for (starting from the inner contour) one month and one year, ten year and hundred year return periods, compared with the wind speed from Eq. (2.18) *(solid line)*

way as year-round data, but the statistical parameters will be different.

The statistical data of H_s for four seasons are given in Table 4.5. The long-term distribution data for each month are given in Table 4.4.

2.7 Weather routing

Weather routing systems are commonly used for sea transport. Weather routing in this context includes altering the course of the ship and varying the speed to avoid areas with adverse weather conditions. The effectiveness of weather routing depends on the quality of the weather forecasts and the software system evaluating the data and the decisions made by the ship's master.

While merchant ships normally maintain a high speed, the speed is typically approximately 5 knots for a towed barge. Adverse weather for a barge tow can be avoided by reducing the speed or halting and waiting for improved weather. There is hence a risk that the tow will be struck by adverse

weather while waiting, and the exact speed and direction of the weather system may not be accurately forecasted. Furthermore, in the case of towline failure, the barge will drift until the towline is reconnected. It may take quite some time before the weather calms down enough to reconnect the towline, and weather routing is therefore not an option.

The minimum required towing speed to be able to perform effective weather routing has not been studied herein. It is instead concluded that the positive effect of weather routing cannot be utilized with respect to the structural capacity in the ultimate limit state, e.g., for the capacity of the grillage and seafastening. Weather routing can, however, be favorable with respect to fatigue damage and fuel consumption.

2.8 Heading control

For sea transport on self-propelled vessels, it may under certain conditions be assumed that the vessel can head up against the wind/waves in adverse weather to limit the rolling. Several requirements, e.g., adequate redundancy in the propulsion system, need to be fulfilled to utilize heading control. Heading control allows for a substantial reduction in the design wave height, such as a 40% reduction in the design significant wave height for beam seas [31] (hence, the significant wave height for beam seas is 60% of the design significant wave height for head seas). Heading control can also be an option for manned barges towed by multiple tugs, where after breakdown of any one tug or failure of any one tow line, the remaining tug(s) have sufficient bollard pull capacity.

For barges towed by a single tug, a tow line failure or tug breakdown will leave the barge drifting until the tow line is reconnected. The probability for this to happen is too high to utilize heading control [31] because a drifting barge may be exposed to beam seas. The probability of these events occurring has not been quantified in this thesis. However, the dynamic loading in the tow line is high [44, 112] and may lead to failure of the tow line, as well as failure of the tow line connection [76]. Regarding tug breakdown, ocean going tugs normally have several engines and propellers; hence, the probability of a total blackout is low. However, a fire in the engine room, for example, could result in a complete blackout even if the machinery itself is redundant. Therefore, the probability of tug breakdown should not be neglected.

Furthermore, depending on the layout of the cargo, the wind area, etc., it might not be possible to keep the barge heading toward the waves in adverse weather even with intact tug and tow line, and there could be a

relatively large yaw angle of the barge.

In the structural reliability analyses, the barge is hence assumed to be exposed to beam seas.

Chapter 3

Wave-induced load effect analysis

3.1 General

For sea transport, wave-induced loads are normally predominant for grillage and seafastening. Generally, wind-induced loads should also be checked, but for heavy cargo transported on barges, the wave-induced loads dominate. For stability, however, wind loading is a main concern but is not discussed herein.

The grillage and seafastening structures are designed to sustain environmental loads dependent on the area, the season of the year, the duration of the transport, etc. In the ultimate limit state, structural failure occurs when the load effect exceeds the structural capacity. Therefore, prediction of the extreme wave-induced load effects during sea transport is vital, and the uncertainties in the characteristic wave-induced load effects must be accounted for in the planning of marine transport.

The wave-induced motions of the transport vessel can be obtained from formulas given in classification rules or design standards. These design criteria are experience-based formulas for calculating the motions based on a limited amount of input, e.g., ship length, breadth, draught, block coefficient, etc. The design forces can be obtained from these design criteria. Alternatively, the wave-induced motions of the transport vessel can be obtained by direct calculations based on hydrodynamic software using 2D strip theory or 3D potential theory, and the extreme vessel motion or loading is then calculated based on the long-term distribution of wave heights by means of scatter diagrams or a given design condition.

For the vessel itself, wave load analysis is performed to calculate the load

effects for the structural design of the vessel. These analyses are performed in relation to new buildings and are normally not required for marine operations as long as the vessel is used in compliance with the standard loading conditions approved by the classification society. However, for heavy cargo, a global capacity check of the transport vessel can be relevant. The transported object must also be documented to be strong enough to resist the loads caused by the vessel motion, as well as the local capacity of the transport vessel adjacent to the supports. Hence, the motion analysis will form the basis for design of the support structures, in addition to capacity checks of the transported object and the vessel itself.

3.2 Wave description

3.2.1 Choice of the wave energy spectrum

A regular wave is described by the wave height (or amplitude) and wave period. A sea state is made up of several individual waves and is described by the significant wave height, H_s, and the zero-crossing period, T_z, or the spectral peak period, T_p. A wave condition might consist of several wave systems, i.e., locally generated wind-driven waves in combination with swell generated in remote areas. The total sea is considered in this thesis; see also Sections 2.3 and 2.5.2.

The wave energy is distributed on frequencies (or periods) and directions, as described by a two-dimensional (2D) wave energy spectrum, as illustrated in Fig. 3.1. A simpler representation is normally used, where the wave energy distribution on the frequency is described by a one-dimensional wave energy spectrum with a main wave propagation direction, possibly combined with a wave spreading function to represent short-crested waves [29]. A one-dimensional spectrum is used in this thesis. Long-crested waves are assumed; hence, no wave spreading function is applied. Because the case analyzed here is a beam sea condition and the roll response dominates, use of long-crested waves will overestimate the response if the waves are in fact short-crested (that would be different if head seas were analyzed, because long-crested waves would then give no roll response, and short-crested waves would govern).

A two-peak spectrum could be applied to model the wave energy separated on wind-dominated and swell-dominated sea states. Several two-peak spectra have been proposed, such as a combination of a Jonswap and a Pierson-Moskowitz spectrum to describe the two wave systems [117] or a combination of two Jonswap spectra [56]. For Norwegian waters, a

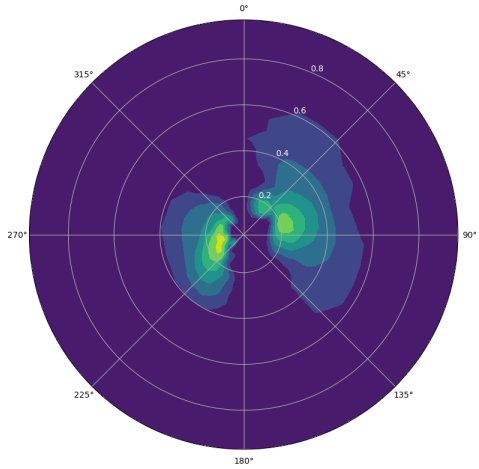

Figure 3.1: Example of a 2D wave spectrum, with directions in degrees and frequencies in Hz [115]

Torsethaugen spectrum [141] is typically used. However, one-peak spectra such as Jonswap and Pierson-Moskowitz can give a reasonably accurate representation of the wave conditions, in particular for severe sea states [10], and in this thesis, a one-peak spectrum is used, as described in Sec. 3.2.3.

3.2.2 Wave direction

The mean wave direction is important for floating vessels when there are restrictions on the vessel heading, e.g., during installations of offshore platforms or subsea equipment. For sea transport in moderate waves, the vessel will head toward the destination and can be exposed to head seas, sideways waves or following waves. For higher sea states, i.e., when the significant wave height exceeds the limit given in the Operation Manual, the master will head the tow or ship up against the waves to minimize the rolling. It is the relative wave direction, which is of interest, and not the absolute direction. It is noted, however, that if the sea state contains wind waves and one or two swell systems, it could be impossible to maintain a heading up against the waves, and there will always be incoming side waves.

3.2.3 Irregular waves

A sea state can be described by a wave energy spectrum. The Jonswap spectrum is given as follows [29]:

$$S(\omega) = \frac{5}{16} A_\gamma H_s^2 \omega_p^4 \omega^{-5} \exp\left[-\frac{5}{4}\left(\frac{\omega}{\omega_p}\right)^{-4} + \ln(\gamma)\exp\left(-\frac{1}{2}\left(\frac{\omega-\omega_p}{\sigma\omega_p}\right)^2\right)\right] \tag{3.1}$$

where

- the significant wave height, H_s, and the peak period, T_p are input values defining the sea state
- $\omega_p = 2\pi/T_p$ is the spectral peak frequency
- $A_\gamma = 1 - 0.287\ln(\gamma)$ is a normalizing factor
- σ is the spectral width parameter, taken as:

$$\sigma = \begin{cases} 0.07, & \text{if } \omega \leq \omega_p \\ 0.09, & \text{if } \omega > \omega_p \end{cases} \tag{3.2}$$

- γ is the peak shape parameter, taken as:

$$\gamma = \begin{cases} 5 & \text{for } \frac{T_p}{\sqrt{H_s}} \leq 3.6 \\ \exp\left(5.75 - 1.15\frac{T_p}{\sqrt{H_s}}\right) & \text{for } 3.6 < \frac{T_p}{\sqrt{H_s}} < 5 \\ 1 & \text{for } \frac{T_p}{\sqrt{H_s}} \geq 5 \end{cases} \tag{3.3}$$

For a given wave spectrum, the nth order moment is calculated as $M_n = \int_0^\infty \omega^n S(\omega)\mathrm{d}\omega$.

The significant wave height and zero-crossing wave period, T_z, can be estimated as follows:

$$H_s = 4M_0 \tag{3.4}$$

$$T_z = 2\pi\sqrt{\frac{M_0}{M_2}} \tag{3.5}$$

The relation between the zero-crossing period and the peak period can be estimated as follows [29]:

$$\frac{T_z}{T_p} = 0.6673 + 0.05037\gamma - 0.006230\gamma^2 + 0.0003341\gamma^3 \tag{3.6}$$

It could be noted that this relationship was previously expressed in a simpler and slightly better looking form as follows [23]:

$$\frac{T_z}{T_p} = \sqrt{\frac{5+\gamma}{11+\gamma}} \tag{3.7}$$

The results from the two expressions are, however, practically the same (maximum 2 % deviation for γ between 1 and 5).

While the Jonswap spectrum is representative of developing seas, the Pierson-Moskowitz spectrum represents a fully developed sea and unlimited fetch. The Pierson-Moskowitz spectrum is a special case of the Jonswap spectrum with $\gamma = 1$ and is expressed as follows [29]:

$$S(\omega) = \frac{5}{16} H_s^2 \omega_p^4 \omega^{-5} \exp\left[-\frac{5}{4}\left(\frac{\omega}{\omega_p}\right)^{-4}\right] \tag{3.8}$$

For this spectrum, the peak period can be calculated from the mean zero-crossing period as $T_p \approx 1.4 T_z$. The Pierson-Moskowitz spectrum was applied in the model tests [109].

3.3 Numerical analyses

3.3.1 Available methods

Several methods are available for motion analyses. The design formulas as given in rules and standards and direct analyses based on potential theory are possible tools. In practical engineering, linear analyses based on potential theory dominate because they are relatively simple to perform, and the results are easily extracted.

For barge transports, forward speed is generally not included in the motion analyses since towing speeds are low. In severe seas, the speed will be close to zero. In small waves, however, there will be a forward speed, but this condition is not governing for the structural design in the ultimate limit state.

The design of transports could also be based on more advanced calculations, including nonlinear effects, e.g., CFD methods based on Reynolds-averaged Navier-Stokes (RANS). In practice, there is often a lack of personnel, financial resources or time to perform such advanced analyses. For practical purposes and preliminary design, there is therefore a need for simplified calculations for vessel motion, as given in ship rules and design

standards. A simplified analysis method often used in planning marine operations is included in Appendix C.1; see also Sec. 3.3.2. The linear analysis approach is discussed in Appendix C.2; see also Sec. 3.3.3. Some comments on the nonlinear method are given in Appendix C.3 and Sec. 3.3.4.

3.3.2 Simplified motion analysis

Vessel motions can be calculated by simplified methods provided by ship rules and design standards. Simplified motion criteria for ships are given by IMO [69] and ISO [72]. Classification societies, e.g., ABS [3], Bureau Veritas [16], DNV GL [25] and Lloyd's Register [85], have class rules where the ship acceleration can be calculated. Motion criteria for transport barges are given by ISO [72], DNV GL [31] and LOC [86]. Based on such criteria, the structural design can be performed. Simplified motion criteria for a transport barge are included in Appendix C.1.

3.3.3 Linear motion analysis in the frequency domain

The wave loads, added mass, linear damping and restoring force may be directly calculated based on potential theory. Wamit [145] and Wadam [129] use the boundary element method to calculate the response amplitude operators, RAOs, i.e., the transfer functions for the six degrees of freedom. Linear analyses are performed in the frequency domain, and the statistical treatment of the results is then simple and robust. Irregular seas are represented by energy density spectra, and the vessel response and load effects are calculated by stochastic analysis. Since the analyses are linear, nonlinear effects such as viscous damping need to be linearized. Assuming narrow banded wave spectra, the individual maxima follow a Rayleigh distribution. The most likely maximum, the expected maximum or the 90th percentile can then easily be calculated, such as that for a three-hour storm.

3.3.4 Nonlinear analysis in the time domain

Nonlinear effects that affect the response include viscous roll damping and water up to the instantaneous free surface elevation. The analysis has to be performed in the time domain and is much more time consuming than linear analysis in the frequency domain.

A "semi" nonlinear method, where the wave loads, added mass and linear damping are calculated based on potential theory, can be used. The dynamic equations of motion are solved in the time domain where the quadratic damping due to vortex shedding is given as input. This approach is used

in Paper 1 and compared with experimental results. The purpose of this analysis was to study the benefits of including nonlinear effects. The wave loads, added mass, potential damping and restoring coefficients for the vessel were calculated by Wadam [129], and the equations of motion were solved in the time domain by Simo [131].

Wadam applied global (earth fixed) coordinates, and Simo used local (ship fixed) coordinates. The body fixed coordinate system in the time domain analysis introduces additional terms in the equations of motions. For small waves and small ship motions, these terms are negligible, but in severe seas, they will affect the solution. This is discussed in Paper 1. To illustrate the effect, the equations of motion are studied in more detail for the special case of barge rolling in Appendix C.3.

3.3.5 Estimate of nonlinear roll damping

The rolling of a floating vessel is sensitive to the damping initiated from vortex shedding at the corner/bilges. Ships are often equipped with bilge keels to improve the roll motion characteristics. Barges, such as the Standard North Sea barges, do not have bilge keels but rounded corners (bilges). Barges can also have sharp corners. Roll damping for a barge with a sharp corner and a bilge radius was studied in Paper 1. Model test results were compared with the results from Tanaka [140] and Ikeda [67], and nonlinear roll damping was estimated and given as input for the motion analyses. The damping had to be linearized to solve the equations of motion in the frequency domain. For irregular sea states, the equivalent stochastic linearization is based on minimizing the expected value of the square of the difference between the nonlinear damping force and the equivalent damping force [120]. The equivalent damping is then given as follows:

$$B_{eq} = B_1 + 2\sqrt{\frac{2}{\pi}}\,\sigma_{\dot{\theta}} B_2 \tag{3.9}$$

where

- B_1 is the linear damping coefficient
- B_2 is the quadratic damping coefficient
- $\sigma_{\dot{\theta}}$ is the standard deviation of the roll velocity

Hence, iterations are required to converge for equivalent stochastic linear damping. (The procedure is as follows: assume (estimate) $\sigma_{\dot{\theta}}^{\{0\}}$, calculate $B_{eq}^{\{0\}}$ from Eq. (3.9), calculate $\sigma_{\dot{\theta}}^{\{1\}}$ from the equations of motion, calculate $B_{eq}^{\{1\}}$ and so on, until convergence.)

3.3.6 The effect of sloshing in tanks

Ballast tanks should be empty or full. However, it could be necessary to have one tank partially filled in order to achieve zero list and the predetermined trim. Sloshing may occur in the partially filled tank, but the effect of sloshing is normally negligible for barge motions [78, Sec. 4.3.4].

3.3.7 The effect of heel from the wind load

The wind load on the transported object will be transferred into the transport vessel through grillage and seafastening. The wind load on the transported object and the vessel itself will introduce a heel that also introduces forces in the seafastening system. For typical barge transport, the initial metacentric height is large, and the initial heel from the wind load is negligible.

The seafastening forces from wind loads are small compared to the forces from the motion of the vessel due to waves in our case. In the transport case considered in Paper 1 [109], the mass of the transported object is 3500 tons, and the wind area is 600 m^2. Based on the criteria shown in Table C.1, the acceleration 15 m above the water line is 0.75 g, and the wind pressure is 1.0 kN/m^2. The inertia force from the rolling of the barge is then 25 MN, while the wind load is 0.6 MN, i.e., the wind load is only 2 % of the load from wave-induced motion. Hence, the wind load is negligible in this case. The wind load must, however, be included when the stability is documented.

3.3.8 Calculation of the loads in the cargo supports

The wave-induced load effects in the structural members of the grillage and seafastening are calculated based on the accelerations and roll/pitch angles derived from the motion analysis of the transport vessel. The calculation can include the effect of elasticity in the transport vessel and the transported object or be based on the assumption of rigid bodies, i.e., calculate the reaction forces based on the dynamic equilibrium of the transported object. Which calculation method to use depends on the layout of the cargo and the transport vessel. If the transported object is supported on more than three supports, the elasticity can be important for the results. If, however, the transported object has vertical supports at the corners, and the transverse and longitudinal directions (i.e., the roll and pitch stoppers) form a statically determinate system, a simplified analysis technique may suffice. For quartering waves, deformation of the transport vessel and the transported object could be important.

In this study, beam sea conditions are considered, and a simple equilibrium analysis is performed. The load effects in the seafastening are then calculated based on dynamic equilibrium [109].

3.4 Model tests

3.4.1 General

The following section gives a brief description of the experiments performed as part of this study. More information on the model tests is given in Appendix D and in Paper 1 [109]. A Standard North Sea barge at a scale of 1:50 was tested at the Marine Cybernetics Laboratory and in the Towing Tank at the Marine Technology Centre at NTNU in Trondheim. The model tests aimed to represent a real sea transport condition, such as the transport shown in Fig. 3.2.

The purpose of the model tests was to study barge motion in severe seas. The most critical wave direction for barge transports is beam seas because roll motion typically governs for forces in the grillage and seafastening system. The rolling of barges is a phenomenon with nonlinear effects due to viscous damping, water on deck, etc., which introduces challenges related to motion analyses. With a draught of 3 m, the deck will be immersed in water, and the barge bottom exits the water for a static roll angle of approximately 12 degrees in still water. This effect is not captured by linear analyses, but it is included in the model tests.

A simple deck layout (a clean deck) was chosen to avoid interference with water on the deck. The cargo is placed 40 mm above the barge deck corresponding to a full-scale module support height equal to 2 m. Any water on deck can then evacuate.

The following tests were performed:

- Forced roll tests by use of hydraulic actuators
- Free decay tests
- Model tests in regular waves
- Model tests in irregular waves

The setup for the model tests is described in Appendix D.

Figure 3.2: A Standard North Sea barge loaded with the Living Quarter to the Kristin platform, towed from Gothenburg, Sweden, to Stord, Norway in 2005. The barge is seen from the tug Bamse*. The picture is taken during tow out of the harbor; during offshore tow, the tow line is much longer. Photo: Asle Natskår.*

3.4.2 Scale effects

The barge model was made on a scale of 1:50. Froude scaling [137] was used, which implies that the gravitational forces (wave load and wave radiation damping) and inertia forces (barge accelerations and added mass) were correctly scaled from the model scale to the full scale. For the viscous damping caused by vortex shedding, the situation is different. The magnitude of the damping depends on the type of flow, analogous to the drag load on a cylinder. The load occurs when there is separation of the flow at the submerged corner of the barge. For a sharp corner, there is always flow separation. For the case with a rounded corner, flow separation with vortex shedding occurs when the Keulegan-Carpenter number, $\mathrm{KC} = UT/D_b$, is larger than approximately 2 [38], where U is the flow amplitude, T is the

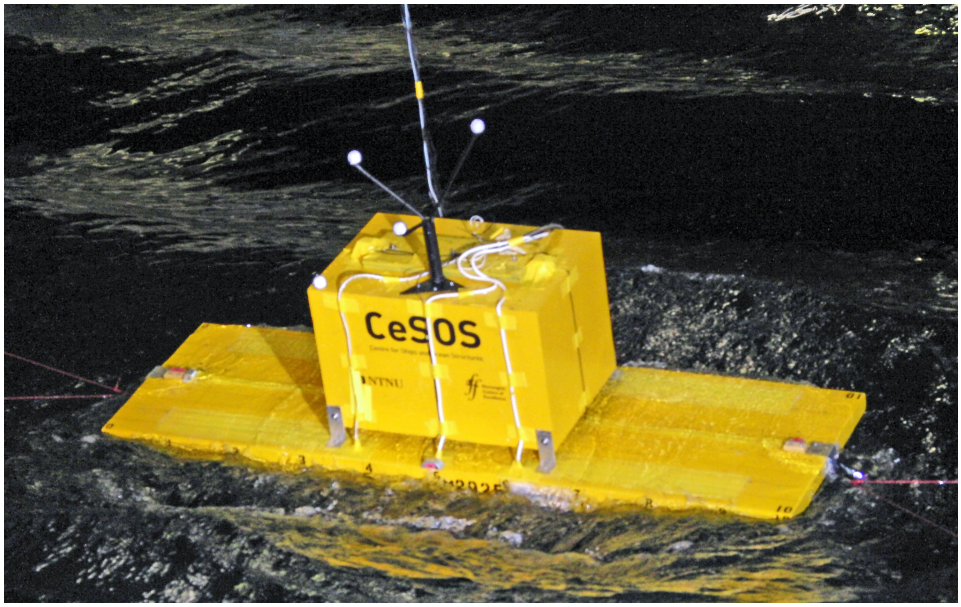

Figure 3.3: The barge model with the transported object and a scale of 1:50. Photo: Asle Natskår.

flow period and D_b is the characteristic length of the body, taken as the bilge diameter. Assuming a roll amplitude of 10° with a full-scale period of $T = 8$ s ($U \approx \omega\theta_0 B/2$ and $D_b = 2r_b$), then KC = 15 in both the model scale and full scale. There will then be separation with vortex shedding at both the model scale and full scale for the barge with a rounded corner. The Reynolds number (Rn $= UD_b/\nu$ [38] where ν is the kinematic viscosity taken equal to 10^{-6} m^2/s) is, however, scale dependent. Rn is equal to $6 \cdot 10^3$ and $2 \cdot 10^6$ in the model scale and full scale, respectively. At the model scale, the flow is in the subcritical regime, and the boundary layer at the bilge is laminar. In full scale, the flow is in the transcritical regime, and the boundary layer upstream from the separation point is turbulent [38]. For the case with a sharp corner, there should not be any significant scale effects, since there will be vortices starting from the corner of the barge cross section in both scales. Since there will also be vortices shed for the barge with rounded corner, and the bilge radius is relatively small, it was concluded that the pressure distribution will be quite similar in both the model scale and full scale, and hence no scale effect was accounted for.

Another effect could also justify neglecting the scale effects, as shown in Fig. 3.4. The effect of the flow regime on the drag coefficient is large

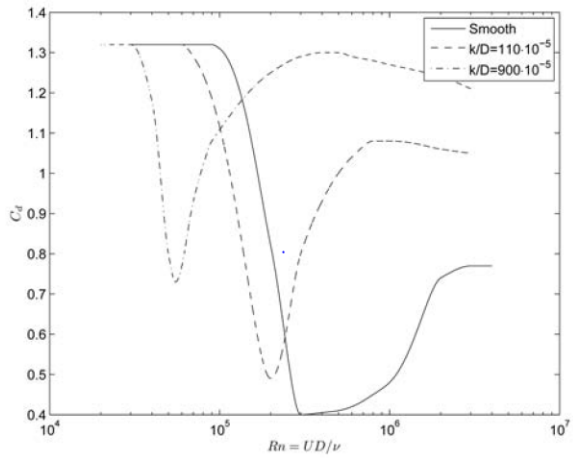

Figure 3.4: Drag coefficient as a function of the Reynolds number for a cylinder with smooth and rough surfaces [4, Fig. 7]. k/D is the roughness, where k is the equivalent sand-grain diameter and D is the diameter of the cylinder.

for a smooth surface and less accentuated for a rough surface. The barge model has a smooth surface (and the roughness is not as important in the subcritical regime ($\mathrm{Rn} < 10^5$)). A full-scale barge is likely to have a rough surface due to paintwork, marine fouling and welding seams [111]. Considering rolling, this will have a positive effect, since it may result in a larger drag coefficient than for a smooth surface in the transcritical regime ($\mathrm{Rn} > 10^6$). (With regard to towing, the effect is negative as it leads to increased towing resistance, however that is not a concern herein.)

From these two effects, the drag coefficient could be slightly lower in full scale (transcritical regime), which in principle could be modeled by introducing a bias. However, this effect is assumed to be negligible, and bias in the uncertainty is set equal to 1.0.

3.4.3 Main results

3.4.3.1 Roll damping

The viscous roll damping was measured for a barge in still water. In waves, the relative velocities between the barge and water particles will be affected by the incoming waves. Standing [136] investigated this effect by calculating the roll response for a barge with and without the effect of the water particle

motions from incoming waves. He analyzed a barge with sharp corners in regular waves with a height of 3 m and in irregular waves with a 9 m significant wave height. He found that the water particle motion had little effect on the barge roll motions because the bilge velocity from barge rolling was larger than the water particle velocity (at least for moderate wave heights) and that the water particle velocity was not in phase with the bilge velocity. Based on this, the measured viscous damping was used directly, and no scaling was performed to account for relative particle motion.

The forced roll and free decay tests gave an estimate of the viscous roll damping. The force at the bilges due to vortex shedding is expressed as a drag force as follows:

$$F_{drag} = \frac{1}{2}\rho C_d A_{wet} r_{cog}^2 |\dot{\theta}|\dot{\theta} \tag{3.10}$$

where

- C_d is the drag coefficient
- A_{wet} is the wet area of the barge (the submerged area)
- r_{cog} is the distance from the center of gravity (the CoG of the cargo and the transport vessel) to the bilges
- $\dot{\theta}$ is the roll velocity of the barge
- $\rho = 1025$ kg/m^3 for sea water

The drag coefficient as a function of B/KG is shown in Fig 3.5 based on Tanaka and the model tests of the barge with a sharp corner. B is the width of the barge, and KG is the vertical distance from the keel to the CoG of the barge and the cargo combined. $B/KG = 2.4$ for the model as tested in irregular waves. This is a case with relatively high CoG due to the large and heavy cargo. For the forced roll case, the barge is rolled about the water line, and $B/KG = 9.1$. This is equivalent to the CoG in the water line, therefore assuming small and light cargo with a low CoG.

The quadratic damping term is estimated by fitting a line through the measured points. First, the equivalent linear damping in regular waves is determined by demanding that the same amount of energy should be dissipated from the linear system as from the nonlinear system. The equivalent linear roll damping is then found by combining the linear roll damping (B_1) and the quadratic roll damping (B_2) as follows:

$$B_{roll,\,linear\,equivalent} = B_1 + \frac{8}{3\pi} B_2 \omega \theta_0 \tag{3.11}$$

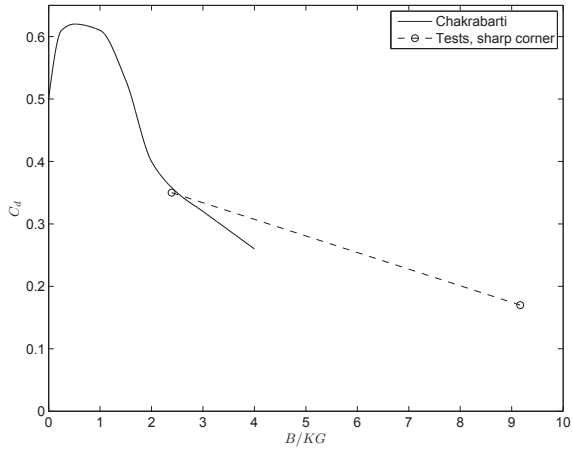

Figure 3.5: The drag coefficient in Eq. (3.10) *as a function of the B/KG ratio [109]. B is the width of the barge, and KG is the vertical distance from the keel to the CoG (for the barge and cargo combined).*

where θ_0 is the roll amplitude and ω is the natural roll period. This means that if the equivalent damping is plotted as a function of $8/(3\pi) \cdot \omega\theta_0$ and a straight line is fitted through the results, then $B_{roll,\,linear}$ and $B_{roll,\,quadratic}$ can be read directly from the plot [38].

There is a certain spread of the measured damping values. The 95% confidence interval of the quadratic damping for the barge with rounded corners in Fig. 3.6 is $B_2 = (7.3 \pm 1.0) Nms^2$ [109], i.e., approximately $\pm 15\%$.

3.4.3.2 Barge motions and support reaction forces

The results from the model tests were compared with results from the numerical motion analyses. The numerical analysis overestimated both the rolling of the barge and the forces in the support points. The expected maximum roll angle based on the model tests was 22 degrees for a significant wave height of $H_s = 9.9$ m and a mean zero-crossing period of $T_z = 9.4$ s. The nonlinear analysis was reasonably good compared with this, while the linear analysis gave an expected maximum roll angle equal to 29 degrees.

To see the sensitivity in the motion analyses with respect to roll damping, the analyses were rerun with the viscous roll damping increased and decreased by 15%, i.e., within the confidence interval of the viscous damping. The results (S_{lin} and $S_{non-lin}$ in Table 3.3) decreased by approximately

Table 3.1: Sea states in the model tests [109]

	Full-scale			Model-scale		
Case	Hs	Tp	Tz	Hs	Tp	Tz
1	5.2	9	7.5	0.1	1.3	1.1
2	5.2	9	7.5	0.1	1.3	1.1
3	6.5	8.8	7.9	0.13	1.3	1.1
4	7.8	9.5	8.3	0.26	1.3	1.2
5	7.2	10.1	8.6	0.14	1.4	1.2
6	9.1	11.6	9.4	0.18	1.6	1.3
7	9.9	12.3	9.4	0.2	1.7	1.3
8	10.6	17	11.6	0.21	2.4	1.6

Table 3.2: Standard deviation and expected maximum values of barge roll angles θ, unit: Degrees [109]

	Standard deviation			Maximum values		
Case	θ_{lin}	$\theta_{non-lin}$	θ_{test}	θ_{lin}	$\theta_{non-lin}$	θ_{test}
1	5.6	5.2	5.7	22	20	17
2	5.6	5.2	5.9	22	20	17
3	6.4	5.6	6.6	25	20	19
4	7.4	6.0	7.4	29	22	20
5	6.8	5.7	6.8	27	22	19
6	7.2	5.6	7.2	28	20	21
7	7.5	5.9	7.6	29	20	22
8	6.2	5.6	6.3	24	21	21

Table 3.3: Standard deviation and expected maximum values of the vertical support forces per side (i.e., per two supports) scaled by the weight of the cargo, $S = \frac{F_{vert}}{mg}$ [109]

	Standard deviation			Maximum values		
Case	S_{lin}	$S_{non-lin}$	S_{test}	S_{lin}	$S_{non-lin}$	S_{test}
1	0.124	0.081	0.085	0.491	0.416	0.308
2	0.124	0.081	0.088	0.491	0.416	0.305
3	0.139	0.088	0.097	0.549	0.435	0.329
4	0.152	0.094	0.102	0.601	0.467	0.349
5	0.136	0.085	0.093	0.536	0.448	0.359
6	0.139	0.089	0.097	0.547	0.422	0.365
7	0.142	0.092	0.098	0.559	0.457	0.360
8	0.114	0.081	0.079	0.45	0.403	0.328

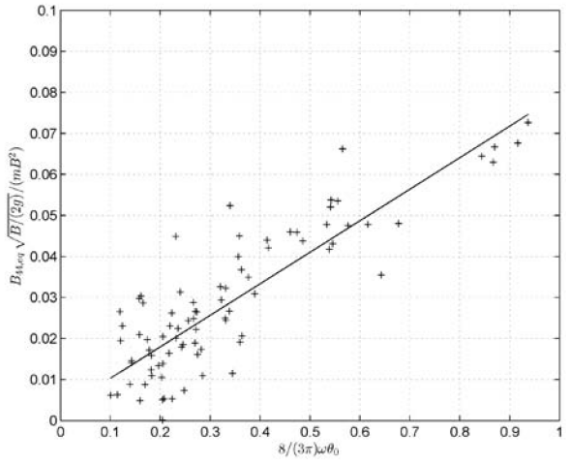

Figure 3.6: Roll damping from the free decay tests and a straight line fitted by linear regression for the barge with rounded corners [109]. The damping is presented in nondimensional form as $b_{lin\,eq} = B_{44,eq}\sqrt{B/(2g)}/(mB^2)$.

5-7%.

The vertical support forces, F_{vert} per side of the cargo (i.e. the sum of the two supports) are shown in Table 3.3. The forces are made nondimensional by dividing them by the weight of the cargo, mg. The bias is estimated by comparing the standard deviations and the maximum values of the responses. The bias is estimated as 0.75-0.94 (bias <1, i.e., conservative analysis results) for the maximum roll angle and 0.65-0.8 for the vertical support force, depending on the type of analysis [109]. The analyzed sea states represented severe seas and had a high steepness for some of the sea states (see Table 3.1). Furthermore, there were nonlinear effects that limited the barge response in the model tests (water on deck, etc.). In the structural reliability analyses, a bias representative for all the sea states included in the long-term distribution should be applied, and hence, a more moderate bias is chosen. The uncertainty is assumed to be a normally distributed stochastic variable with a bias of 0.9 and a COV of 0.1.

Chapter 4

Structural reliability analysis

4.1 Introduction

In a narrow sense, structural reliability is the probability that a structure will not exceed any of a specified set of limit states during a specified reference period. This means that the structure is in a safe set and will survive. The complementary quantity to being safe is the failure probability, P_f, defined in a simple case with a single resistance and load effect variable, by $P_f = P[R \leq S]$, where R is the resistance and S represents the load effect. Depending on how R and especially S are related to time, the failure probability will also depend on some reference time period. For a normal operation, the reference period could be a year or the service lifetime. For marine operations, the reference period is typically equal to the duration of the operation.

Structural design standards based on limit state formulations are typically calibrated by using reliability methods [90]. Structural reliability analysis (SRA) can be used to calculate the probability of failure for structures that have been designed for relevant limit states. The failure probability is calculated based on random variables describing the load effects and the structural capacity. In this thesis, SRA is used to calculate the failure probability for temporary structures designed by a semiprobabilistic method.

The concept of structural reliability analysis is briefly described in Sec. 4.3.11. More details about SRA may be found in the literature, including the text books by Ditlevsen and Madsen [22], Madsen et al. [88] and Melchers and Beck [95].

4.2 Limit state design check

4.2.1 Calculation of the ultimate strength

The ultimate strength is calculated for all the structural components. In addition to the capacity of the grillage and seafastening, which are normally specifically built for each individual transport, the capacity of the transported object as well as the local ship structure adjacent to the grillage and seafastening is checked. These existing structures are already given once the transport ship is nominated, and local reinforcements for one single transport should be avoided. Hence, the capacity of the existing structure should be checked in parallel with the design of the grillage and seafastening.

The design standards for marine operations [31, 72] describe the principles for the operations and provide guidance and requirements for planning them. They do not cover the design of structures beyond giving the principles but refer to recognized codes and standards as the basis for the detailed design and the fabrication requirements of structural components. Many design codes are thus available for calculating the ultimate structural capacity. In Norwegian waters, Eurocode and Norsok standards are typically used, e.g., [36, 113]. In other areas, ISO and API standards are widely used, e.g., [8, 73].

A case where the load effects are caused by the self-weight and wave-induced vessel motion is considered. A typical case is shown in Fig. 4.1. An example of a support structure, the grillage beams, is shown in Fig. 4.2. This is a typical structure for the distribution of support forces for a ship or a barge. Hand calculations of the moment and sectional forces would normally suffice for a design check in ULS. A finite element analysis may be required for more complicated structures and for details. The internal barge structure also needs to be documented. A typical barge bulkhead, i.e., a 10-20 mm thick plate with horizontal stiffeners and transverse web frames typically every 2.4 m, is shown in Fig. 4.2. More information about a typical North Sea barge is given in Appendix B.

In short, the structural strength must be verified for the following subsystems:

- Transported object
- Grillage and seafastening
- Transport vessel

The main discussion below is related to the vertical supports (the grillage beams). The local capacity of the transport vessel, notably the longitudinal

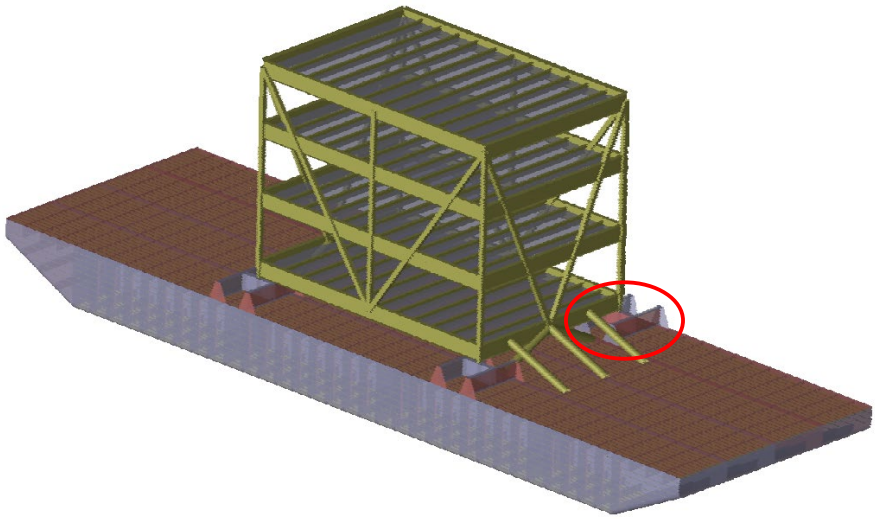

Figure 4.1: Typical flat-top barge with grillage beams and seafastening (roll and pitch stoppers) and the transported object (only the structural steel is shown, not the mechanical equipment and the outfitting)

bulkheads, is also discussed. The transported object is not discussed further.

4.2.2 Ultimate limit state design check

In the design checks, it is demonstrated that the structural capacity is larger than the load effects. The design capacity is equal to the characteristic capacity divided by a material factor. The characteristic loads are multiplied by load factors to achieve the design loads. The design check can then be expressed as:

$$\frac{R_c}{\gamma_m} \geq \gamma_G S_{G,c} + \gamma_E S_{E,c} \tag{4.1}$$

R_c represents the capacity, typically the characteristic yield or buckling stress multiplied by the cross sectional area or section modulus for a beam. The load factors for the ultimate limit state, ULS, are given in the design codes. $S_{G,c}$ is the characteristic static load effect, typically due to gravity. $S_{E,c}$ is the dynamic load effect, typically due to environmental loads, i.e., the wave induced load in this thesis. The capacity check in Eq. (4.1) can be written on an alternative form, assuming the capacity is fully utilized:

$$R_c = \gamma_m(\gamma_G S_{G,c} + \gamma_E S_{E,c}) \tag{4.2}$$

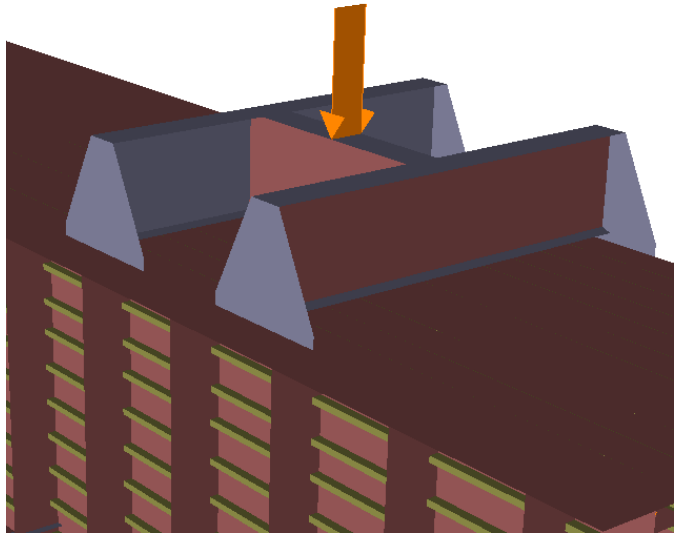

Figure 4.2: The grillage beams in one corner of the transported object (from Fig. 4.1), the vertical loading onto the grillage is indicated. The grillage beams are connected to the barge by wing plates welded to the deck. The longitudinal bulkhead with horizontal stiffeners is also seen.

In many design cases, R_c is somewhat larger than required (i.e., ">" in Eq. (4.2) instead of "="), but in this thesis, exact fulfillment is assumed. The load factors for the ultimate limit state capacity check are given in Table 4.1. The material factor depends on the type of material and the type of

Table 4.1: Load coefficients for the ultimate limit state [31] G=Permanent actions (e.g., due to self-weight) and E = Environmental actions (e.g., due to wave-induced loads).

Action combination	Load factors	
	γ_G	γ_E
ULS-A	1.3	0.7
ULS-B	1.0	1.3

capacity check. For steel structures, $\gamma_m = 1.15$ is typical for capacity checks based on the yield stress and 1.3 is typical for the weld capacity based on the ultimate stress [28, 113]. For welding on board a barge or transport ship, an increased material factor of 1.5 is imposed [31].

4.2.3 Wave-induced load effects in the design check and in SRA

Two different approaches are used to calculate the load effects for the design capacity check and the structural reliability analyses. The characteristic load effect, $S_{E,c}$, in Eqs. (4.1) and (4.2) are applied in the design checks. The load effects due to wave-induced barge motions could have been calculated from a hydrodynamic analysis using a 3D panel model. That is not done in this thesis. The characteristic load effects are instead calculated using a method given in a design standard for marine operations [31].

The wave-induced load effects in the structural reliability analyses, S_E in Eq. (4.6), are calculated based on a 3D panel model. The wave-induced load effects are described by a response surface [122] for the standard deviation of the response. The method is further discussed in Sec. 4.3.10, and the response surface is given in Eq. (4.15). The purpose in this section is to clearly indicate how the characteristic load effect, $S_{E,c}$, is determined and demonstrate that the random variable S_E used in SRA is calculated by a different approach.

The most probable maximum support load is shown in Fig. 4.3 as a function of the significant wave height. (The support load is calculated using a modified version of Eq. (4.7) by integrating over T_z only and solving for s_E from $s_E(h_s) = F_{S|H_s}(e^{-1})$ for given values of h_s.) The load is shown for exposure times of 3 and 24 hours. A typical storm duration is three hours; hence, for large sea states, the solid line in Fig. 4.3 is the most representative. For moderate sea states, the time period with a more or less constant sea state can be much longer, as indicated by the dotted line in Fig. 4.3 calculated for a 24-hour exposure time. The design forces from the design standard [31] are also shown and are in the same range as the forces from the stochastic analysis.

4.3 Structural reliability analysis method

4.3.1 Formulation of the failure probability

As mentioned, the probability of failure can be expressed as follows:

$$P_f = P[R \leq S] \tag{4.3}$$

where
R is the structural capacity, defined in Eq. (4.4) and
S is the load effect, defined in Eq. (4.6)

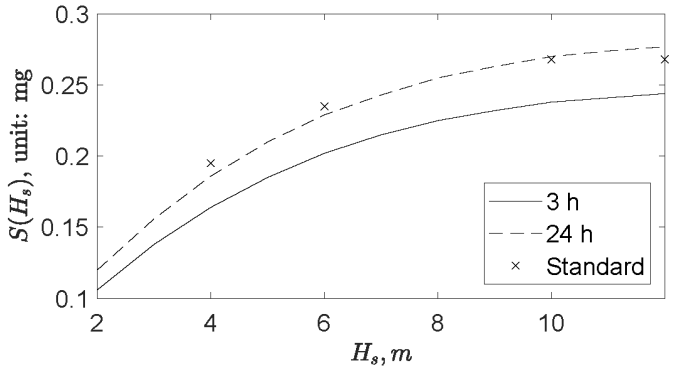

Figure 4.3: Most probable maximum vertical force, $S(H_s)$, at one support point as a function of the significant wave height based on Eq. (4.7) *for an exposure time equal to 3 and 24 hours. The design forces calculated according to a design standard [31] for $H_s = 4$ m and 6 m and a weather-unrestricted transport ($H_s \geq 10$ m) are also shown.*

4.3.2 Modelling the structural capacity

The structural capacity may be expressed as follows:

$$R = \chi_R R_c \tag{4.4}$$

where

- χ_R is a variable to account for uncertainty in the calculated capacity
- R_c is the characteristic capacity calculated from Eq. (4.2)

The statistical parameters for the yield stress of the steel for use in the SRA were estimated by the JCSS approach, where a probabilistic model for the random vector $\boldsymbol{X} = [f_y, f_u, E, \nu, \epsilon_u]^T$ is given [77, Table A]. The model can be used for steel grades with yield stress up to 380 MPa, which may be defined in terms of nominal values verified by standard mill tests (e.g., following the procedures of EN 10025 [35] for the sampling and selection of test pieces and the requirements of EN 10002-1 (superseded by [74]) for testing) or in terms of the minimum values given in the material specifications (e.g., [35]). The main concern here is the yield stress. The mean value of the true yield stress used in the SRA is calculated according to the following formula [77]:

$$E[f_y] = f_{ysp} a e^{-u \cdot COV} - C \tag{4.5}$$

where

- The COV for the yield stress is set equal to 0.07
- f_{ysp} is the code specified or nominal value for the yield stress used in the design check
- a is the spatial position factor. It is equal to 1.05 for webs of hot rolled sections and 1 otherwise; a=1 is used in this thesis
- u is a factor related to the fractile of the distribution used in describing the distance between the code specified or nominal value and the mean value; u is in the range of -1.5 to -2.0
- C is a constant for reducing the yield strength as obtained from usual mill tests to obtain the static yield strength; a value of 20 MPa is recommended [77]

Based on the above, the mean value and the standard deviation for the yield stress are $\mu = 1.12 f_{ysp} - 20$ and $\sigma = 0.07\mu$.

This model is combined with the random variable, which represents the uncertainty in the calculated capacity, that is assumed to follow a lognormal distribution. The capacity of the bulkheads in the barge has a mean value of 1.21 and a COV of 0.15, and the grillage beams have a mean value of 1.0 and a COV of 0.05. [107]. When the uncertainty in the yield stress is combined with the model uncertainty, the mean value is 1.25, and the COV is 0.17 for the vertical load acting at the bulkheads. For the grillage beams, the resulting mean value is 1.07, and the COV is 0.09.

4.3.3 Overview of the uncertainties in the load effects

The modeling of the uncertainty in the load effect will depend on the effects being studied. The aleatoric and epistemic uncertainties, including the model uncertainties, are discussed below. The static loads from gravity and dynamic loads from waves were included in this study. Generally, wind loading can also be important but is not included here because wave loading dominates the case studied in this thesis. For this purpose, the load effect in the reliability model can be formulated as follows:

$$S = \chi_{S,G} S_G + \chi_{S,E} S_E B_{oper} \tag{4.6}$$

where

- S_G is the static load effect

- S_E is a stochastic variable representing the wave-induced load effect, accounting for the uncertainty in the significant wave height and wave period; see Sec. 4.3.10 (note that S_E is different from the characteristic load effect in Eq. (4.1))
- $\chi_{S,G}$ represents the uncertainty in the calculated static load effect
- $\chi_{S,E}$ represents the uncertainty in the calculated dynamic load effect
- B_{oper} accounts for the uncertainty related to heavy weather avoidance

In the case studies, $\chi_{S,G}$ is modeled as a normal distributed variable with a mean value of 0.95. The COV is set equal to 0.1.

The uncertainty in the calculated dynamic wave-induced load effect, $\chi_{S,E}$, depends on:

- the wave data
- the calculated motions of the transport vessel, $\chi_{S,E,1}$
- the method for the calculation of the structural load effects due to the vessel motions, $\chi_{S,E,2}$

The effect of the uncertainty in the wave data is included in the calculation of the load effect, S_E; see Sec. 4.3.10. The last two items are combined to give the resulting uncertainty estimated by $\chi_{S,E} = \chi_{S,E,1} \cdot \chi_{S,E,2}$. The model uncertainty associated with the response analysis covers uncertainties related to the analysis of the barge motions as well as the calculation of the load effects in the supports. The prediction of the barge motions for the structural reliability analyses is based on hydrodynamic analysis using linear 3D potential theory, and nonlinear effects, such as barge deck immersion, are not included. The viscous roll damping is linearized by stochastic linearization. For high waves with large steepness, there may be a significant bias in the calculated barge motions [109]. However, in the structural reliability analyses, a bias that represents all the sea states included in the long-term distribution is needed, as discussed in Sec. 3.4.3.2. Consequently, the model uncertainty in the hydrodynamic analysis, $\chi_{S,E,1}$, is assumed to follow the normal distribution with a mean value of 0.9 and a COV of 0.1. The uncertainty resulting from the calculation of the dynamic load effect is assumed to be the same as that for the static load effect. Even if a simple statistical model is chosen here, the uncertainty in the calculated load effect could in a real case depend on the ballast condition and the relative stiffness between the supports. The uncertainty $\chi_{S,E,2}$ is assumed to follow

a normal distribution with a mean value equal to 0.95 and a COV equal to 0.1. The uncertainty in the calculated dynamic load effect is added to the uncertainty in the hydrodynamic analysis. The total model uncertainty[1] is then assumed to follow a normal distribution with a mean value of 0.86 and a COV of 0.14 [107].

For the structural reliability analysis of the supports, the extreme values of the support forces need to be calculated. The calculation must include the effect of the uncertainty in the environmental conditions. For short-term analyses based on weather forecasts, the forecast uncertainty is described in Sec. 4.3.4. For long-term analyses, see Sec. 4.3.5. The load effect is further described in Sec. 4.3.10.

4.3.4 Uncertainty in the forecasted wave height

The uncertainty in the forecasted significant wave height is assumed to follow a lognormal distribution [108]. The mean value and standard deviation depend on the forecast lead time. No additional uncertainty to account for the uncertainty in the hindcast data has been included; see also Sec. 4.3.7.

4.3.5 Uncertainty in the long-term significant wave height

Descriptions of the long-term environmental conditions are available from many sources. Traditionally, the data from BMT [64] have been applied for marine transports. However, as BMT data are based on visual observations of the environmental conditions from ships, they may contain the effects of adverse weather avoidance. Another source for obtaining weather data is hindcasting [123]. The hindcast data are independent of ship observations and are hence better suited to describe the true long-term environmental condition.

The long-term description of the environmental conditions used here is based on hindcast data from the North Sea. A three-parameter Weibull distribution is fitted to the long-term wave conditions. The long-term distribution describes the fundamental variation, but the meteorological data and the hindcast method are subjected to uncertainties; see also Sec. 4.3.7.

4.3.6 Uncertainties due to the amount of environmental data

The amount of data available for estimating the statistical parameters will affect the uncertainty. The effect of varying amounts of data is important,

[1] For the product of two statistically independent variables, $\chi = \chi_1 \cdot \chi_2$, the mean value is $\mu_\chi = \mu_{\chi 1} \cdot \mu_{\chi 2}$, and the coefficient of variation is COV$\approx \sqrt{(\mathrm{COV}_{\chi_1})^2 + (\mathrm{COV}_{\chi_2})^2}$ [95].

and an interesting study related to the time variability of the wave climate in the northern North Sea was performed by Moan et al. [100]. Data recorded by wave rider buoys in the northern North Sea over a period of 29 years were available. The extreme values of H_s were estimated by applying all 29 individual scatter diagrams and groups of every 2 and every 4 independent years together with the 29-year scatter diagram as a whole.

The observed maximum values of the significant wave height in each scatter diagram for a 1-, 2- and 4-year period are shown in the histogram in Fig. 4.4. The histogram based on the annual data shows larger scatter than that of the 2- and 4-year data. The variations in the predicted extreme

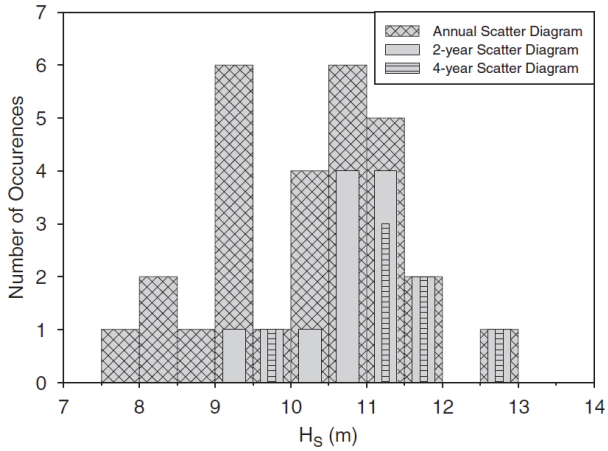

Figure 4.4: Histogram of the observed maxima of H_s in the scatter diagrams for 1, 2 and 4 years [100]

values based on the data in different years can be illustrated by the annual and 100-year extreme values of the significant wave height. The expected annual maximum H_s obtained by the 29 years of data was 10.5 m, while the 100-year value was 14.2 m. The variation in the estimated extreme values is shown in Table 4.2. The mean value of H_s and the coefficient of variation are also shown. It is evident that the effect of the data collection period affects the statistical results to a large extent.

4.3.7 Uncertainties in the gathered environmental data

In the previous section, the uncertainty related to the length of the data collection period was discussed. An additional uncertainty is included through the data used for estimating the statistical parameters. Data at a specific

Table 4.2: Variation in the annual and 100-year values of the extreme H_s as well as the mean value and COV of the Hs for statistics based on 1, 2, 4 and 29 years of data [100]

Reported value	1-year	2-year	4-year	29-year
1 year return H_s (m)	8.1-12.9	9-12.1	9.3-11.3	10.5
100 year return H_s (m)	10.3-19.2	11.8-16.8	12.2-15.4	14.2
Mean H_s (m)	2.3-3.2	2.5-2.9	2.6-2.8	2.7
COV of mean H_s	0.26	0.096	0.077	-

location are typically measured by wave rider buoys or radar, and the accuracy obtained in the measurements is of interest [91]. The same point can be considered for hindcast data. In this thesis, hindcast data from NORA10 [2, 123] have been used. Based on the discussion in Sec. 2.4.1, it was concluded that the uncertainty in the hindcast H_s-values was small, and the effect was not included in the SRA.

4.3.8 Uncertainty in the wave period

The forecasted wave period could be treated similarly to the significant wave height to account for the uncertainty in the wave peak period related to the forecasted wave period. This was considered in Paper 2 [108], but the wave period was seen to be more uncertain than the forecasted significant wave height. The wave period was therefore modeled as a lognormal distributed variable conditional on the significant wave height [11, 63]. The wave periods based on the statistical distribution at Location 2 in Fig. 2.6 were used.

If the design checks are based on a stochastic analysis, a range of wave periods as given in the design standards would be used, see, for example, Eq. (2.12). The wave period that gives the largest response governs. However, the design approach in this study is based on formulas from the marine operation standard [31]; see Sections 4.2.3 and C.1. The wave period is not included as a separate parameter in that design method, but the wave periods are implicit in the design formulas.

4.3.9 Operational uncertainty

During sea transport, the captain will normally seek to avoid heavy weather. Based on weather forecasts and the captain's experience, the speed and/or course may be altered during transport. For coastal transport, it may be possible to seek shelter and to a large extent avoid forecasted adverse weather (see Fig. 2.1). For overseas transport or in coastal areas where

it is not possible to seek shelter, course and speed alterations are the only options. In reliability analyses, the effect of the latter options could in principle be included through a bias factor [130].

As discussed in Sec. 2.7, the speed of a transport ship, even a bulk carrier, is relatively high. However, the speed of a towed barge is low, typically not more than 5 knots. The ability for heavy weather avoidance will therefore normally be limited, and speed reduction or halting and waiting for adverse weather ahead of the tow to pass by are the only practical alternatives. Furthermore, towing line failure will leave the barge adrift, in which case heavy weather avoidance will not be possible. Based on these considerations, the operational bias factor, B_{oper}, is set equal to 1.0 in Eq. (4.6), and the random uncertainty is neglected for barge transports in this study.

4.3.10 Load description

The long-term cumulative extreme value distribution of the wave-induced individual maxima, S_E, used in Eq. (4.6) is defined as follows [104]:

$$F_{S_E}(s_E) = \int_0^\infty \int_0^\infty F_{S_E|H_s,T_z}(s_E|h_s,t_z) f_{H_s,T_z}(h_s,t_z)\,\mathrm{d}h_s\,\mathrm{d}t_z \tag{4.7}$$

where

- $F_{S_E|H_s,T_z}(s_E|h_s,t_z)$ is the cumulative extreme value distribution for the individual support force conditional on the significant wave height and the mean zero-crossing wave period
- $f_{H_s,T_z}(h_s,t_z)$ is the joint probability density function for the significant wave height and the mean zero-crossing wave period

The distribution of the individual response maxima within a sea state, i.e., for given H_s and T_z, is assumed to be the extreme value distribution based on the Rayleigh distributed individual maxima:

$$F_{S_E|H_s,T_z}(s_E|h_s,t_z) = \left(1 - \exp\left[-\frac{1}{2}\left(\frac{s_E}{\sigma_{S_E}(h_s,t_z)}\right)^2\right]\right)^{N(h_s,t_z)} \tag{4.8}$$

$\sigma_{S_E}(h_s,t_z)$ is the standard deviation, the RMS-value (the root mean square value), of the support force. The load effect is a function of both the significant wave height and the period because it is caused by the wave-induced motion of the transport vessel. The load effect is estimated by the response surface method [122].

The total number of response cycles during marine operation for a given sea state is $N(h_s, t_z) = T_R \cdot \nu_0^+(h_s, t_z)$, where T_R is the duration of the operation and $\nu_0^+(h_s, t_z)$ is the mean zero-upcrossing rate of the response. The mean zero-upcrossing rate of the support force in beam sea conditions is practically independent of the significant wave height; hence, $N(t_z) \approx T_R \nu_0^+(t_z)$. $\nu_0^+(t_z)$ can be estimated by fitting an exponential curve to the actual mean zero-upcrossing rate. The following estimate was used in this thesis [107]:

$$\nu_0^+(t_z) = 0.12 + 0.87e^{-0.64t_z} \tag{4.9}$$

where T_z is given in seconds and the unit for ν_0^+ is s^{-1}.

The joint probability density function of H_s and T_z is expressed by the relation:

$$f_{H_s,T_z}(h_s, t_z) = f_{T_z|H_s}(t_z|h_s) f_{H_s}(h_s) \tag{4.10}$$

where the distribution of H_s depends on the category of marine operation [107]. A lognormal distribution was used for weather-restricted operations as follows:

$$f_{H_s}(h_s) = \frac{1}{h_s \cdot \sigma_{\ln H_s}\sqrt{2\pi}} \exp\left[-\frac{1}{2}\left(\frac{\ln h_s - \mu_{\ln H_s}}{\sigma_{\ln H_s}}\right)^2\right] \tag{4.11}$$

The parameters in the distribution are [108]:

$$\mu_{\ln H_s} = \ln(h_{s,fc}) + \mu_{\ln \chi} \tag{4.12a}$$

$$\sigma_{\ln H_s} = \sigma_{\ln \chi} \tag{4.12b}$$

where $h_{s,fc}$ is the maximum forecasted significant wave height during the operation, given in meters. The stochastic variable χ represents the uncertainty in the weather forecasts ($\chi = H_{s,hindcast}/H_{s,forecast}$). The numerical values are given in Table 2.1.

For weather-unrestricted operations, a three-parameter Weibull distribution was used (see Eq. (2.2)).

The statistical distribution of the mean zero-crossing period, T_z, conditional on H_s, is given as a lognormal distribution [11, 63]:

$$f_{T_z|H_s}(t_z|h_s) = \frac{1}{t_z \cdot \sigma_{\ln T_z|H_s}\sqrt{2\pi}} \exp\left[-\frac{1}{2}\left(\frac{\ln t_z - \mu_{\ln T_z|H_s}}{\sigma_{\ln T_z|H_s}}\right)^2\right] \tag{4.13}$$

The mean value and the standard deviation for $\ln(T_z)$ are calculated as follows:

$$\mu_{\ln T_z|H_s} = a_1 + a_2 h_s^{a_3} \tag{4.14a}$$

$$\sigma_{\ln T_z|H_s} = b_1 + b_2 e^{b_3 h_s} \tag{4.14b}$$

The parameters a_i and b_i, $i = 1, 2, 3$, are estimated from hindcast data in this study, see Table 4.6.

The RMS value of the support force is estimated by a response surface as follows [122]:

$$\sigma_{S_E}(H_s, T_z) = (A_1(T_z) + A_2(T_z)H_s + A_3(T_z)H_s^2)mg \tag{4.15}$$

where mg is the weight of the transported object (with mass m) and the parameters A_1, A_2 and A_3 are estimated from:

$$A_i(T_z) = k_{i1} + k_{i2}T_z + k_{i3}T_z^2 \; for \, i = 1, 2, 3 \tag{4.16}$$

The coefficients k_{ij} are estimated based on results from a numerical analysis [107].

4.3.11 Basic formulation of the reliability problem

For a seafastening structure in the ultimate limit state, where the structural capacity and the load effect are modeled by the stochastic variables R and S, respectively, the *failure function* can be expressed as follows:

$$g(\boldsymbol{X}) = R(\boldsymbol{X}) - S(\boldsymbol{X}) \tag{4.17}$$

where $g(\boldsymbol{X}) \leq 0$ represents failure. $\boldsymbol{X}$ is a vector of variables representing the load effects and the capacity. The probability of structural failure is defined as follows:

$$P_f = P(g(\boldsymbol{X}) \leq 0) \tag{4.18a}$$

$$= \int ... \int_{g(\boldsymbol{X}) \leq 0} f_{\boldsymbol{X}}(\boldsymbol{x}) \, \mathrm{d}\boldsymbol{x} \tag{4.18b}$$

$$= \int ... \int_{\boldsymbol{X}} I[g(\boldsymbol{x}) \leq 0] f_{\boldsymbol{X}}(\boldsymbol{x}) \, \mathrm{d}\boldsymbol{x} \tag{4.18c}$$

where $I[\circ]$ is an indicator function that is equal to 1 if $[\circ]$ is "true" and 0 if $[\circ]$ is "false". The joint probability density, $f_{\boldsymbol{X}}(\boldsymbol{x})$, includes all the variables involved.

In some special cases, the failure probability can be expressed analytically. This applies for cases when both R and S are time-invariant, and they have either a normal or a lognormal distribution. Generally, the failure probability is calculated by numerical methods. When R and S are statistically independent, then $f_{\boldsymbol{X}}(\boldsymbol{x})\mathrm{d}\boldsymbol{x} = f_{\boldsymbol{R}}(\boldsymbol{r}) f_{\boldsymbol{S}}(\boldsymbol{s})\mathrm{d}\boldsymbol{r}\mathrm{d}\boldsymbol{s}$ in Eq. (4.18).

4.3.12 Time-independent reliability analyses with FORM/-SORM

The failure function is defined by Eq. (4.17). The structural capacity is assumed to be time invariant, and the load effects are calculated from Eq. (4.7). The failure probability shown in Eq. (4.18) in a reference period equal to the duration of the operation may then be determined by time-independent reliability analysis. It is generally not possible to use analytic integration for the failure probability in Eq. (4.18). Several numerical methods are available for time-independent reliability analyses, notably simulation and FORM/SORM methods. The first order reliability method (FORM) is an efficient method for calculating the failure probability. The second order reliability method (SORM) is a more refined method than FORM, which takes the curvature of the failure surface at the design point into account. SORM is used to calculate failure probabilities in this thesis. Experience has shown that FORM is sufficient for many structural engineering problems [103], and using either FORM or SORM gives practically equal results in this thesis.

In FORM/SORM analyses, the integral is solved by transforming the problem from the space of physical variables, $\boldsymbol{X}$, to a standard normal space, $\boldsymbol{U}$, and approximating the failure surface by a linear/quadratic surface that is tangential to the initial failure surface at the point with the shortest distance from the origin. This point is called the β-point or the *design point*. The procedure is schematically illustrated in Fig. 4.5, where the first step is to map the limit state from the real space to the standard normal space. The reliability index, β, is uniquely related to the failure probability, P_f. It is defined as [99]:

$$\beta = -\Phi^{-1}(P_f) \tag{4.19}$$

where $\Phi(\cdot)$ is the cumulative standard normal distribution. It is evident from Fig. 4.5 that β can also be expressed as follows [134]:

$$\beta = |\boldsymbol{u}^*| = \sqrt{(u_i^*)^2 + (u_j^*)^2} \tag{4.20}$$

An alternative to the FORM/SORM methods include the simulation methods, e.g., Monte Carlo simulations. The failure probability calculated by a Monte Carlo simulation will converge toward the true value if the number of simulations is large enough. A disadvantage of Monte Carlo simulations is that they are time consuming for problems with many random variables and/or low failure probability. However, Monte Carlo simulation is a valuable tool for checking the accuracy of the results from reliability analysis based on FORM/SORM for complicated problems. In this thesis,

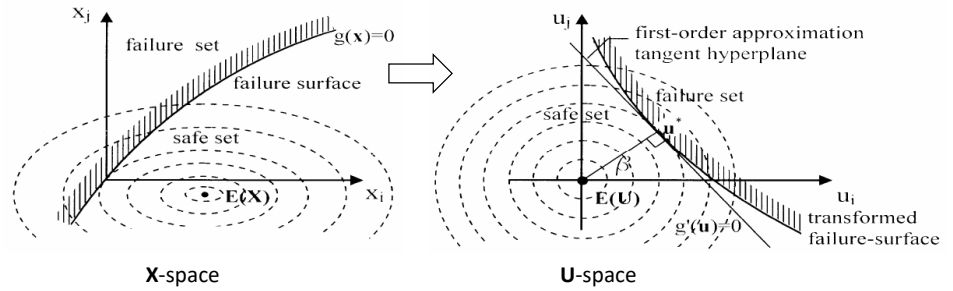

Figure 4.5: Schematic illustration of FORM/SORM analyses for a general $g(\boldsymbol{X})$- function [99]. While FORM uses a tangent hyperplane approximation as indicated in the figure, SORM is based on a quadratic approximation of the failure-surface.

the computer program Proban [143] has been used to perform reliability analyses.

4.3.13 Uncertainty importance factors

The uncertainty importance factors provide information on the influence of the variables in $g(\boldsymbol{X})$ from Eq. (4.17) on the failure probability. The importance factors represent the percentage of the total uncertainty in the reliability index, β, due to the corresponding random variable or group of random variables. The importance factors are defined as $100\alpha_i^2$, where α_i are the sensitivity factors defined as follows [89]:

$$\alpha_i = \frac{\partial \beta}{\partial u_i}\Big|_{\boldsymbol{u}^*} \tag{4.21}$$

where $\boldsymbol{u}^*$ is the design point in u-space (see Fig. 4.5). The importance factors are calculated by FORM/SORM using Proban [121, 143]. FORM and SORM give equal results here because the tangent hyperplane in $\boldsymbol{u}^*$ is the same in both methods. If an importance factor is low, the corresponding variable has little influence on the failure probability and can be defined as a fixed value instead of a random variable.

4.4 Case studies of a seafastening structure in barge transport

4.4.1 General

The barge transport of a large and heavy object was studied in this thesis. The grillage and seafastening were designed to resist the loading calculated by a deterministic method. Based on that particular design, reliability analyses were carried out, calculating the failure probability of Eq. (4.3) to demonstrate how P_f depends on various factors. This included the model uncertainty in the load effects and structural capacity, as well as the uncertainty in the environmental conditions and seasonal variations.

In Sec. 4.4.2, the input to the SRA is described. Some selected results from the SRA [107] are presented in Sec. 4.4.3, and a discussion on the results is included in Sec. 4.4.4.

4.4.2 Input data for the structural reliability analyses

4.4.2.1 Stochastic variables in the case studies

The failure probability was defined as $P_f = P[R \leq S]$ in Eq. (4.3). The variables R and S were defined in Eqs. (4.4) and (4.6), respectively. Information on the variables is given in Table 4.3.

4.4.2.2 Long-term distribution of the significant wave height

In Table 4.4, the parameters for the three-parameter Weibull distribution for the significant wave height are given for each month and year-round. The significant wave heights with a return period equal to one year are also shown. (This is the value of H_s with 8% probability of being exceeded during one month and 63% probability of being exceeded during 12 months). Seasonal parameters are given in Table 4.5. The data are grouped into four seasons: winter (December - February), spring (March - May), summer (June - August) and autumn (September-November).

4.4.2.3 Distribution of the wave period conditional on H_s

The parameters in the lognormal distribution of the mean zero-crossing period conditional for the significant wave height (Eq. (4.13)) are given in Table 4.6.

Table 4.3: Mean value and COV of the variables in the case studies

Variable	Description	Distribution	Mean	COV
χ_R	Uncertainty in the structural capacity of the bulkhead	Lognorm.	1.25	0.17
R_c	Characteristic structural capacity	Fixed	Eq. (4.2)	-
$\chi_{S,G}$	Uncertainty in the calculated static load effect	Normal	0.95	0.1
$\chi_{S,E}$	Uncertainty in the calculated dynamic load effect	Normal	0.86	0.14
S_E	Vertical dynamic load effect	Eq. (4.7)	-	-
H_s	Significant wave height	Eq. (4.10)	-	-
T_z	Mean zero-crossing wave period	Eq. (4.13)	-	-
ν_0^+	Mean zero-upcrossing rate of the response	Sec. 4.3.10	-	-

4.4.3 Results from the case studies

4.4.3.1 Seafastening structure designed for weather-restricted transport

For weather-restricted transport designed by standard criteria for a H_s of 4 m, the failure probability was calculated with and without considering the uncertainty in the weather forecasts according to the Alpha factor method described in Sec. 1.4.6. The following was done:

1. The maximum allowed forecasted H_s required to start the operation was taken according to the design H_s multiplied by the Alpha factor [31]; hence, the maximum allowed forecasted H_s was equal to 3.0 m for a one-day operation, 2.8 m for two days and 2.7 m for three days.

2. The uncertainty in the forecasted significant wave height was accounted for by a lognormal distribution; see Sec. 4.3.4, with the mean and standard deviation taken from Table 2.1; hence, $\mu_{ln\chi} = 0.055$ and $\sigma_{ln\chi} = 0.112$ for a one-day operation, and so on.

3. The failure probability was calculated according to Eq. (4.18) for 24, 48 and 72 hours.

Table 4.4: Parameters in the three-parameter long-term Weibull distribution of the significant wave height (ref. Eq. (2.2)) for each month and year-round, for the northern North Sea. The significant wave height with a one-year return period is also shown.

Month	α (m)	β (-)	γ (m)	$H_{s,1y}$ (m)
January	2.87	1.58	0.88	11.6
February	2.67	1.57	0.70	10.7
March	2.39	1.52	0.75	10.2
April	1.60	1.30	0.72	8.6
May	1.24	1.26	0.59	7.1
June	1.04	1.23	0.56	6.2
July	0.94	1.21	0.54	5.8
August	1.02	1.19	0.58	6.4
September	1.49	1.23	0.77	8.8
October	2.13	1.43	0.81	10.0
November	2.42	1.54	0.92	10.2
December	2.73	1.54	0.90	11.4
Year-round	2.05	1.31	0.54	10.6

As a quick check of how reasonable the forecast limits seem, the uncertainty given in Table 2.1 is considered. For a forecasted significant wave height of 4 m, the mean value plus two standard deviations after 48 hours is $(1.08 + 2 \cdot 0.13) \cdot 4 \text{ m} \approx 5.4 \text{ m}$, which is well above the design H_s. When the forecast indicates a significant wave height of no more than 2.8 m over the next two days, as required above, the mean value plus two standard deviations equals 3.8 m, which is close to the design value. Hence, the reduction in design H_s to reach the forecast H_s seems plausible.

When the forecast uncertainty is *not* considered, the forecast limit to start the operation is not reduced; the operation can start when the forecasted H_s is equal to 4 m. This is a hypothetical situation because it implies that the weather forecasts are exact and that the true H_s is identical to the forecasted H_s. The purpose was to quantify the effect of the forecast uncertainty on P_f. Under this assumption, the failure probability is calculated for one, two and three days, all with $H_s = 4$ m. When the forecast uncertainty *is* considered, the maximum allowed forecasted H_s required to start the transport is 3 m for an operation period of one day, reducing to 2.7 m for a period of 3 days. The failure probability accounting for the fore-

Table 4.5: Parameters in the three-parameter long-term Weibull distribution of the significant wave height (ref. Eq. (2.2)) for each season for the northern North Sea. The significant wave height with a one-year return period is also shown.

Month	α (m)	β (-)	γ (m)	$H_{s,1y}$ (m)
Winter (Dec.-Feb.)	2.77	1.56	0.82	11.3
Spring (Mar.-May)	1.79	1.29	0.63	9.5
Summer (Jun.-Aug.)	1.00	1.20	0.56	6.2
Autumn (Sep.-Nov.)	2.11	1.41	0.75	10.0

Table 4.6: Parameters for the conditional distribution of T_z (ref. Eq. (4.14)) based on year-round data for the northern North Sea

Parameter	a_1	a_2	a_3	b_1	b_2	b_3
Value	1.277	0.378	0.441	0.005	0.195	-0.169

cast uncertainty is shown in Table 4.7, together with the failure probability when forecast uncertainty is neglected, i.e., for $H_s \equiv 4$ m. The forecasted significant wave height is taken to be constant during the operation period. This assumption is discussed in Sec. 4.4.4.

The failure probability increases with increasing duration both with and without forecast uncertainty because the maximum forces (extreme values) increase over time for a given H_s. When the forecast uncertainty is included, there is an additional effect because the forecast uncertainty also increases with time. However, the increased uncertainty is counteracted by the reduced limit for the forecasted H_s for longer operations. In fact, the reduced startup criterion accounts for the uncertainty and results in a lower failure probability when the forecast uncertainty is included.

4.4.3.2 The effect of seasonal versus year-round data for weather-unrestricted transport

The ISO standard for Marine Operations [72] requires that the weather conditions used for the design of weather-unrestricted operations "shall reflect the statistical extremes for the area and season concerned". According to the DNV GL standard for Marine Operations [31], the seasons *may* be accounted for when planning sea voyages. Traditionally, the use of seasonal

Table 4.7: The failure probabilities of the vertical supports are shown for a weather-restricted operation based on a design value of $H_s = 4$ m. When the effect of the forecast uncertainty is included, P_f is calculated for a forecasted H_s equal to the maximum allowed according to design standards [31, 107], as shown in the column for $H_{s,fc}$. When the forecast uncertainty is excluded, $H_s \equiv 4$ m is used as a deterministic variable.

No. of days	$H_{s,fc}$ [1)] (m)	P_f Uncert. excl.	P_f Uncert. incl.
1	3.0	$1.4 \cdot 10^{-3}$	$6.2 \cdot 10^{-4}$
2	2.8	$1.8 \cdot 10^{-3}$	$6.2 \cdot 10^{-4}$
3	2.7	$2.1 \cdot 10^{-3}$	$6.6 \cdot 10^{-4}$

Note 1: $H_s \equiv 4$ m with no forecast uncertainty

variations has been optional. The normal approach has generally been to use year-round data and utilize seasonal variations when it is beneficial in the sense that the loads are reduced.

A weather-unrestricted seafastening design was considered, and P_f was calculated based on environmental data from January and year-round data, as shown in Table 4.8. For that particular design, the failure probability was 2-3 times higher based on January statistics than for year-round data.

Table 4.8: Failure probability for a weather-unrestricted operation based on wave data for January and year-round

No. of days	P_f Jan.	P_f Year-round
3	$1.6 \cdot 10^{-4}$	$6.1 \cdot 10^{-5}$
7	$2.2 \cdot 10^{-4}$	$8.5 \cdot 10^{-5}$
14	$2.8 \cdot 10^{-4}$	$1.1 \cdot 10^{-4}$
21	$3.2 \cdot 10^{-4}$	$1.3 \cdot 10^{-4}$

Assuming a duration equal to seven days, P_f for each month was compared with that calculated with year-round data. The P_f value based on year-round data was $8.5 \cdot 10^{-5}$, while P_f based on monthly data varied, as shown in Fig. 4.6.

While the increased P_f in winter compared with year-round analysis was moderate (2-3 times higher), P_f during summer was reduced by a factor of 10.

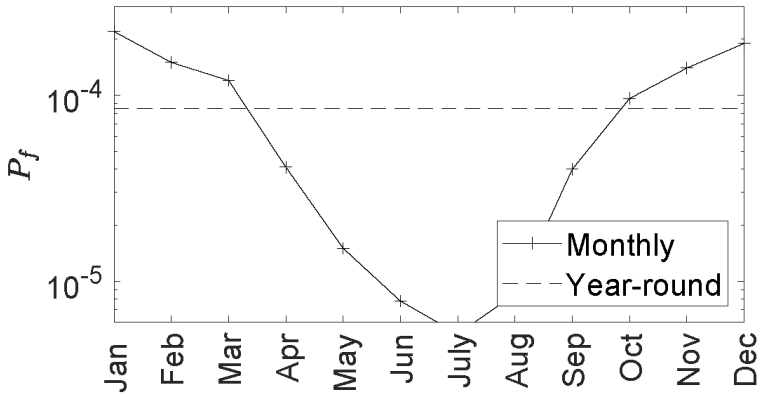

Figure 4.6: Failure probability for a weather-unrestricted operation with a duration of seven days based on monthly and year-round wave data [107]

4.4.3.3 Sensitivity study

The importance factors (see Sec. 4.3.13) for two selected cases, one weather-restricted operation and one weather-unrestricted operation, are shown in Table 4.9. In the weather-restricted case, the seafastening was designed for a significant wave height equal to 4 m, and the duration of the operation was three days (72 h). The forecasted H_s was 2.7 m. In the weather-unrestricted case, the duration was seven days, and the significant wave height was based on year-round long-term statistics. Vertical support was designed for weather-unrestricted transport.

The base cases and alternatives with changed bias and the COV on the capacity and one alternative with increased COV on the uncertainty in the calculated dynamic load effect are considered. The details on the alternatives and the importance factors, as well as the reliability index and the failure probability, are given in Table 4.9. The importance factor for the structural capacity, χ_R, dominates in all cases. For weather-unrestricted operations, the wave-induced load, S_E, contributes significantly more to the failure probability than for weather-restricted operations. As expected, the failure probability increases when the bias on χ_R is reduced and when the COV of $\chi_{S,E}$ is increased. In Alternative 4, an increase in the COV for the capacity leads to a substantial increase in the failure probability. The main observation is that the uncertainty in the structural capacity dominates in the structural reliability analyses. The capacity depends on the structural design and fabrication for actual marine operations, and a focus on this aspect is suggested in the grillage and seafastening design for the transport

Table 4.9: Importance factors (in %) for a weather-restricted (WR) operation and a weather-unrestricted (UR) operation with durations of three and seven days, respectively. The reliability index and failure probability are also given. Index 0: Base case with variables from Table 4.3. Index 1: Alternative 1 with the bias for χ_R changed from 1.25 to 1.15. Index 2: Alternative 2 with the COV for $\chi_{S,E}$ changed from 0.14 to 0.20. Index 3: Alternative 3 with the COV for χ_R changed from 0.17 to 0.15. Index 4: Alternative 4 with the COV for χ_R changed from 0.17 to 0.20.

			Importance factors, %			
Case	β	P_f	χ_R	$\chi_{S,E}$	S_e	$\chi_{S,G}$
WR-0	3.21	$6.6{\cdot}10^{-4}$	77	7	8	8
WR-1	2.78	$2.7{\cdot}10^{-3}$	76	7	8	8
WR-2	3.10	$9.5{\cdot}10^{-4}$	72	13	9	7
WR-3	3.54	$2.0{\cdot}10^{-4}$	72	9	10	9
WR-4	2.81	$2.5{\cdot}10^{-3}$	82	6	6	6
UR-0	3.76	$8.5{\cdot}10^{-5}$	60	8	27	4
UR-1	3.38	$3.6{\cdot}10^{-4}$	59	8	29	5
UR-2	3.63	$1.4{\cdot}10^{-4}$	55	14	28	4
UR-3	4.05	$2.5{\cdot}10^{-5}$	57	10	29	5
UR-4	3.38	$3.6{\cdot}10^{-4}$	65	6	25	4

of heavy objects.

4.4.4 Discussion of the results

The case studies focus on the structural reliability of a seafastening structure that is designed according to standard motion/acceleration criteria for a barge, while the structural reliability analysis is based on the direct calculation of motions and accelerations.

A weather-restricted transport designed for $H_s = 4$ m was discussed in Sec. 4.4.3.1 (a similar case for $H_{s,design} = 6$ m was included in Paper 3). It was assumed that the forecasted significant wave height was constant during the operation. This condition does not necessarily hold, as the forecasted H_s could (and generally does) vary over time. However, for moderate sea states, the significant wave height can be approximately the same over several consecutive days. Hence, for a transport with a limited duration (one, two and three days), the calculated failure probabilities represented a realistic transport case. It was evident that the Alpha factor approach

effectively compensated for the uncertainty of the forecasting in this case.

Next, the effect of seasonal versus year-round data for weather-unrestricted transport was studied in Sec. 4.4.3.2. For weather-unrestricted transport, the significant wave height is not constant but follows a long-term distribution, as discussed in Chapter 2. This distribution varies throughout the year. From an analysis point of view, it is convenient to apply year-round data because that is readily available and provides flexibility in the planning at an early stage before the transport date is defined. However, as indicated in Fig. 4.6, the failure probability for seafastening structures designed for weather-unrestricted transports then strongly depends on the time of the year. It is evident that P_f is very low if the transport is executed during the summer period. This is good from a safety perspective, but a too low P_f could be seen as (unnecessary) conservatism by use of the weather-unrestricted design option for the summer period and introduce an (unnecessary) high cost. For practical transport, a design H_s could be calculated based on a long-term distribution or the return period approach described in Sec. 2.6 (if the design H_s was below 4 or 6 m, the standard method in App. C.1 may be used.) It should be noted that for planning real marine operations, it is necessary to check the capacity also using environmental data for the preceding and/or succeeding month [31], but that has not been considered in this thesis.

In reality, the duration of a marine operation is a stochastic variable, but in the analyses above, it was assumed to be a deterministic variable, estimated as described in Sec. 2.2. The duration could be modeled as a stochastic variable, and revised failure probabilities could be calculated. However, from the case studies above, it is evident that P_f is not very sensitive to the duration; hence, it is reasonable to model the duration as a fixed variable.

In Sec. 4.4.3.3, a sensitivity study was performed in which importance factors were calculated for weather-restricted and weather-unrestricted marine operations. The sensitivity analyses showed that the structural capacity had the largest importance factors of all the parameters examined. Consequently, the failure probabilities were sensitive to variations in the bias and COV for the structural capacity, and the structural capacity, in particular that of a bulkhead with horizontal stiffeners exposed to vertical loading, was an important input for the structural reliability analyses.

The above analyses are all based on the barge transport case where the seafastening structure is designed for various environmental conditions. To obtain a further understanding of how the results from the SRA relate to the planning of marine operations in practice, other case studies could be

performed. It would also be of interest to extend the period of weather-restricted operations. The uncertainty in the forecasted value of H_s was quantified for operations lasting up to seven days in Paper 2 (see Table 2.1 above). Hence, the method for weather-restricted marine operations could be applied for transports with a duration of up to seven days, and the results could be compared with weather-unrestricted operations. This has not been done in this thesis but is proposed as future research (see Sec. 5.4.3).

Chapter 5

Conclusions and recommendations for future research

5.1 General

The objective of the research presented in this thesis is to study the structural integrity of typical support structures for sea transport of large and heavy objects in a structural reliability framework, considering both weather-restricted and weather-unrestricted operations. This thesis addresses the uncertainty assessment of wave-induced motions of a transport barge and the capacity of the selected elements as implemented in the structural reliability analyses. The focus in this research work is on three topics. First, an investigation of the motion of a transport barge in severe beam seas and the associated support loads is conducted by numerical methods supported by the model tests. Second, the uncertainty of forecasted significant wave height is evaluated. Finally, the structural reliability analysis of the supports in the ultimate limit state is performed. The conclusions and original contributions of the research work in this thesis and recommendations for future research are presented below.

5.2 Conclusions

The main conclusions in this thesis are presented in the published papers focusing on the three topics related to sea transports, namely, the wave-induced load effects, uncertainty in weather forecasts and structural relia-

bility of the cargo supports during sea transport. The main conclusions and findings are summarized in the following.

- *Maximum roll angle.*
  For severe sea states, the model test results were compared with calculations in the frequency domain using stochastic linearization of the viscous roll damping. They were also compared with the results from a nonlinear analysis in which the equations of motion were solved in the time domain. The ratio between the maximum expected roll angle for a three hour storm period and the standard deviation was 3.4-3.9 for the nonlinear analysis, i.e., close to the results from a linear analysis. The similar ratio from the model tests was between 2.7 and 3.2. The reason for this lower ratio was concluded to be that the roll amplitude was limited upwards by physical effects that were not captured by the numerical analyses. The maximum expected roll amplitude from the model tests was 22 degrees for a three hour storm period. The linear analyses overestimated the maximum roll angle, while the nonlinear analysis compared well.

- *Model uncertainty in support force.*
  The barge motions for high sea states are calculated by linear and nonlinear analyses and compared with results from the model tests. It was found that the bias varied with the response. The bias was estimated to be 0.75-0.94 for the maximum roll angle and 0.65-0.8 for the vertical support force, depending on the type of analysis. Accounting for the effect of high wave steepness and non-linearity in the model tests, e.g., water on the deck in high sea states, the bias for the vertical support force from the model tests was set to 0.9 together with a COV of 0.1. The uncertainty in the calculated load effect was represented by a random variable with a mean value of 0.95 and COV of 0.1. The model uncertainty was then assumed to be normal distributed with a mean value of 0.86 and COV of 0.14 for long-term environmental conditions for use in the structural reliability analysis to represent the general environmental conditions.

- *Duration of weather-restricted operations.*
  Operations with planned durations less than three days are designed as weather-restricted marine operations. The weather forecasts from the Norwegian Sea that were studied in this thesis did not reveal any specific increase in the forecast uncertainty that would require an exact 72-h limit for weather-restricted operations, even if the uncertainty in the forecasts increases with the lead time up to a lead time of seven

days. For example, the bias in the forecasted significant wave height increases from 1.09 to 1.10 from three to four days, while the coefficient of variation increases from 0.13 to 0.15.

- *Forecasted wave period.*
  A similar approach as used for the significant wave height can been used for the forecasted wave period. However, the correlation between forecast and hindcast data is lower for wave periods than for significant wave heights for a given lead time, indicating that forecasted wave periods are more uncertain than forecasted wave height. The wave period for weather-restricted operations is therefore modeled by a statistical distribution similar to the distribution used for weather-unrestricted operations.

- *Target reliability level.*
  An important question in applying structural reliability analyses in decision making is to specify the target reliability level. Some design standards recommend a certain target reliability level for the design depending on the consequences of failure. However, in practice, it may be difficult to relate such target levels directly to the reliability analyses. However, as long as the reliability level is considered to be adequate, the target reliability level can be chosen to be the same as that obtained by using the current design standards. The adequacy of the current practice is demonstrated through a low experienced failure rate and general acceptance by the industry and insurance companies.

  In engineering practice, the uncertainty in weather forecasts is accounted for by applying a risk reduction factor called the Alpha factor. This factor was implemented in the structural reliability analyses, and the failure probability was calculated by this approach as well as by assuming perfect weather forecasts (and hence there was no forecast uncertainty to compensate for). The standard Alpha factor approach was seen to effectively compensate for the uncertainty inherent in the weather forecast in the cases studied in this thesis.

- *Structural capacity.*
  The structural capacity was considered for the grillage beams and for the barge bulkheads, considering the model uncertainty and the uncertainty in the material parameters. The ultimate strength of the bulkheads was found to be governing, and it was found adequate to model the resulting capacity by a random variable following a lognormal distribution with a bias of 1.25 and a COV of 0.17.

- *Results from the structural reliability analysis.*
  For a weather-unrestricted operation planned using standard all-year criteria for load calculation, the failure probability depends on the time of the year in which the operation is executed. For example, it was noticed that for a given cargo support design:

  – the failure probability was 1.5 times higher using environmental data for November instead of seasonal data for autumn (September - November)
  – the failure probability calculated using statistical data for January was 3 times higher than that calculated using data for the entire year
  – the failure probability in July was less than 1/10 of the failure probability in October

  The differences in the failure probabilities are not dramatic in the first two cases. In the third case, however, the difference is rather large and should be further considered. It is evident that to use the weather-unrestricted all-year criteria for summer transport introduces conservatism. This is acceptable from a safety point of view but increases cost. Hence, the design of grillage and seafastening should be optimized by applying a reduced design sea state for weather-unrestricted summer transports based on available hindcast or measured wave data.

  The following main conclusions are drawn from this study:

  – For a weather-restricted operation, the reduction in the allowable significant wave height according to the so-called Alpha factor method to account for the forecast uncertainty is a good approach with respect to the failure probability.
  – The use of seasonal data for planning weather-unrestricted operations is optional according to some regulatory bodies and mandatory according to other regulatory bodies. The use of seasonal or year-round data will affect the failure probability for a given operation, as seasonal data for the winter gives a higher failure probability than year-round data.
  – The calculated failure probabilities for a given operation depend on the season in which it is executed, the duration of the operation, etc. However, the calculated probabilities are of the same order of magnitude as the target value generally accepted for marine operations, of 10^{-4} per operation.

The overall conclusion is that for the North Sea, the failure probability by use of the simplified design criteria compares well with the target level. However, because the uncertainty in the strength dominates and the strength depends on temporary solutions for each transport, a focus on this aspect is recommended in the integrity management of the grillage and seafastening in connection with the transport of heavy objects.

- *A simple design formula for the wind speed.*
  For a weather-unrestricted operation, the wind speed corresponding to a given design wave height needs to be determined. While the significant wave height can be determined based on available long-term statistics, such statistics are not always available for the design wind speed. A simple approach is proposed to estimate the design wind speed for open sea areas as a function of the design significant wave height. This easy-to-use engineering method provides a design wind speed with reasonable accuracy and could be used in planning transports where wave-induced loading dominates and where a design significant wave height is given.

5.3 Summary of the original contributions

This thesis addresses the structural reliability related to the seafastening of heavy cargo during sea transport on barges. The original contributions of this thesis are summarized as follows:

- *Establishing a method for calculating the viscous damping for rolling of a barge.*
  This was based on the original methods by Tanaka and Ikeda for ships and extended to include wider vessels such as a transport barge (i.e., increased B/KG ratios).

- *Model test of the transport barge exposed to severe seas with steep waves giving large barge motions.*
  The purpose was to study the motions of a barge in storm conditions during weather-unrestricted transport. The wave periods were close to the natural roll period to investigate the effect of resonant barge motion in severe seas.

- *Uncertainty assessment of the environmental conditions.*
  Weather forecasts of the significant wave height were studied, and the

uncertainty was quantified. The uncertainty was implemented in the reliability analyses.

- *A formula for the design wind speed.*
  A simple formula to calculate the design wind speed corresponding to a design significant wave height was proposed. The purpose was to provide a simple method for engineering purposes in estimating the wind speed and hence the wind-induced loading acting on the transported object.

- *Structural reliability analyses including modeling of uncertainties, especially the uncertainty in weather forecasts.*
  A reliability model that accounted for the uncertainty inherent in the weather forecasts was established. This model was used to study the effect of the forecast uncertainty on the structural reliability by providing a comparison with a (fictitious) condition without forecast uncertainty.

- *Structural reliability analyses to study the effect of seasons, etc.*
  A reliability model in which the long-term statistical distribution of the environmental conditions was modeled was used to study seasonal variations and the failure probability as a function of the duration for weather-unrestricted operations.

5.4 Suggestions for future research

5.4.1 Additional model tests

The model tests included free decay and forced roll tests, and the barge was exposed to beam seas. In the free decay tests, the CoG was in one position, and in the forced roll tests, the model was rolled about an axis in the water surface.

Several additional tests could have been performed to obtain a broader set of data to analyze the roll damping and barge motion. Additional model tests could include:

- free decay tests with several vertical CoG positions of the cargo
- forced roll tests with the axis of rotation at several elevations
- waves from several directions in addition to the beam seas, e.g., head seas and beam quartering seas

5.4.2 Uncertainty assessments of wave forecasts

In this thesis, the significant wave height for the total sea was used for comparison of the forecast and hindcast. In the weather forecasts and hindcast data, the significant wave height was given for the wind driven waves, swell and total sea. An alternative to the chosen approach could be to compare wind sea and swell separately, and this might be part of a future research project.

Many marine operations are sensitive to wave periods, e.g., vessel motions close to natural periods. The maximum allowable significant wave height for a weather-restricted operation, e.g., for an offshore crane installation or sensitive sea transport, may vary as a function of the wave period (T_p or T_z) for such operations. The margin on the forecasted wave period required to achieve the required safety level is not clearly defined in the design standards. (For example, if the analysis has shown that the operation can be started when $H_s \leq 2$ m and $T_z \leq 9$ s, the forecasted maximum H_s is $\alpha \cdot 2$ m, where Alpha is found in design standards. However, the maximum acceptable T_z in the weather forecast to start the operation is unknown.) The uncertainty in the forecasted wave period could be further addressed in future studies.

5.4.3 Maximum duration of weather-restricted operations

The maximum duration of weather-restricted operations is generally three days according to design standards. This is often a challenge in planning marine operations because exceeding that limit imposes design environmental conditions based on long-term statistics, which is normally much more severe than the limits defined for weather-restricted operations. It would therefore be a great benefit for the industry if the limit for weather-restricted operations could be extended. In the study of the forecast uncertainty in the significant wave height performed in this thesis, no clear reason to limit the duration of a weather-restricted operation to three days was observed. However, that was an observation that was based on a limited amount of data, and a possible extension of the three-day limit based on a broader data set considering wind and waves could be a topic for future research.

5.4.4 Ultimate strength assessment

Some assumptions and simplifications regarding the strength have been made in this thesis. The support forces were calculated based on the dynamic equilibrium of the transported object. In future work, a refined

method could be applied for the strength assessment. The support forces could have been calculated by finite element analysis methods, including the calculation of the relative stiffness of the barge and transported object. The uncertainty in the capacity of stiffened plate panels in bulkheads was estimated based on previous experiments and analyses described in the literature. More sophisticated evaluations of the bulkheads could be performed by methods such as nonlinear finite element analyses or experiments.

The event defined to represent failure in an ultimate capacity context is not a physical collapse but a defined upper limit for the capacity. Hence, a violation of the ultimate limit state capacity will not necessarily lead to structural failure. For the same reason, even several load cycles exceeding the ULS capacity due to events such as rolling of the barge in heavy seas that do not have to lead to a total loss. Following the buckling failure of a bulkhead below the cargo supports, the deck plate of the barge will be able to resist a substantial amount of loading due to membrane stresses, and hence, there is a reserve that is not accounted for in the calculated capacity. Buckling of a bulkhead would lead to local damage of the barge, but a total degradation of the cargo support would not occur. This reserve capacity has not been quantified in this study. The calculated failure probability refers to a defined capacity limit and not necessarily to a physical collapse. Such reserves could lead to a larger bias for the structural capacity, hence reducing the failure probability. It could also lead to lower consequences of failure by limiting the damage and avoiding total collapse. Such effects could be interesting to study in future work.

Another interesting subject is how conditions during fabrication could affect the ultimate strength. Construction work is generally performed indoors or under cover in adverse weather conditions outdoors. Normally, fabrication is performed over a long period of time, and weld inspection can easily be planned to comply with the required waiting time before performing NDT (nondestructive testing) on the welds. The fabrication of grillage and seafastening for sea transports of offshore structures is normally performed under controlled conditions in a yard. However, welding of the grillage beams and seafastening to the vessel and the transported object is performed outdoors. Building weather shielding is time consuming and not always done. A tight schedule may lead to a limited waiting time before performing NDT. Hence, the challenges for marine operations are different than those for general fabrication. The effect of weather conditions on the quality of welded joints and thereby the uncertainty in the structural strength is also relevant for future work.

5.4.5 The effect of costs

In this thesis, no cost-safety benefit analysis is performed. The reliability analyses do not include the effect of costs. It is then assumed that the planning and execution is carried out under the ALARP regime by minimizing all the risks as much as reasonable practicable and satisfying the required safety level with respect to loss of life. The application of the ALARP principle could be a topic for future research.

References

[1] A.B. Aalbers and C.J.G. van Dongen. Weather routing: Uncertainties and the effect of decision support systems. In *Proceedings of the Marine Operations Specialty Symposium (MOSS), Baltimore, USA*, 2008.

[2] O. J. Aarnes, Ø. Breivik, and M. Reistad. Wave Extremes in the Northeast Atlantic. *Journal of Climate*, 25:1529–1543, 2012.

[3] ABS. Rules for Building and Classing Steel Vessels. American Bureau of Shipping, Houston, USA, July 2019.

[4] E. Achenbach. Influence of surface roughness on the cross-flow around a circular cylinder. *Journal of Fluid Mechanics*, 46(2):321–335, 1971.

[5] P. Ø. Alvær. HLV transports - DNV guidelines for calculation of cribbing friction. In *Proceedings of the Royal Institution of Naval Architects (RINA) International Conference, London, UK*, 2005.

[6] P. Ø. Alvær. The VMO Standard & ISO 19001-6 Marine Operations. In *Proceedings of the Second Marine Operations Specialty Symposium (MOSS), Singapore*, 2012.

[7] P. Ø. Alvær. The new marine operation standard DNVGL-ST-N001. In *Proceedings of the Third Marine Operations Specialty Symposium (MOSS), Singapore*, 2016.

[8] API RP 2A-LRFD. Recommended practice for planning, designing and constructing fixed offshore platforms - load and resistance factor design. American Petroleum Institute, Washington, D.C., USA., 2019.

[9] J.R. Bidlot. Twenty-one years of wave forecast verification. Newsletter Number 150 – Winter 2016/17, European Centre for Medium-range Weather Forecasts (ECMW), Reading, UK, 2017.

[10] E. M. Bitner-Gregersen and A. Toffoli. Uncertainties of Wind Sea and Swell Prediction From the Torsethaugen Spectrum. In *Proceedings of the 28th International Conference on Offshore Mechanics and Arctic Engineering, Hawaii, Honolulu*, 2009.

[11] E.M. Bitner-Gregersen and S. Haver. Joint environmental model for reliability calculations. In *ISOPE. Proc. 1st Int. Offshore and Polar Eng. Conf., Edinburgh, UK*, volume 1, pages 246–253, 1991.

[12] A.K. Brook and R.G. Standing. A theoretical and experimental investigation of barge roll damping. In *Proceedings of the Fourth international conference on stability if ships and ocean vehicle, STAB '90, Naples, Italy*, 1990.

[13] D. C. Brooker, G. K. Cole, and J. D. McConochie. The influence of hindcast modeling uncertainty on the prediction of high return period wave conditions. *Proceedings of the International Conference on Offshore Mechanics and Arctic Engineering - OMAE, Vancouver, British Columbia, Canada*, 2004.

[14] D. T. Brown, R. Eatock Taylor, and M. H. Patel. Barge motions in random seas - a comparison of theory and experiment. *Journal of Fluid Mechanics*, 129:385–407, 1983.

[15] K. Bruserud and S. Haver. Comparison of wave and current measurements to NORA10 and NoNoCur hindcast data in the northern North Sea. *Ocean Dynamics*, 66:823–838, 2016.

[16] Bureau Veritas. Rules for the Classification of Steel Ships. Part B - Hull and Stability. NR 467.B1 DT R12 E , Paris, France, January 2020.

[17] K.V. Bury. *Statistical Distributions in Engineering*. Cambridge: Cambridge University Press., 1999.

[18] S. Chakrabarti. Empirical calculation of roll damping for ships and barges. *Ocean Engineering*, 28(7):pages 915–932, 2001.

[19] H.S. Chan, E. Armaoglu, M. Thomson, M Garner, A Parisotto, and S. Sovilla. Response forecasts for a suspended wellbay module and flare tower during transit to shore. In *Proceedings of the Twenty-ninth International Ocean and Polar Engineering Conference, ISOPE, Honolulu, Hawaii, USA, June 16-21*, 2019.

[20] R.P. Dallinga, A.B. Aalbers, and J.W.W. van der Vegt. Design Aspects for Transport of Jackup Platforms on a Barge. Offshore Technology Conference (OTC), Houston, 1984. Paper no. OTC1984-4733.

[21] M. Deelen and J. B. de Jonge. An operational based method for determining the design sea states of heavy transport vessels. *Marine Heavy Transport and Lift IV, London, UK, 29-30 October*, 2014.

[22] O. Ditlevsen and H.O. Madsen. *Structural Reliability Methods*. Department of Mechanical Engineering, Technical University of Denmark, 2007. http://od-website.dk/books/OD-HOM-StrucRelMeth-Ed2.3.7.pdf [Accessed 2020-08-27].

[23] DNV. Rules for Planning and Execution of Marine Operations, 1996/2000. Det Norske Veritas, Oslo, Norway.

[24] DNV GL. When Noble met Denton, 2015. `https://www.dnvgl.com/oilgas/perspectives/when-noble-met-denton.html` [Accessed 2020-08-27].

[25] DNV GL. Rules for classification - Ships, July 2020. Oslo, Norway.

[26] DNV-OS-H101. Marine Operations, General, 2011. Det Norske Veritas, Oslo, Norway.

[27] DNV-OS-H202. Sea transport operations, 2015. Det Norske Veritas, Oslo, Norway.

[28] DNVGL-OS-C101. Design of offshore steel structures, general - LRFD method. DNVGL, Oslo, Norway, July 2019.

[29] DNVGL-RP-C205. Environmental Conditions and Environmental Loads. DNV GL, Oslo, Norway, December 2019.

[30] DNVGL-RP-N101. Risk management in marine - and subsea operations. DNVGL, Oslo, Norway, September 2019.

[31] DNVGL-ST-N001. Marine Operations and Marine Warranty. DNV GL, Oslo, Norway, 2020.

[32] G. Dong and T. Moan. Prediction of ultimate behaviour of plate girders in transverse frames. *Proceedings of the Sixteenth International Offshore and Polar Engineering Conference, ISOPE, San Francisco, California, USA*, 2006.

[33] M.J. Downie, P.W. Bearman, and J.M.R Graham. Effect of vortex shedding on the coupled roll response of bodies in waves. *Journal of Fluid Mechanics*, 189:243–261, 1988.

[34] I.N. Dragos. Risk control - marine warranty survey. *Journal of Engineering Studies and Research*, 18(2):66–76, 2012.

[35] EN 10025-1. Hot rolled products of structural steels. Part 1: General technical delivery conditions. European Committee for Standardization, Brussels, Belgium, 2005.

[36] EN 1993-1-1. Eurocode 3. Design of steel structures - Part 1-1: General rules and rules for buildings. European Committee for Standardization, Brussels, Belgium, 2005.

[37] W.A. Ewers, P.E. Freathy, K. Lindemann, and K. Børresen. Barge Motions Research Projects, Phase 2 Report, Part 3 Further work on viscous roll damping, for a consortium of companies organised by Noble Denton and Associates Ltd. Technical report, 1979. Atkins Research & Development, Surrey, UK, and Det Norske Veritas, Oslo, Norway.

[38] O.M. Faltinsen. *Sea Loads on Ships and Offshore Structures*. Cambridge: Cambridge University Press., 1990.

[39] O.M. Faltinsen. *Hydrodynamics of High-Speed Marine Vehicles*. Cambridge University Press, New York, USA, 2005.

[40] A.C. Fernandes and A.C. Oliveira. The roll damping assessment via decay model testing (new ideas about an old subject). *Journal of Marine science and application*, 8(2):144–150, June 2009.

[41] S. Fjeld. Reliability of Offshore Structures. *Journal of Petroleum Technology*, 30(10):1486–1496, October 1978.

[42] W. Froude. *On the Rolling of Ships*. Parker, Son and Bourn, London, UK, 1861.

[43] FugroOceanor. http://www.oceanor.no/services/. Accessed 2020-08-27.

[44] I.J. Fylling. Analysis of towline forces in ocean towing systems. Technical report, Department of Marine Technology - The Norwegian Institute of Technology, Nov. 1979.

[45] O. Gaidai, G. Storhaug, and A. Naess. Extreme Value Statistics of Ship Rolling. In *Proceedings of PRADS 2010, the 11th International Symposium on Practical Design of Ships and other Floating Structures, Rio de Janeiro, Brazil*, September 2010.

[46] S. Ghosh, M.A. Jacobs, and J.A. Mercier. Role of marine warranty surveyors and their requirements for selected items. *Proceedings of the International Conference on Offshore Mechanics and Arctic Engineering - OMAE, Vancouver, British Columbia, Canada*, pages 647–662, 2004.

[47] GL Noble Denton. General Guidelines for Marine Projects. Technical Standard Committee, London, UK, 2013.

[48] GOMO. Guidelines for Offshore Marine Operations, UK/Norway. www.g-omo.info, 2020.

[49] J.M.R. Graham. The forces on sharp-edged cylinders in oscillatory flow at low Keulegan-Carpenter numbers. *Journal of Fluid Mechanics*, 97:331–346, 1980.

[50] J.M.R Graham. Calculation of Hydrodynamic Damping of Offshore Structures. In *Proceedings of the International Conference on Behaviour of Offshore Structures, BOSS. Trondheim, Norway*, pages 579–590, 1988.

[51] J.M.R. Graham and M.J. Downie. Viscous damping of floating bodies in waves. In *Proceedings of the ASME 2015 34th International Conference on Ocean, Offshore and Arctic Engineering, OMAE*, 2015.

[52] J.M.R. Graham and T.E. Kendon. Viscous Damping of Large Floating Structures. *IUTAM Symposium on Fluid-Structure Interaction in Ocean Engineering, © Springer Science+Business Media B.V.*, 8:69–78, 2008.

[53] Grillage and Seafastening Design. Guidelines No. VMO 1.2. 1989. Det Norske Veritas, Oslo, Norway.

[54] W. Guachamin Acero, L. Li, Z. Gao, and T. Moan. Methodology for assessment of the operational limits and operability of marine operations. *Ocean Engineering*, 125:308–327, 2016.

[55] O. T. Gudmestad. Risk Assessment Tools for Use During Fabrication of Offshore Structures and in Marine Operations Projects. *Journal*

of Offshore Mechanics and Arctic Engineering, 124:153–161, August 2002.

[56] C. Guedes Soares. Representation of double-peaked sea wave spectra. *Ocean Engineering*, 11(2):185–207, 1984.

[57] G.R. Gunnu. *Safety and efficiency enhancement of anchor handling operations with particular emphasis on the stability of anchor handling vessels*. PhD thesis, Department of Marine Technology, Norwegian University of Science and Technology (NTNU), Trondheim, Norway, 2017.

[58] H. Haakenstad, Ø. Breivik, M. Reistad, and O. J. Aarnes. NORA10EI: A revised regional atmosphere-wave hindcast for the North Sea, the Norwegian Sea and the Barents Sea. *International Journal of Climatology*, 40(10):4347–4373, 2020.

[59] Ø. Hagen and B. Riise. Ensemble Forecasts Used for Extreme Wave Warning and Platform Unmanning Strategies. In *ASME 2012 31st International Conference on Ocean, Offshore and Arctic Engineering Volume 2: Structures, Safety and Reliability, Rio de Janeiro, Brazil*, July 2012.

[60] A.R. Harrison. Marine warranty surveying for offshore projects and issues faced in the current market. *Annual Conference of the Maritime Law Association of Australia & New Zeeland*, 23(2), 2009.

[61] S. Haver. Uncertainties Related to Hindcast Wave Data. *Proceedings of the International Conference on Offshore Mechanics and Arctic Engineering - OMAE, Houston, Texas, USA*, 1994.

[62] S. Haver. Metocean modelling and prediction of extremes. Haver & Havet, University in Stavanger (UIS), Norway, August 2020.

[63] Sverre Haver. Wave climate off northern Norway. *Applied Ocean Research*, 7(2):85–92, April 1985.

[64] N. Hogben, N. M. C. Da Cunha, and G. F. Olliver. *Global wave statistics*. British Maritime Technology Ltd, Brown Union, London, UK, 1986.

[65] E. Hollnagel. *Barriers and Accident Prevention*. Ashgate Publishing Limited, Hampshire, UK, 2004. ISBN 0 7546 4301 8.

[66] D.M. Hunns and B.K. Daniels. Paired comparisons and estimates of failure likelihood. *Design Studies*, 2(1):9–18, Jan. 1981.

[67] Y. Ikeda, T. Fujiwara, and T. Katayama. Roll damping of a sharp-cornered barge and roll control by a new-type stabilizer. *Proceedings of the Third International Offshore and Polar Engineering Conference, ISOPE, Singapore*, 1993.

[68] Y. Ikeda, Y. Himeno, and N. Tanaka. Components of Roll Damping of Ships at Forward Speed. Report No. 00404, Department of Naval Arhitecture, University of Osaka Prefecture, August 1978.

[69] IMO. *Code of Safe Practice for Cargo Stowage and Securing, Annex 13*. International Maritime Organization, London, UK, 1991.

[70] IMO. *Guidelines for Safe Ocean Towing*. International Maritime Organization, London, UK, 1998.

[71] ISO 17776. Petroleum and natural gas industries - Offshore production installations - Major accident hazard management during the design of new installations. International Organization for Standardization, Geneva, Switzerland, 2016.

[72] ISO 19901-6. Petroleum and natural gas industries. Specific requirements for offshore structures. Part 6: Marine Operations. International Organization for Standardization, Geneva, Switzerland, 2009.

[73] ISO 19902. Petroleum and natural gas industries - Fixed steel offshore structures. International Organization for Standardization, Geneva, Switzerland, 2013.

[74] ISO 6892-1. Metallic materials - Tensile testing - Part 1: Method of test at room temperature. International Organization for Standardization, Geneva, Switzerland, 2016.

[75] ITTC Specialist Committee on Stability in Waves. Numerical Estimation of Roll Damping. In Proceedings of the 26th International Towing Tank Conference, Rio de Janeiro, Brazil, 2011.

[76] R.L. Jack, D.R. Noble-Smith, and J. Huntington. Risk Reduction in Towing Offshore Structures. *Journal of Petroleum Technology*, Volume 32, Number 1(1):21–26, January 1980.

[77] JCSS. Probabilistic model code. Part 3: Material properties. *Joint Committee on Structural Safety (JCSS), https://www.jcss-lc.org*, 2000.

[78] H. Jia. *Structural Reliability Analysis of Intact and Damaged Ships in a Collision Risk Analysis Perspective.* PhD thesis, Department of Marine Technology, Norwegian University of Science and Technology (NTNU), Trondheim, Norway, 2011.

[79] J. M. J. Journée. Motions of rectangular barges. In *Proceedings of the 10th International Conference on Offshore Mechanics and Arctic Engineering, OMAE, Stavanger, Norway. Publ. by ASME, Vol 1, Part B*, pages 641–650, 1991.

[80] H. Kato. Effect of Bilge Keels on the Rolling of Ships. *Memories of the defence Academy, Japan*, 4(3):369–384, 1966.

[81] J.A. Keuning and W. Beukelman. Hydrodynamic coefficients of rectangular barges in shallow water. In *Proc. Second Int. Conf. on the Behaviour of Off-Shore Structures (BOSS), London, UK, AUG. 28-31*, pages 105–124, 1979.

[82] B.O. Kvamme, A.P. Orimolade, S. Haver, and O.T. Gudmestad. Marine operation windows offshore norway. *Proceedings of the ASME 2016 35th International Conference on Ocean, Offshore and Arctic Engineering, OMAE*, 2016.

[83] A. Kvitrud, G. Ersdal, and R.L. Leonhardsen. On the risk of structural failure on norwegian offshore installations. In *Proceedings of the Eleventh International Offshore and Polar Engineering Conference Stavanger, Norway, June 17-22*, 2001.

[84] K. Lindemann. Extreme Value Statistics and Exposure Time: A Simple Method to Establish Well Defined Criteria for Marine Operations. In *In proceedings of the 18th Annual Offshore Technology Conference (OTC), Houston, Texas, USA*, number 5142, pages 519–525, May 1986.

[85] Lloyds. Rules and Regulations for the Classification of Ships. Lloyd's Register Group Limited, London, UK, July 2019.

[86] LOC. Guidelines for Marine Operations. London Offshore Consultants Limited, Ledbury, Herefordshire, UK, 1997.

[87] Ø. Lundby. Marine operations rules, revised Alpha factor - Joint Industry Project. Report No. 2006-1756, Rev. 03. Technical report, DNV, Oslo, Norway, 2007.

[88] H. Madsen, S. Krenk, and N.C. Lind. *Methods of Structural Safety.* Prentice-Hall Inc., Englewood Cliffs, New Jersey, USA, 1986.

[89] H.O. Madsen. Omission sensitivity factors. *Journ. of Structural Safety*, 5:35–45, 1988.

[90] M.A. Maes, S. Abelatif, and R. Frederking. Recalibration of partial load factors in the Canadian offshore structures standard CAN/CSA-S471. *Can. J. Civ. Eng.*, 31:684–694, 2004.

[91] A.K. Magnusson. What is true sea state? *11th International Workshop on Wave Hindcasting and Forecasting and Coastal Hazard Symposium, Halifax, Canada, October 18-23*, 2009.

[92] Marin. Safetrans, the safe design and operation of marine transports. Wageningen, The Netherlands. https://www.marin.nl/storage/uploads/2375/files/SafeTrans.pdf, Accessed 2020-08-27.

[93] Matlab. Ver. 7.11. The MathWorks Inc., Natick, Massachusetts, USA, 2010.

[94] R.E. Melchers. Human error in structural reliability assessments. *Reliability Engineering*, 7(2):61–75, 1984.

[95] R.E. Melchers and A.T. Beck. *Structural Reliability Analysis and Prediction.* John Wiley & Sons Ltd, Hoboken, New Jersey, USA, third edition, 2018.

[96] T. Moan. Safety Level Across Different Types of Structural Forms and Materials - Implicit in Codes for Offshore Structures. Technical report, SINTEF Report No. STF70 A95210. Trondheim, Norway, 1995.

[97] T. Moan. Safety of offshore structures. Technical Report No. 2005-04, Centre for Offshore Research & Engineering. National University of Singapore, 2005.

[98] T Moan. Integrity management of offshore structures and its implication on computation of structural action effects and resistance. *IOP Conference Series: Materials Science and Engineering*, 276:012033, December 2017.

[99] T. Moan, P.K. Das, X.K. Gu, P. Friis-Hansen, L. Hovem, G. Parmentier, E. Rizzuto, T. Shigemi, and J. Spencer. Reliability based structural design and code development. In *16th international ship and offshore structures congress, Southampton, UK*, Aug. 2006.

[100] T. Moan, Z. Gao, and E. Ayala-Uraga. Uncertainty of wave-induced response of marine structures due to long-term variation of extratropical wave conditions. *Marine Structures*, 18(4):359–382, May 2005.

[101] B. Molin. On the frictional damping in roll of ship sections. *International Shipbuilding Progress*, 51(1):59–85, 2004.

[102] A. Naess and O. Gaidai. Estimation of extreme values from sampled time series. *Structural Safety*, 31(4):325–334, 2009.

[103] A. Naess and T. Moan. *Probabilistic design of offshore structures. In: S. Chakrabarti (ed.), Handbook of offshore engineering, vol. 1.*. Elsevier, 2005.

[104] A. Naess and T. Moan. *Stochastic dynamics of marine structures.* Cambridge University Press, 2013.

[105] L.S. Nascimento, L.V.S. Sagrilo, and G.B. Ellwanger. On the extreme value analysis of jack-up dynamic response parameters. *Marine Systems and Ocean Technology*, 6(2):75–86, Dec. 2011.

[106] A. Natskår and T. Moan. An Experimental Investigation of Barge Roll in Severe Beam Seas. In *Proceedings of PRADS 2010, the 11th International Symposium on Practical Design of Ships and other Floating Structures, Rio de Janeiro, Brazil*, volume 1, pages 415–425, 2010.

[107] A. Natskår and T. Moan. Structural reliability analysis of the seafastening structure for sea transports of heavy objects. *Issued for publication in Ocean Engineering*, 2020.

[108] A. Natskår, T. Moan, and P. Ø. Alvær. Uncertainty in forecasted environmental conditions for reliability analyses of marine operations. *Ocean Engineering*, 108:636–647, 2015.

[109] A. Natskår and S. Steen. Rolling of a transport barge in irregular seas, a comparison of motion analyses and model tests. *Marine Systems and Ocean Technology*, 8(1):5–19, 2013.

[110] Naval Sea Systems Command. *U.S. Navy Towing Manual.* SL740-AA-MAN-010, Washington, D.C., USA, 2013.

[111] J. N Newman. *Marine Hydrodynamics*. Cambridge: The MIT Press, 1977.

[112] F. G. Nielsen. Lecture notes in marine operations. Department of Marine Technology, Norwegian University of Science and Technology (NTNU), Trondheim, Norway, 2007.

[113] NORSOK. N-004 Design of steel structures. Norwegian Technology Standards, Oslo, Norway, February 2013.

[114] NORSOK. N-003, Actions and action effects. Norwegian Technology Standards, Oslo, Norway, 2017.

[115] Norwegian Meteorological Institute. 2D wave energy spectra. Email received 2020-05-25 from Anne Hesby Palm.

[116] NTNU. https://www.ntnu.edu/imt/lab/cybernetics. Accessed 2020-09-13.

[117] M. K. Ochi and E. N. Hubble. On Six-Parameters Wave Spectra. *Proceedings of the 15th Coastal Engineering Conference*, 1:301–328, 1976.

[118] M. Pakkan, D. Heng, and O.T. Gudmestad. Polar Lows and Their Implications on Marine Operations: Survivability Criteria. In *Proceedings of the ASME 2013 32nd International Conference on Ocean, Offshore and Arctic Engineering OMAE*, 2013.

[119] M. Prevosto. Distribution of Maxima of Non-Linear Barge Rolling with Medium Damping. In *Proceedings of the Eleventh International Offshore and Polar Engineering Conference, ISOPE, Stavanger, Norway, June 17-22*, volume III, pages 307–316, 2001.

[120] W. G. Price and R. E. D. Bishop. *Probabilistic theory of ship dynamics*. ISBN 0-412-12430-0. Chapman and Hall, London, UK, 1974.

[121] Proban. *Theory Manual*, 2004. Det Norske Veritas, Oslo, Norway.

[122] M. R. Rajashekhar and B. R. Ellingwood. A new look at the response surface approach for reliability analysis. *Structural Safety*, 12(3):205–220, 1993.

[123] M. Reistad, Ø. Breivik, H. Haakenstad, O. J. Aarnes, B. R. Furevik, and J.R. Bidlot. A high-resolution hindcast of wind and waves for the North Sea, the Norwegian Sea, and the Barents Sea. *J. Geophys. Res.*, 116:18, 2011.

[124] W. Rettedal and T. Aven. *Integrating QRA and SRA methods within a predictive Bayesian approach: An example from offshore projects.* Safety and Reliability of Industrial Products, Systems and Structures - Guedes Soares (ed), Taylor & Francis Group, London, UK, 2010.

[125] W. K. Rettedal. *Quantitative Risk Analysis and Structural Reliability Analysis in Construction and Marine Operations of Offshore Structures.* PhD thesis, Aalborg University, Denmark and Stavanger University College, Norway, 1997.

[126] J. B. Roberts, J. F. Dunne, and A. Debonos. Estimation of Ship Roll Parameters in Random Waves. *J. Offshore Mech. Arct. Eng*, 114:114–121, May 1992.

[127] G. Rodriguez, C. Guedes Soares, and U. Machado. Uncertainty of the sea state parameters resulting from the methods of spectral estimation. *Ocean Engineering*, 26:991–1002, 1999.

[128] V. Rumawas. *Human Factors in Ship Design and Operation: Experiential Learning.* PhD thesis, Department of Marine Technology, Norwegian University of Science and Technology (NTNU), Trondheim, Norway, 2016.

[129] SESAM. *User Manual - Wadam. Wave Analysis by Diffraction and Morison Theory*, January 2016. DNV GL, Oslo, Norway.

[130] Z. Shu and T. Moan. Effects of Avoidance of Heavy Weather on the Wave-Induced Load on Ships. *Journal of Offshore Mechanics and Arctic Engineering*, 130(2), 2008.

[131] SIMO. *Simulation of Marine Operations.* Sintef Ocean, Trondheim, Norway, https://www.sintef.no/globalassets/upload/marintek/pdf-filer/sofware/simo.pdf. Accessed 2020-08-27.

[132] Sintef Ocean. https://www.sintef.no/en/all-laboratories/towing-tanks/. Accessed 2020-09-13.

[133] S. Sklet. Safety barriers: Definition, classification, and performance. *J. Loss Prev. Process Ind.*, 19:494–506, 2006.

[134] J.D. Sørensen. Notes in structural reliability theory and risk analysis, 2004. Institute of Building Technology and Structural Engineering Aalborg University, Denmark.

[135] R. G. Standing, G. E. Jackson, and A. K. Brook. Experimental and theoretical investigation into the roll damping of a systematic series of two-dimensional barge sections. In *Proceedings of the 6th International Conference on Behaviour of Offshore Structures (BOSS), London, UK*, volume 2, pages 1097–1111, 1992.

[136] R.G. Standing. Prediction of viscous roll damping and response of transportation barges in waves. In *Proceedings of the First International Offshore and Polar Engineering Conference, ISOPE, Edinburgh, UK, 11-16 August*, pages 409–419, 1991.

[137] S. Steen. Experimental Methods in Marine Hydrodynamics. Faculty of Engineering Science and Technology - Norwegian University of Science and Technology, NTNU, Trondheim, Norway, August 2014.

[138] M.G. Stewart and R.E. Melchers. Simulation of human error in a design loading task. *Structural safety*, 5:285–297, 1988.

[139] W.P. Stewart and W.A. Ewers. Wave induced motions of marine deck cargo barges. In *Proceedings of the Second International Conference on the Behaviour of Off-Shore Structures (BOSS79), London, UK. 28-31 August*, 1979.

[140] N. Tanaka. A study on the Bilge Keels. (Part 4. On the eddy making resistance to the rolling of a ship hull). *Journal of Society of Naval Architecture, Japan*, 109:205–212, 1961.

[141] K. Torsethaugen and S. Haver. Simplified Double Peak Spectral Model for Ocean Waves. In *Proceedings of the Fourteenth International Offshore and Polar Engineering Conference, Toulon, France*, 2004.

[142] V.M. Trbojevic, O.T. Gudmestad, and W.K. Rettedal. Accounting for management and organisational factors in risk analysis of marine operations. In *Proceedings of the European Safety and Reliability Conference, ESREL - Risk, Reliability and Societal Safety, Stavanger, Norway, 25-27 June*, 2007.

[143] L. Tvedt. Proban probabilistic analysis. *Journal of Structural Safety*, 28:150–163, 2006.

[144] J. H. Vugts. The hydrodynamic coefficients for swaying heaving and rolling cylinders in a free surface. Report No. 194, Laboratorium voor Scheepsbouwkunde, Technische Hogeschool Delft, the Netherlands, January 1968.

[145] Wamit. *User Manual, Version 7.3*. Wamit Inc., Chestnut Hill, Massachusetts, USA, 2019.

[146] S. Wilcken. Alpha factors for the calculation of forecasted operational limits for marine operationsinthe barents sea. Master's thesis, Faculty of Science and Technology, University of Stavanger, Norway, 2012.

[147] WMO Lead Centre for Wave Forecast Verication LC-WFV. Intercomparison of operational wave forecasting systems against in-situ observations, Part I: Significant wave height (SWH). European Centre for Medium-Range Weather Forecasts, ECMWF, Reading, UK, 2019.

Appendix A

Appended papers

A.1 Paper 1

Paper 1:
Rolling of a Transport Barge in Irregular Seas, a Comparison of Motion Analyses and Model Tests.
Authors: Asle Natskår and Sverre Steen.
Published in *Marine Systems & Ocean Technology*, Vol. 8 No. 1, pp. 05-19, June 2013.

A.2 Paper 2

Paper 2:
Uncertainty in forecasted environmental conditions for reliability analyses of marine operations.
Authors: Asle Natskår, Torgeir Moan and Per Ø. Alvær.
Published in *Ocean Engineering*, Vol. 108, pp. 636-647, 2015.

Ocean Engineering 108 (2015) 636–647

Contents lists available at ScienceDirect

Ocean Engineering

journal homepage: www.elsevier.com/locate/oceaneng

Uncertainty in forecasted environmental conditions for reliability analyses of marine operations

Asle Natskår [a,*], Torgeir Moan [a], Per Ø. Alvær [b]

[a] Centre for Ships and Ocean Structures (CeSOS), Norwegian University of Science and Technology (NTNU), Trondheim, Norway
[b] DNV GL Marine Operations, VMO, Norway

ARTICLE INFO

Article history:
Received 3 September 2014
Accepted 24 August 2015

Keywords:
Marine operations
Weather forecast
Weather criteria
Forecast uncertainty

ABSTRACT

Marine operations, e.g., the sea transport of heavy objects and the installation of offshore units and equipment, need to be planned and executed with proper consideration for environmental conditions and operational limits with respect to vessel motions and structural loads. Marine operations with a limited duration, usually less than 72 h, are typically designed as weather-restricted operations. The environmental design criteria are thus predefined, and the actual weather conditions are confirmed by weather forecasts issued immediately prior to the start of such an operation. Marine operations of longer duration are typically designed as weather-unrestricted operations, and the environmental conditions are calculated based on long-term statistics, possibly depending on the season. More detailed information about uncertainties in weather forecasts could increase the feasible duration of weather-restricted operations. The uncertainty inherent in weather forecasts, notably that in the significant wave height, is studied. Further, a method to assess the reliability of weather forecasts is described. Data from the Norwegian Sea are used to quantify the uncertainty in forecasted data. The probability of exceeding the design criteria used in the planning of a weather-unrestricted marine operation can be estimated based on forecast statistics. The corresponding uncertainty can be incorporated into structural reliability analyses.

1. Introduction

The work presented in this paper is part of a research project regarding the level of reliability inherent in marine operations. The uncertainty in the environmental conditions, and hence in the wave- and wind-induced load effects, that are considered in the planning of an operation is important with respect to the overall reliability level. The scope of this paper encompasses the study of methods to account for the uncertainty inherent in weather forecasts for marine operations. This is of interest, e.g., with regard to structural design for sea fastening (i.e., the design of structures to secure a transported object to the transport vessel), but the approach is more general. The marine operations considered herein are specially planned, non-routine operations of limited duration related to the load transfer, transport and installation of objects, typically in the offshore oil and gas industry. The need for special planning may arise because the transported object is large and/or heavy or has a high economic value or a long replacement time. Therefore, the consequences of severe damage to or total loss of such a transported object are large, involving economic loss and possibly pollution of the environment. Most likely, there will also be delays in the project, and some loss of reputation may be suffered by the companies involved. It is therefore necessary to quantify the uncertainties inherent in such an operation. The environmental conditions are important input for the planning of marine operations, particularly with regard to the motion analysis of floating vessels. Hence, the uncertainty in the environmental conditions and how it is accounted for in the planning/design exert a considerable effect on the safety level of such an operation.

Marine operations can be designed in accordance with several Standards and Guidelines. These operations are generally defined as either weather-restricted or weather-unrestricted operations, depending on their duration. For weather-restricted operations planned in accordance with DNV (2011) or GL Noble Denton (2013), the uncertainty inherent in the weather forecasts of the significant wave heights and wind speeds is accounted for by a so-called α-factor; see Eq. (2). For weather-unrestricted operations, the weather criteria cannot be based on forecasts but instead must be based on long-term statistical data on the environmental conditions.

The uncertainty in the forecasting of significant wave heights is quantified by comparing the forecasted wave heights with the

* Corresponding author.
E-mail address: natskar@ntnu.no (A. Natskår).

http://dx.doi.org/10.1016/j.oceaneng.2015.08.034

actual waves at the location. Instead of observed/measured significant wave heights, hindcast data are used. The uncertainty is described by estimating the mean values and standard deviations of the difference and ratio between the hindcasted and forecasted wave heights. Data from the Norwegian Sea are applied to quantify the uncertainty in the forecasted data.

The objective is to incorporate the uncertainty resulting from weather forecasts into reliability analyses for marine operations. For most marine operations, the environmental loads govern the planning and structural design, and hence, the uncertainty in forecasted environmental conditions is important input for these analyses. The uncertainty in the forecasted significant wave height is studied in this paper. The intent is to address reliability analyses in a separate paper.

2. Planning of marine operations

2.1. Design standards for marine operations

Marine operations must be designed in accordance with certain standards/guidelines. We are aware of two such standards and two such guidelines:

- DNV-OS-H101, Marine Operations, General, DNV (2011).
- GL Noble Denton (2013), General Guidelines for Marine Projects.
- ISO 19901-6 (2009) Petroleum and natural gas industries. Specific requirements for offshore structures. Part 6: Marine Operations.
- London Offshore Consultants Limited, Guidelines for Marine Operations, LOC (1997).

A key parameter for a marine operation is the duration. It is defined as the best estimate plus an ample margin to account for inaccuracies in schedule and delays. This is the approach used in all referenced standards. Using the notation from DNV (2011), the operation reference period, T_R, is defined as follows:

$$T_R = T_{POP} + T_C \tag{1}$$

where T_{POP} is the planned operation period and T_C is the estimated maximum contingency time. (The estimated maximum contingency time is often between 50% and 100% of the planned operation period, unless more accurate information is known.)

2.2. Weather-restricted operations

If the duration of the operation is less than 72 h, then the operation can be defined as a weather-restricted operation. An operation can also be defined as weather restricted if it can be halted and the handled object brought into safe conditions during the same period. For a sea transport operation, this means that the route must be divided into several legs, and ports or areas of shelter along the transport route must be predefined. Updated weather forecasts are received regularly throughout the entirety of such an operation.

Traditionally, the maximum duration of a weather-restricted operation has been three days including contingency time, i.e., $T_R \leq 72$ h. This limit is stated in ISO 19901-6 (2009), GL Noble Denton (2013), LOC (1997), NORSOK (2007). DNV (1996/2000) also adhered to this limit until 2011. In DNV (2011), however, the maximum operation period was increased to four days including contingency provided that the planned operation period is less than three days.

For marine operations in areas and seasons in which it can be demonstrated that weather forecasts are capable of predicting any extreme weather conditions over a longer period, the operation reference period may be increased accordingly. By contrast, in areas and/or seasons in which the corresponding reliable weather forecasts are not considered realistic, a shorter limit is to be applied.

If an operation is weather restricted, then the design environmental criteria are defined in an early phase of the project. Weather-restricted operations are beneficial because the owner, or his representative, may define the necessary environmental criteria (with the understanding that more strict environmental criteria may lead to more wait time before the operation can commence). The operation may commence when the weather forecasts indicate acceptable environmental conditions. The uncertainty in the weather forecasts and how to include this uncertainty in the planning of the operation thus become key issues.

To account for the uncertainty in weather forecasts, the operational environmental limits must be less than those considered in the design. According to DNV (2011) and GL Noble Denton (2013), the operational limit on the significant wave height can be expressed as

$$H_{s,oper} = \alpha H_{s,design} \tag{2}$$

where α is a parameter (≤ 1) that depends on both the duration of the operation and the level of forecasting and/or monitoring. In DNV (2011), α also depends on the significant wave height used in the design. The parameters for the base case, with one weather forecast available, are shown in Table 1. The α-factor can be increased if the wave height at the site of the operation is monitored and if there is a meteorologist on site (because the presence of a meteorologist will increase the confidence in weather forecasts at that location). In the DNV method, α accounts for the uncertainty in the weather forecast based on the planned duration ($T_{Dur} = T_{POP}$), but the forecasted wave height must be less than $H_{s,oper}$ for the operation reference period, T_R. In the GL Noble Denton method, α is based on the operation reference period ($T_{Dur} = T_R$). It should be noted that the safety formats (load and material factors) are somewhat different in the DNV and GL Noble Denton formulations and that the corresponding αs may not be directly comparable.

2.3. Weather-unrestricted operations

Operations with durations longer than three days are typically weather unrestricted. The separation between these two categories is important, as these two types of operations will be designed differently with respect to environmental loads.

Weather-unrestricted marine operations are not planned based on weather forecasts, because the duration of such an operation is longer than the duration over which weather forecasts are considered reliable. Instead, the environmental conditions used for planning must be based on long-term statistics. The environmental

Table 1
The parameter α as a function of operation duration from DNV (2011) and GL Noble Denton (2013) for the case of one weather forecast and no wave monitoring. In DNV (2011), the parameter definition is valid only for the North Sea and the Norwegian Sea and is given as a function of the design wave height.

T_{Dur} (h)	DNV			GL Noble Denton
	$H_s = 2$ m	4 m	≥ 6 m	
12	0.76	0.79	0.8	0.69
24	0.73	0.76	0.78	0.65
48	0.68	0.71	0.74	0.59
72	0.63	0.68	0.72	0.54

loads will then be based on a set of conditions with a given (low) probability of being exceeded.

In the planning of an unrestricted operation, the environmental criteria for the design must be based on long-term statistics accounting for

- the geographical area,
- the season of the year and
- the duration of the operation.

The extreme values of the wave heights may be calculated based on scatter diagrams, e.g., those from BMT Ltd (1986) or DNV (2014). It should be noted that the scatter diagrams from DNV are based on visual observations of the sea and may therefore, to some extent, include the effects of heavy weather avoidance (i.e., the largest waves are never observed).

For commercial projects, more accurate data may be purchased, e.g., from Fugro Oceanor. Data from Fugro Oceanor are derived from hindcast models and are calibrated against satellite data and, where available, in situ wave buoy data (FugroOceanor, 2012).

A study by Shu and Moan (2008) of a VLCC (very large crude carrier) and a bulk carrier indicated that the use of data from Fugro Oceanor yielded amidships bending moments that were approximately 15% larger than those deduced from the scatter diagrams of DNV (2014).

Another alternative is the computer program Safetrans from Marin (2007), which contains a large environmental database and can provide wave statistics for certain transport routes and seasons.

3. Description of environmental conditions

3.1. Weather forecasts

Several global systems are available for weather forecasters, e.g., those from the European Centre for Medium-Range Weather Forecasts (ECMWF) and the US-based National Centers for Environmental Prediction (NCEP).

The ECMWF system includes atmospheric variables, such as wind, temperature and precipitation, in addition to waves for offshore applications. The forecasts are based on the Ensemble Prediction System (EPS) (see, e.g., Saetra and Bidlot, 2004). The dynamical weather system is then simulated several times, each time changing the initial conditions slightly. The forecasters receive data from the ECMWF and perform their own evaluations and interpretations of the results, on which the weather forecasts are then based. The forecasts from different meteorologists may therefore differ for the same location and time.

For projects involving the installation of structures at offshore locations, weather forecasts are issued throughout the project period, which may be several years. In this paper, we will consider forecasted data for the Skarv oil and gas field, which is located 210 km west of Sandnessjoen, Norway, at a water depth of 350–450 m. The weather forecasts are provided by BP.

The forecasts include, amongst other information, the significant wave height H_s and the zero-crossing period T_z for wind-generated waves, swell and the total sea. The relation between these significant wave heights is $H_{s,total\ sea} = (H^2_{s,wind\ waves} + H^2_{s,swell})^{0.5}$. Only the total sea, i.e., the significant wave height resulting from both wind generated waves and swell, has been assessed in this paper. The lead time is defined as the numbers of hours from the time when the forecast is issued until the time for which it applies. The first set of forecasted values is for a three-hour lead time. Forecasted values are generally given every three hours for the first 72 h (for some forecasts, 69 h) and every six hours thereafter until the 168th hour. The data are for the year 2011 and include 1150 forecasts (generally three forecasts per day, with four forecasts for certain days).

3.2. Hindcast data

The formula given in Eq. (23) is a simple hindcast model, in which the significant wave height is estimated from the wind speed. This model does not, however, include the effects of wind

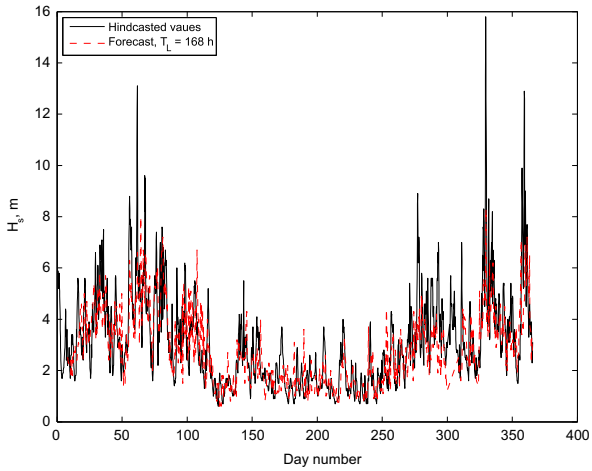

Fig. 1. Forecasted and hindcasted significant wave heights for a lead time of seven days.

fluctuations in time and space or any effects of the sea bottom topology, etc. A surface ocean wave model that does include such effects is used by meteorologists to hindcast wave data.

The hindcast data used in this study were provided by the Norwegian Meteorological Institute (DNMI, http://www.met.no). The data are based on the WAM Model of the Wamdi Group (1988). The quality of these hindcast data compared with the observed data is very good; see, e.g., Reistad et al. (2011). Therefore, in this paper, these hindcast data are used instead of observed data.

3.3. Comparing forecast and hindcast data

Forecasted and hindcasted wave heights are shown in Fig. 1. The figure shows the significant wave height in the year 2011 as a function of time in days (the first of January is day no. 1, and so on). The hindcasted significant wave height is shown in black. The forecasted significant wave height shown in red is given for a lead time of 168 h, i.e., these data represent the weather as forecasted seven days before (e.g., the wave height shown on day 30 is taken from the weather forecast issued on day 23, and so on). No details can be seen from the plot, but it is apparent that the trend is predicted quite well, even if the maximum significant wave heights (the peak values) are not forecasted. The maximum significant wave height at this location in 2011 was 15.8 m on day no. 329 (i.e., on 2011-11-25) at 18.00 h. In Fig. 2, the wave heights a few days before and after this date are shown together with the forecasted wave heights issued 72 and 168 h before. The maximum wave height was not captured in any of the forecasts, but the three-day forecast was, as expected, closer than the seven-day forecast.

The difference between the hindcasted and forecasted significant wave heights is also illustrated for two different lead times in Fig. 3 for one two-week period in June and one in December.

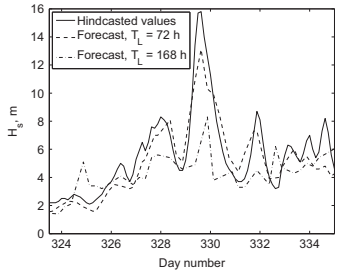

Fig. 2. Forecasted H_s values for lead times of three days and seven days together with hindcast H_s values for November 20 (day no. 324) to 30, 2011

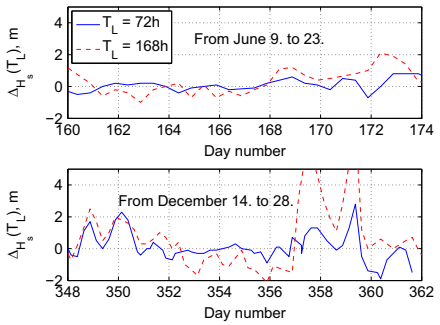

Fig. 3. The difference between hindcasted and forecasted significant wave heights ($\Delta_{H_s}(T_L)$ in Eq. (5)) for one two-week period in June and one in December 2011 for lead times of three and seven days

4. Model uncertainty in weather forecasts

4.1. Statistical models

The environmental conditions are an important input for marine operations. The significant wave height and wind speed are key information obtained from weather forecasts. For certain marine operations, the wave periods and wave directions may also be important. The uncertainties inherent in the environmental conditions predicted by forecasts, e.g., the significant wave height, can be quantified using two different mathematical models, one additive and one multiplicative model. The statistical parameters for these models are estimated based on hindcasted and forecasted data. The additive model is formulated as follows:

$$\Delta = Z_{true} - Z_{predicted} \tag{3}$$

where Δ is a stochastic variable. In our case, the predicted values are obtained from weather forecasts, whereas the true values are the hindcast data. In the multiplicative model, the stochastic variable χ is defined as follows:

$$\chi = \frac{Z_{true}}{Z_{predicted}} \tag{4}$$

Because the stochastic variable (Δ or χ) depends on the wave height, lead time (or forecasting period) and season, the mean value and the standard deviation of this variable are also functions of these parameters.

The statistical parameters necessary for a realization of the stochastic variable Δ (or χ) are calculated via the standard formulas using the software package (Matlab, 2010).

4.2. Uncertainty as a function of lead time

We now consider the significant wave height given in a weather forecast and define a stochastic variable $\Delta_{H_s}(T_L)$ as follows:

$$\Delta_{H_s}(T_L) = H_{s,hindcast} - H_{s,forecast}(T_L) \tag{5}$$

where T_L is the lead time. (A similar definition may also be used in the multiplicative model.) In Fig. 6, Δ_{H_s} is shown as a function of lead time.

The correlation between the forecasted and hindcasted significant wave heights is shown for several lead times in Fig. 4. As expected, the correlation is initially high and decreases with increasing lead time. In Fig. 5, the wave periods (spectral peak periods, T_p) are shown in a similar manner. It is apparent that the correlation between forecasted and hindcasted significant wave heights is higher than the correlation between forecasted and hindcasted wave periods. In fact, it seems preferable to use a fitted conditional probability distribution for the wave period but to base the wave height solely on the weather forecast.

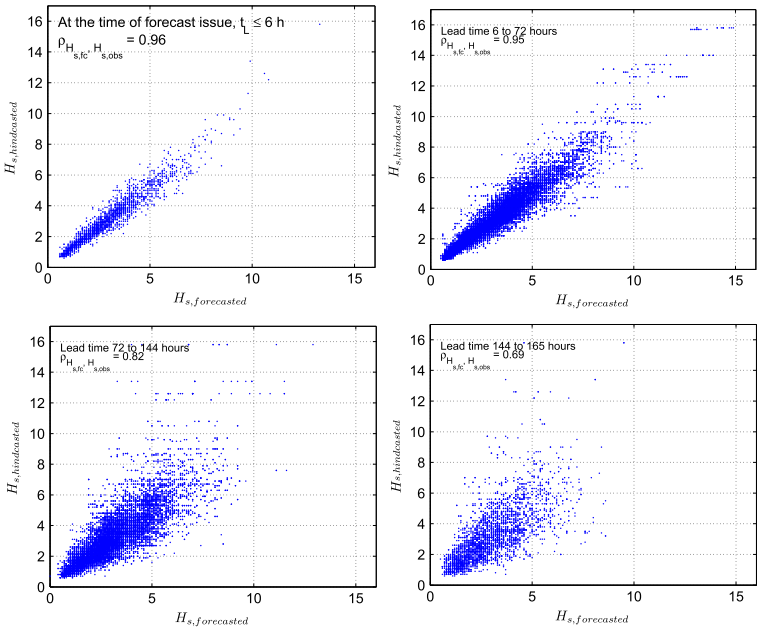

Fig. 4. Forecasted versus hindcasted significant wave height; note that for the longest forecast period, the largest waves are not forecasted

4.3. Uncertainty within a forecast period

In Eq. (5), the forecasting uncertainty is considered as a function of the lead time alone. For most marine operations, however, the primary concern is not whether a certain weather condition occurs exactly when forecasted but rather whether it occurs at all during the marine operation. Given the maximum wave height that is predicted to occur during a certain period, the probability that this wave height will be exceeded can be estimated.

A stochastic variable can be defined based on the additive model as follows:

$$\Delta_{H_{s,max}}(T_R) = H_{s,hc,max} - H_{s,fc,max} \tag{6}$$

where

$$H_{s,fc,max} = \max_{\tau}\{H_{s,forecast}(\tau)\} \quad \text{for } t \le \tau \le t + T_R \tag{7}$$

is the maximum forecasted significant wave height during the operation reference period and

$$H_{s,hc,max} = \max_{\tau}\{H_{s,hindcast}(\tau)\} \quad \text{for } t \le \tau \le t + T_R \tag{8}$$

is the maximum hindcasted significant wave height during the same period. Similarly, a stochastic variable can be defined based on the multiplicative model as follows:

$$\chi_{H_{s,max}}(T_R) = \frac{H_{s,hc,max}}{H_{s,fc,max}} \tag{9}$$

4.4. Quantification of model uncertainty

The methodology for estimating the uncertainty is as follows:

- Establish the observed data and weather forecasts for a certain period of time at a chosen location.
- Calculate $\Delta_{H_{s,max}}(T_R)$ from Eq. (6) and $\chi_{H_{s,max}}$ from Eq. (9).
- Calculate the statistical parameters.
- Choose the statistical distribution for the variables. For each data set, fit the distribution to the data.
- Extract percentile values for Δ_{H_s} and χ_{H_s} as functions of lead time and forecasted H_s, either based on the chosen statistical distribution or directly from the data sets.

The mean values and standard deviations for realizations of these stochastic variables (i.e., for the data from 2011) are shown in Figs. 7 and 8 for the additive and multiplicative models, respectively. (Note that whereas a perfect weather forecast would yield a mean value of 0 m for $\Delta_{H_{s,max}}$, the corresponding mean value would be equal to 1.0 for $\chi_{H_{s,max}}$.)

Figs. 7 and 8 present all-year data. However, the majority of marine operations are performed during the summer season, and therefore, seasonal data may be more relevant to use for analysing the uncertainties in weather forecasts. The data are therefore divided into two seasons: the summer season, from April to September, and the winter season, from October to March. (Data are often divided into four seasons or into monthly data, but because the data for only one year are considered here, only two seasons are defined.)

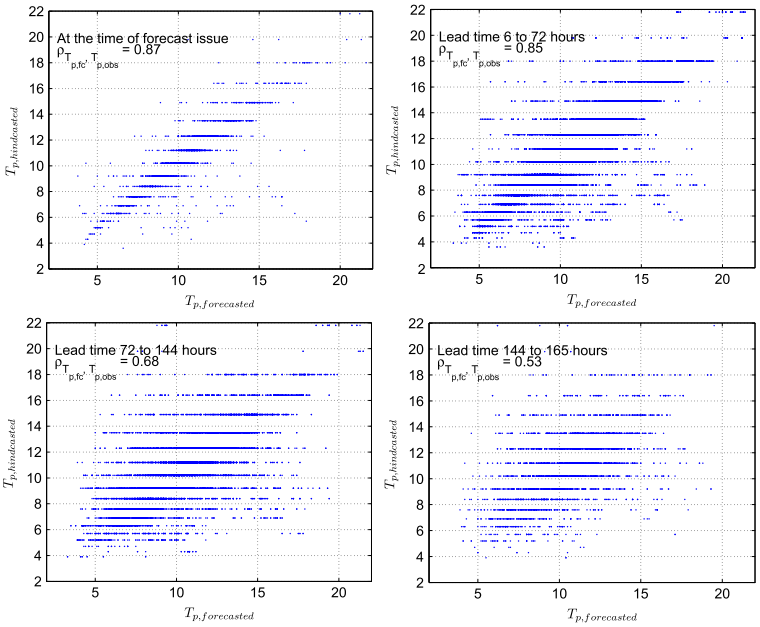

Fig. 5. Forecasted versus hindcasted peak wave periods

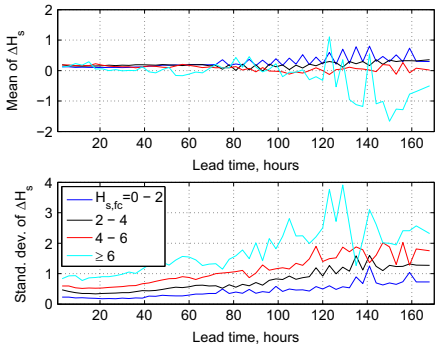

Fig. 6. Mean values and standard deviations of the stochastic variable Δ_{H_s} as a function of *lead time* for four groups of forecasted significant wave heights: 0–2 m, 2–4 m, 4–6 m and >6 m.

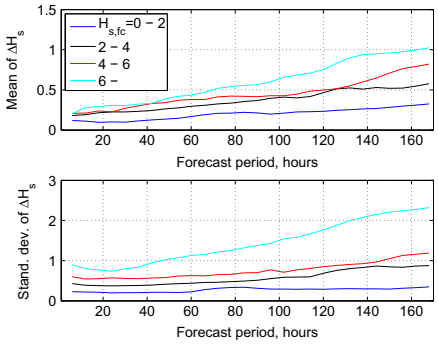

Fig. 7. Statistical parameters for the stochastic variable $\Delta_{H_s,max}$, based on the additive model, as functions of the *forecast period* for four groups of forecasted significant wave heights: 0–2 m, 2–4 m, 4–6 m and >6 m

In Figs. 9 and 10, the means and standard deviations of $\Delta_{H_s,max}$ are given for the summer and winter seasons for two groups of forecasted wave heights. The corresponding parameters for the variable $\chi_{H_s,max}$ are shown in Figs. 11 and 12.

It is evident that the means and standard deviations of $\Delta_{H_s,max}$ depend on the size of the forecasted significant wave height; this is particularly apparent from the all-year data presented in Fig. 7 and is, to some extent, also observed for the seasonal data presented in Figs. 9 and 10. In the groups corresponding to significant wave heights of 2–4 m and 4–6 m, the mean and the standard deviation are both larger during the winter season than during the summer season, except for H_s for the 4–6 m group for forecast periods of less than 50 h. (Notably, this variation could also, to some extent, be attributed to the fact that the forecasted wave

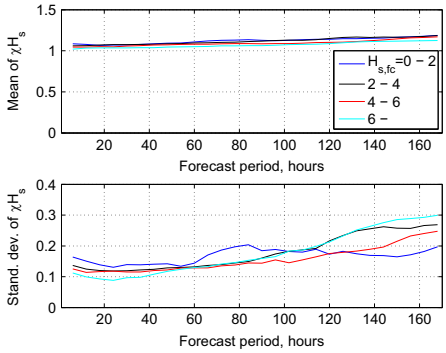

Fig. 8. Statistical parameters for the stochastic variable $\chi_{Hs,max}$, based on the multiplicative model, as functions of the *forecast period* for four groups of forecasted significant wave heights: 0–2 m, 2–4 m, 4–6 m and >6 m.

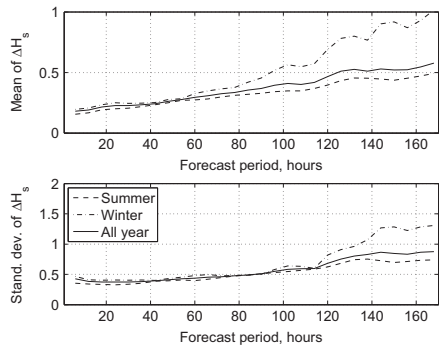

Fig. 9. Statistical parameters for the additive model as functions of the forecast period for the summer (April–September) and winter (October–March) seasons for forecasted significant wave heights between 2 and 4 m.

heights are larger during the winter season and could thus reflect behaviour similar to that observed in Fig. 7 rather than an actual seasonal variation.)

The effects of the forecasted wave height and season are smaller for $\chi_{Hs,max}$. In Fig. 8, the mean values are essentially identical for all wave height groups, and the spread in the estimated standard deviation also appears not to depend on the forecasted wave height.

Based on the above findings, we choose to use the multiplicative model and to include all wave heights in a single group when performing the analysis. The behaviours of the statistical parameters in this analysis are shown in Fig. 13.

4.5. Uncertainty in point estimates

The uncertainties in the model parameter estimates are calculated via a bootstrap method using Matlab (2010). The 95% confidence interval for the mean value in Fig. 13 is found to be within ±1% of the estimates. For the standard deviation, the

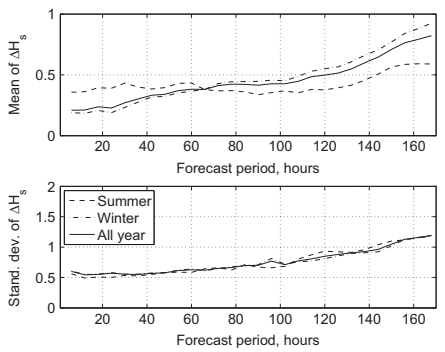

Fig. 10. Statistical parameters for the additive model as functions of the forecast period for the summer (April–September) and winter (October–March) seasons for forecasted wave heights between 4 and 6 m

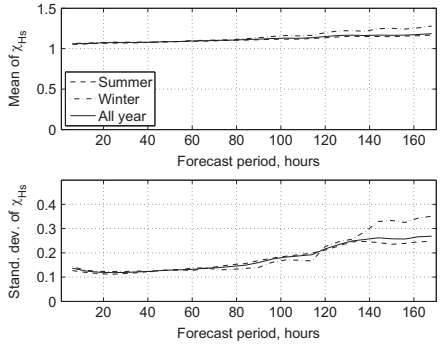

Fig. 11. Statistical parameters for the multiplicative model for the summer (April–September) and winter (October–March) seasons for forecasted wave heights between 2 and 4 m

corresponding interval ranges from −5% to +10% of the estimates. For the skewness and kurtosis, the uncertainties are much larger. The 95% confidence interval varies with the forecast period, but it ranges from approximately −50% to +100% of the estimates (hence, single values in the confidence interval may be from 0.5 times to 2 times the corresponding estimates). It is well known that estimates of skewness and kurtosis suffer from a relatively large uncertainty for data sets of limited size. However, these parameters are used here only to identify a plausible statistical distribution to be fitted to the data set, and hence, the uncertainties are considered acceptable.

5. Statistical description of environmental conditions

5.1. Significant wave heights

A short-term sea state is described by a significant wave height and a wave period and possibly also by other wave spectral parameters (bandwidth parameter, doubly peaked spectrum, etc.).

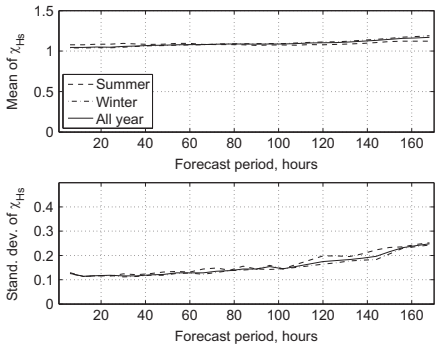

Fig. 12. Statistical parameters for the multiplicative model for the summer (April–September) and winter (October–March) seasons for forecasted wave heights between 4 and 6 m.

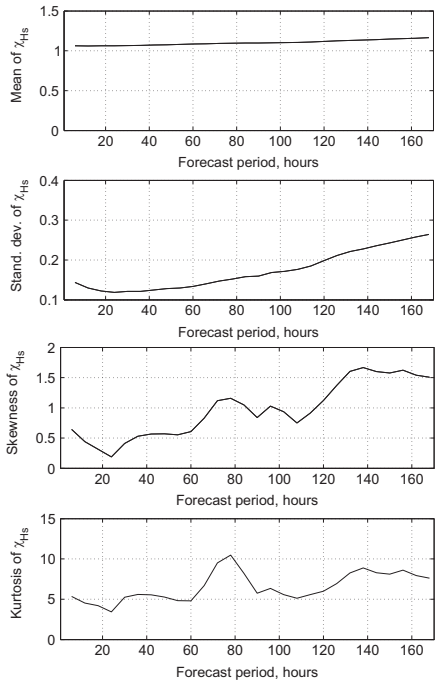

Fig. 13. Mean value, standard deviation, skewness and kurtosis of the stochastic variable $\chi_{Hs,max}$, based on the multiplicative model, as functions of the forecast period.

Given a forecasted significant wave height (i.e., the maximum predicted value during the forecast period) $h_{s,fc}$, the maximum significant wave height to be used in an operational design may be defined as a stochastic variable. In the additive model, this variable is defined as follows:

$$H_{s,max} = h_{s,fc} + \Delta_{Hs,max} \tag{10}$$

where $\Delta_{Hs,max}$ is defined in Eq. (6). The mean value and the standard deviation are equal to

$$\mu_{Hs,max} = h_{s,fc} + \mu_{\Delta Hs,max} \tag{11a}$$

$$\sigma_{Hs,max} = \sigma_{\Delta Hs,max} \tag{11b}$$

In the multiplicative model, the maximum wave height is expressed as follows:

$$H_{s,max} = \chi_{Hs,max} \cdot h_{s,fc} \tag{12}$$

where $\chi_{Hs,max}$ is defined in Eq. (9). The mean value and the standard deviation are equal to

$$\mu_{Hs,max} = h_{s,fc} \cdot \mu_{\chi Hs,max} \tag{13a}$$

$$\sigma_{Hs,max} = h_{s,fc} \cdot \sigma_{\chi Hs,max} \tag{13b}$$

It is evident from Fig. 13 that the skewness is positive and that the kurtosis is larger than three. Thus, the log-normal distribution may be suitable (see, e.g., Hahn and Shapiro, 1967, Fig. 6-1).

Under the assumption of a log-normal distribution, the probability density function for the maximum significant wave height during the operation reference period for a given weather forecast may be expressed as follows:

$$f_{Hs,max}(h_{s,max}) = \frac{1}{\sigma_{\ln Hs} h_{s,max} \sqrt{2\pi}} e^{-(1/2)((\ln h_{s,max} - \mu_{\ln Hs})/\sigma_{\ln Hs})^2} \tag{14}$$

where the mean value and the standard deviation of the logarithm of H_s are calculated as follows:

$$\mu_{\ln Hs} = \ln(h_{s,fc}) + \mu_{\ln \chi} \tag{15a}$$

$$\sigma_{\ln Hs} = \sigma_{\ln \chi} \tag{15b}$$

where $h_{s,fc}$ is given in meters and

$$\sigma_{\ln \chi} = \sqrt{\ln\left(1 + \left(\frac{\sigma_{\chi Hs,max}}{\mu_{\chi Hs,max}}\right)^2\right)} \tag{16a}$$

$$\mu_{\ln \chi} = \ln(\mu_{\chi Hs,max}) - \frac{1}{2}\sigma^2_{\ln \chi} \tag{16b}$$

The cumulative distribution function is

$$F_{Hs,max}(h_{s,max}) = \Phi\left(\frac{\ln(h_{s,max}) - \mu_{\ln Hs}}{\sigma_{\ln Hs}}\right) \tag{17}$$

where $\Phi(\,)$ is the cumulative distribution function for the standard normal distribution.

5.2. Wave period

The wave period is given in the weather forecast and may be included in the analysis in a similar manner as is the wave height. However, because of the relatively low correlation between forecasted and hindcasted periods (see Fig. 5), this is not done here. The uncertainty in the wave periods can instead be accounted for using a statistical distribution that is conditional upon the

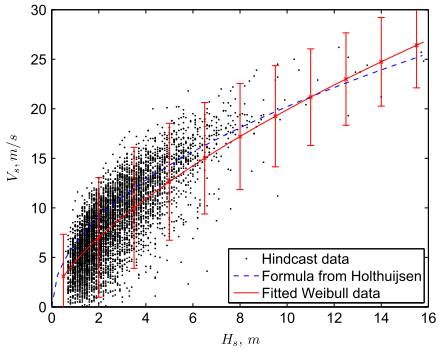

Fig. 14. Wind speed at a height of 10 m averaged over one hour versus significant wave height (hindcast data) at the Skarv field for 2010 and 2011, together with the wave-wind relation obtained from Holthuijsen's formula, Eq. (24), and the fitted Weibull distribution, i.e., the mean value from Eq. (20) with error bars of $\pm 2\sigma_{V|H_s}$ (see Eq. (21))

Table 2
Coefficients obtained by fitting Eq. (19) to the data from the Skarv field for 2010 and 2011.

Coefficient	Fitted value
c_1	1.23
c_2	0.55
c_3	1.17
c_4	0.00
c_5	5.19
c_6	0.61

Table 3
Mean wind speeds and standard deviations based on the conditional Weibull distribution (see Eqs. (19)–(21)) with coefficients from Table 2.

H_s (m)	$\mu_{V\|H_s}$ (m/s)	$\sigma_{V\|H_s}$ (m/s)
1	4.6	2.7
2	7.0	3.0
4	10.9	3.0
6	14.2	2.9
8	17.2	2.7
10	19.9	2.5
12	22.4	2.4
14	24.7	2.2

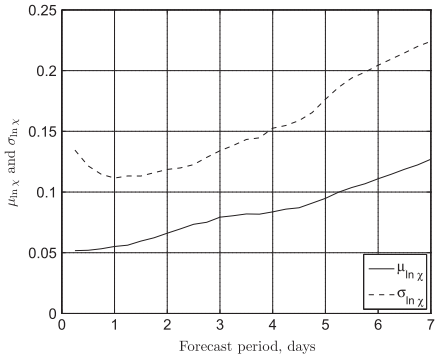

Fig. 15. Mean value ($\mu_{\ln\chi}$) and standard deviation ($\sigma_{\ln\chi}$) of the logarithm of χ in the multiplicative model, based on the previously mentioned Skarv data for all forecasted wave heights, as a function of the operation period.

significant wave height. The period may be described by a log-normal distribution, as shown by Bitner-Gregersen and Haver (1991). For design purposes, the distribution of the zero-crossing period, T_z, follows a log-normal distribution that is conditional on H_s:

$$f_{T_z|H_s}(t|h) = \frac{1}{\sigma_{\ln T_z} t\sqrt{2\pi}} e^{-(1/2)((\ln t - \mu_{\ln T_z})/\sigma_{\ln T_z})^2} \tag{18}$$

with parameters $\mu_{\ln T_z} = a_1 + a_2 h^{a_3}$ and $\sigma_{\ln T_z} = b_1 + b_2 e^{b_3 h}$ (see, e.g., DNV, 2014). The coefficients a_i and b_i, with $i = 1, 2, 3$, are estimated from real data.

For engineering purposes, the upper and lower bounds on the wave periods are given as functions of the significant wave height by, e.g., DNV (2011), GL Noble Denton (2013), and LOC (1997).

5.3. Wind speed

The wind speed may be treated in a similar manner as the wave heights, namely, by comparing forecasted values with observed values, resulting in a statistical description of the deviation. Alternatively, the wind speed can be inferred based on the joint probability density function of wind speed and wave height.

The significant wave height for wind-driven waves is typically conditional upon the wind speed, as the wind creates such waves; see, e.g., Johannessen et al. (2002).

However, in our scenario, the wind speed must be determined for a given significant wave height.

The joint probability distribution of wave height and wind speed is $f_{V,H_s}(v, h) = f_{H_s}(h) f_{V|H_s}(v|h)$, where the conditional distribution of the wind speed can be described by a two-parameter Weibull distribution; see Bitner-Gregersen (2005):

$$f_{V|H_s}(v|h) = k\frac{v^{k-1}}{V_C^k} e^{-(v/V_C)^k} \tag{19}$$

where the shape parameter is $k = c_1 + c_2 h^{c_3}$ and the scale parameter is $V_C = c_4 + c_5 h^{c_6}$. The coefficients c_i, $i = 1, 2, \ldots, 6$, are estimated from real data. The mean value of the conditional wind speed is

$$\mu_{V|H_s} = E[V|H_s] = V_C \Gamma\left(1 + \frac{1}{k}\right) \tag{20}$$

and the variance is

$$\sigma^2_{V|H_s} = V_C^2\left(\Gamma\left(1 + \frac{2}{k}\right) - \Gamma^2\left(1 + \frac{1}{k}\right)\right) \tag{21}$$

where Γ is the gamma function ($\Gamma(t) = \int_0^\infty x^{t-1}e^{-x}\,dx$).

In Fig. 14, the hindcasted significant wave height and the hindcasted wind speed at a height of 10 m averaged over one hour are plotted. Values are given for every three hours at the Skarv field in 2010 and 2011 (Table 3). In the same figure is also plotted the wind speed indicated by the conditional Weibull distribution from Eq. (19), which is plotted with error bars equal to $\pm 2\sigma_{V|H_s}$ (i.e., approximately the 95% confidence interval). The parameters used in Eq. (19) are given in Table 2.

Table 4
Select numerical values of $\mu_{\ln\chi}$ and $\sigma_{\ln\chi}$, from Fig. 15.

No. of days (–)	T_R (h)	$\mu_{\ln\chi}$ (–)	$\sigma_{\ln\chi}$ (–)
1	24	0.055	0.112
2	48	0.066	0.119
3	72	0.079	0.134
4	96	0.084	0.153
5	120	0.095	0.176
6	144	0.111	0.204
7	168	0.127	0.224

6. Environmental conditions for weather-unrestricted operations

6.1. Design environmental conditions

For weather-unrestricted operations, the environmental design conditions are based on long-term statistics, possibly accounting for seasonal variations. According to ISO 19901-6, weather-unrestricted operations may be planned using environmental criteria with return periods estimated as a multiple of the operation duration. A minimum of 10 times the duration of the operation may be used (ISO 19901-6, 2009). (However, for operations with durations of up to seven days, environmental criteria based on seasonal data with a return period of one year are recommended.)

An alternative is a method proposed by Lindemann (1986) for calculating the design significant wave height as a function of the duration with a defined exceedance probability of 10%. This method is used by DNV (2011).

6.2. Exceedance probabilities for the wave height

Consider a marine operation with a given duration and in a given season for which the long-term statistics for the geographical area yield a significant wave height for the design that is equal to $h_{s,d}$. Based on the log-normal distribution from Eq. (17), the probability that the actual (observed) significant wave height will be larger than the design value can be expressed as follows:

$$P_e = P(H_{s,max} \geq h_{s,d}) = 1 - \Phi\left(\frac{\ln(h_{s,d}) - \mu_{\ln H_s}}{\sigma_{\ln H_s}}\right) \tag{22}$$

$\mu_{\ln H_s}$ and $\sigma_{\ln H_s}$ are calculated from Eq. (15) for the maximum forecasted wave height, $h_{s,fc}$, during the operation period, T_R.

6.3. Simplified numerical values for the weather forecasting uncertainty

Using the expressions given in Eqs. (22) and (15), the probability of exceeding the design criteria over a period of several days can be estimated based on a given weather forecast. The mean and the standard deviation of χ are given in Fig. 13 for all-year data. In Fig. 15, the mean and the standard deviation of the logarithm of χ as calculated using Eq. (16) are shown. Select values of $\mu_{\ln\chi}$ and $\sigma_{\ln\chi}$ are given in Table 4.

6.4. Simplified design wind speed

A simple relationship between the significant wave height and the wind speed is given in Holthuijsen (2007, Section 6.3.2):

$$H_s = 0.24\frac{V^2}{g} \tag{23}$$

where V is the sustained wind speed (10-min average) 10 m above the sea surface. Similar expressions with slightly varying constants

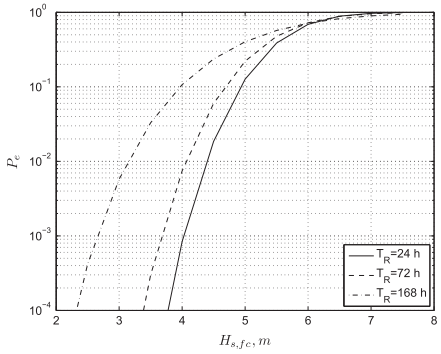

Fig. 16. Probability of exceeding $H_s = 6$ m as a function of the forecasted significant wave height for three operation reference periods: 24 h, three days and seven days

are also given by other authors, e.g., Gran (1992, Eq. 3.4.63), with a coefficient of 0.18 instead of 0.24 (for a wind speed V observed 10–20 m above the sea surface). Note that the spread (e.g., the standard deviation) of the H_s data is not described by this formula. Inverting Eq. (23) yields the wind speed as a function of the significant wave height:

$$V = \sqrt{\frac{H_s g}{0.24}} \tag{24}$$

The wind speed according to Eq. (24) is also shown in Fig. 14. (The wind speed in Eq. (24) is averaged over 10 min, whereas the hindcasted wind speed, which is approximately 10% lower, is averaged over one hour.) The significant wave height in Eq. (23) represents wind-generated waves. By contrast, the significant wave height assumed in long-term wave distributions describes the total sea, i.e., it also includes swells. This means that when the wind speed is calculated via Eq. (24) using a significant wave height from a long-term distribution representing the total sea, the wind speed will be overestimated.

In engineering, a simple method of calculating the wind speed corresponding to a specified significant wave height is useful for operation design. As a simplification, the wind speed may be taken to be a deterministic function of the wave height if a formula similar to Eq. (24) is fitted to the upper limit in Fig. 14 (i.e., to $\mu_{V|H_s} + 2\sigma_{V|H_s}$; see Eqs. (20) and (21)). The factor 0.24 is then replaced with 0.15; hence, $V_{one\ hour} = \sqrt{H_s g/0.15} \approx 8\sqrt{H_s}$. (A more sophisticated curve could also be used, but Eq. (24) is both simple and convenient and has the traditional form.) This formula could be used for planning operations in the Norwegian Sea, bearing in mind that it is based on two years of data. Because the formula is valid for wind speeds averaged over one hour, it should be transformed to correspond to the actual averaging time used in the case under consideration. A one-minute averaging time is often used, in which case the wind speed is approximately 20% higher than the one-hour wind speed (see, e.g., DNV, 2011). The one-minute design wind speed can thus be approximated as follows:

$$V_{one\ minute} \approx 10\sqrt{H_s} \tag{25}$$

where H_s is given in m and the wind speed is given in m/s. Note that this is merely an approximate formula for wind speed and is a function of the significant wave height only. The relation between wave height and wind speed at a certain location may depend on

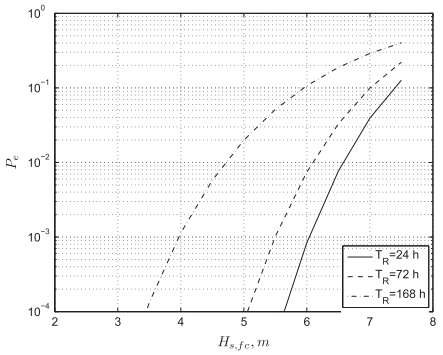

Fig. 17. Probability of exceeding $H_s = 9$ m as a function of the forecasted significant wave height for three operation reference periods: 24 h, three days and seven days.

the wind and wave directions, storm duration, fetch, water depth and possibly other covariates. However, Eq. (25) can be used for engineering or feasibility studies and is valid for deep water and unlimited fetch.

For structural reliability analyses, the conditional probability distribution given in Eqs. (19)–(21) may be used.

7. Reliability of a weather forecast

The probability of exceeding a certain significant wave height given a certain forecasted wave height and operation period can be estimated from Eq. (22).

In Fig. 16, the probability of exceeding a significant wave height of 6 m is plotted as a function of the forecasted wave height for three different operation periods. Similarly, the probability of exceeding a significant wave height of 9 m is plotted in Fig. 17.

It is observed that if the forecasted wave height is, e.g., 4 m, then the probability that the actual wave height will be greater than 6 m after 24 h is approximately 10^{-3}; after three days, it is approximately 10^{-2}; and after seven days, the probability of exceedance is 10^{-1}. The probability that the actual wave height will be greater than 9 m is negligible after either 24 h or three days. After seven days, the probability of exceeding a wave height of 9 m is approximately 10^{-3}. It is also apparent from Fig. 17 that if the forecasted wave height is 6 m, then the probability of exceeding a 9 m wave height after seven days is approximately 10^{-1}. Hence, the weather forecasts still provide interesting information even after one week. Because the results are sensitive to the tail of the distribution when extreme values are considered, the values here should be taken as examples only.

The primary concern in engineering is not the probability of exceedance but rather how to calculate a design wave height. The design wave height can be estimated for a given probability of exceedance and a forecasted wave height. By substituting Eq. (15) into Eq. (22) and solving for $H_{s,d}$, the maximum significant wave height can be calculated as follows:

$$H_{s,d} = h_{s,fc} \exp(\mu_{\ln\chi} + \sigma_{\ln\chi}\Phi^{-1}(1 - P_e)) \tag{26}$$

The probability of exceedance, P_e, should correspond to the safety format used in the design of the marine operation. The safety factors used in the structural design (typically load and material factors) will depend on the probability of exceeding a certain load level. A probability of 10% that the design wave will be exceeded is used in DNV (2011) for weather-unrestricted operations.

As an example, suppose that the maximum allowed forecasted significant wave height for a certain marine operation is 5 m. (Hence, the operation cannot begin before the forecasts indicate $H_s \leq 5$ m for the entire duration of the operation.) Using the values from Table 4, the maximum significant wave heights obtained from Eq. (26) are 6.4 m for a three-day operation and 7.6 m for a seven-day operation, with P_e=0.1. (These would then be the characteristic values to be used in design.)

The ratio between the forecasted wave height and the design wave height for a three-day operation is 5/6.4 = 0.78. This value can then be compared with the values from the design standards. The ratio between the forecasted wave height and the design wave height for a 72-h operation is 0.72 according to DNV (2011) (for $H_{s,design} \geq 6$ m) and 0.54 according to GL Noble Denton (2013); see Table 1. Hence, these standards yield conservative results compared with our data set in this case.

For a seven-day operation period, no ratio is given by the design standards, but the ratio between the forecasted and design wave heights according to the results from Table 4 is 5/7.6 = 0.66.

In general, standards for marine operations do not allow the planning and design to be based on weather forecasts when the operation duration is more than three days unless it can be demonstrated that the relevant weather forecasts can predict any extreme weather conditions over a longer period. The method described in this paper may be used to assess the reliability of such weather forecasts, preferably based on a more extensive data set. Because only weather forecasts for a single location are included in the data set considered in this paper, the results cannot be directly applied elsewhere. However, they are considered to be representative of extratropical conditions.

Because only one year of data is included, there will be a rather large uncertainty in the calculated values; see, e.g., Moan et al. (2005).

8. Conclusions

The uncertainty in environmental conditions based on weather forecasts has been studied. Forecasted significant wave heights have been compared with hindcasted values using an additive and a multiplicative statistical model. In the additive model, the mean value and the standard deviation are more strongly dependent on the forecasted wave height than in the multiplicative model, making the latter the preferred model in this study.

The uncertainty in the forecasts increases with increasing lead time, reducing the correlation between the forecasted and hindcasted data. The correlation between forecasted and hindcasted data is lower for wave periods than for significant wave heights for the same lead time. Therefore, it is preferable to model the wave period conditionally upon the wave height.

The wind speed may be modelled using a Weibull distribution that is conditional upon the wave height. For marine operations in which the governing environmental load is caused by waves and the corresponding wind speed must be estimated, a simple engineering method is proposed. The relationship between wind speed and wave height was developed for wind-driven waves. Hence, if the waves in fact contain swells in addition to wind-driven waves, then the wind speed may be overestimated. Moreover, in sheltered water or other cases in which there may be high wind speeds but small or no waves, this method is not applicable. In such cases, it will be necessary to determine the wind speed using other methods, e.g., the return period approach based on the duration of the operation.

According to the design standards for marine operations, only operations with planned durations of less than three days are generally planned as weather-restricted marine operations, unless it can be demonstrated that the relevant weather forecasts are able to predict any extreme weather conditions over a longer period. In that case, the operation reference period may be increased. The data from the Norwegian Sea used in this paper do not reveal any specific limitations of the weather forecasts that would require a 72-h limit for weather-restricted operations. The method described in this paper may be used to assess the quality of weather forecasts for a period longer than three days based on forecasts for the area of interest.

The results may be used as input for structural reliability analyses of marine operations.

Although the statistical model described in this paper considers the significant wave heights, several other effects might have been included. Seasonal variations and the dependences of the forecasted wave height have been discussed to some extent, but other covariates may also influence the results. The wave and wind directions, water depth, geographical area, forecast provider or other covariate effects could be included in these analyses. To obtain the parameters for the engineering of an operation at a certain location, data reflecting the area of interest should be analysed.

Acknowledgements

The first author's work was financed by the Research Council of Norway (RCN) through the Centre for Ships and Ocean Structures (CeSOS) at the Norwegian University of Science and Technology (NTNU) as well as by support from the Education Fund of Det Norske Veritas. This support is greatly appreciated.

Hindcast data were received from Magnar Reistad at the Norwegian Meteorological Institute and are also much appreciated.

References

Bitner-Gregersen, E., Haver, S., 1991. Joint environmental model for reliability calculations. In: ISOPE. Proceedings of the First International Offshore and Polar Engineering Conference, vol. 1, Edinburgh, UK, pp. 246–253.

Bitner-Gregersen, E.M., 2005. Joint probabilistic description for combined seas. In: OMAE2005, p. 67382.

BMT Ltd, 1986. Global Wave Statistics.

DNV, 1996/2000. Rules for Planning and Execution of Marine Operations.

DNV, 2011. Marine Operations, General. DNV-OS-H101.

DNV, 2014. Environmental Conditions and Environmental Loads. DNV-RP-C205.

FugroOceanor, 2012. ⟨http://www.oceanor.no/services/⟩.

GL Noble Denton, 2013. General Guidelines for Marine Projects.

Gran, S., 1992. Developments in Marine Technology. A Course in Ocean Engineering, vol. 8. Elsevier, Amsterdam.

Hahn, G., Shapiro, S., 1967. Statistical Models in Engineering. 1967. John Wiley & Sons, Inc, New York (reprinted 1994).

Holthuijsen, L.H., 2007. Waves in Oceanic and Coastal Waters. Cambridge University Press, Cambridge, United Kingdom.

ISO 19901-6, 2009. Petroleum and Natural Gas Industries. Specific Requirements for Offshore Structures. Part 6: Marine Operations.

Johannessen, K., Meling, T.S., Haver, S., 2002. Joint distribution for wind and waves in the northern North Sea. Int. J. Offshore Polar Eng. 12 (March), 1.

Lindemann, K., 1986. Extreme value statistics and exposure time: a simple method to establish well defined criteria for marine operations. In: Offshore Technology Conference, No. 5142 in OTC. OTC, Houston, pp. 519–525, May.

LOC, 1997. Guidelines for Marine Operations. London Offshore Consultants Limited, Ledbury, United Kingdom.

Marin, 2007. Safetrans. ⟨http://www.marin.nl/web/JIPsNetworks/Public/Safetrans.htm⟩.

Matlab, 2010. Ver. 7.11. The MathWorks Inc., Natick, MA.

Moan, T., Gao, Z., Ayala-Uraga, E., 2005. Uncertainty of wave-induced response of marine structures due to long-term variation of extratropical wave conditions. Mar. Struct. 18 (May (4)), 359–382.

NORSOK, 2007. N-003, Actions and Action Effects.

Reistad, M., Breivik, Ø., Haakenstad, H., Aarnes, O.J., Furevik, B.R., Bidlot, J.-R., 2011. A high-resolution hindcast of wind and waves for the North Sea, the Norwegian Sea, and the Barents Sea. J. Geophys. Res. 116, 18.

Saetra, Ø., Bidlot, J.-R., Potential benefits of using probabilistic forecasts for waves and marine winds based on the ECMWF ensemble prediction system. Weather Forecast. 19 (4), 673–689, August.

Shu, Z., Moan, T., 2008. Effects of avoidance of heavy weather on the wave-induced load on ships. J. Offshore Mech. Arct. Eng. 130, 2.

Wamdi Group, 1988. The WAM model—a third generation ocean wav prediction model. J. Phys. Oceanogr. 18, 1778–1810.

A.3 Paper 3

Paper 3:
Structural reliability analysis of a seafastening structure for sea transport of heavy objects.
Authors: Asle Natskår and Torgeir Moan.
Issued for publication in *Ocean Engineering.*

Appendix B

Structural layout of a transport barge

B.1 Introduction

Transport barges have a large range of sizes and have various deck layouts and equipment. Semisubmersible barges have superstructures (towers) to maintain hydrostatic stability under submerged conditions. For ordinary sea transports, such equipment is not required, and the flat top barge will suffice. The smallest barges can simply be steel structures without ballast systems and without anchors. Larger barges will typically have their own ballast system, anchor, winch for retrieving the towing gear, etc. The structural capacity of a flat top barge is considered, and the equipment is not important here.

B.2 Layout of the barge and the transported object

B.2.1 Positioning of the transported object

In Fig. B.1, a barge loaded with a typical object is illustrated. Load-out of the cargo will typically be performed by crane lifting, skidding or multiwheel transporters (trailers). The transported object is accurately positioned and set down on preinstalled grillage beams and seafastened. For small objects, the seafastening can be chain lashings, while for larger objects, the seafastening will typically be conducted with roll and pitch stoppers welded to the object and to the barge deck.

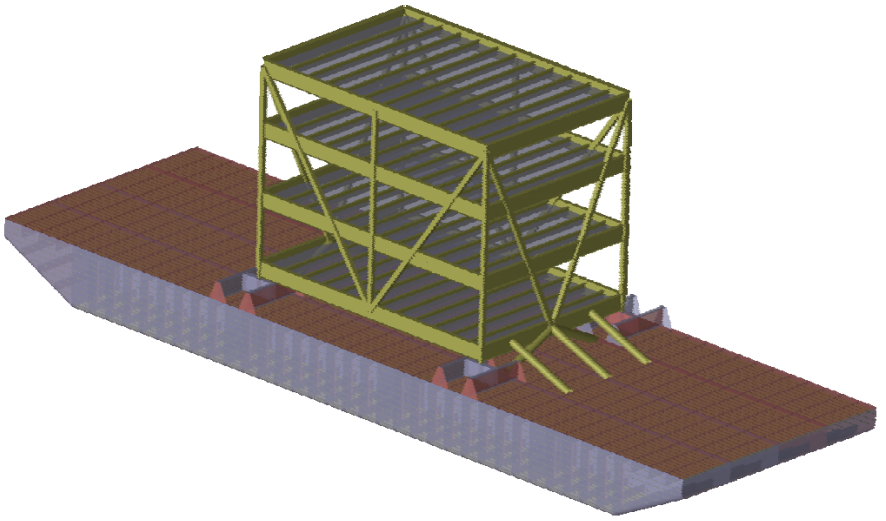

Figure B.1: Barge with transported object, grillage and seafastening.

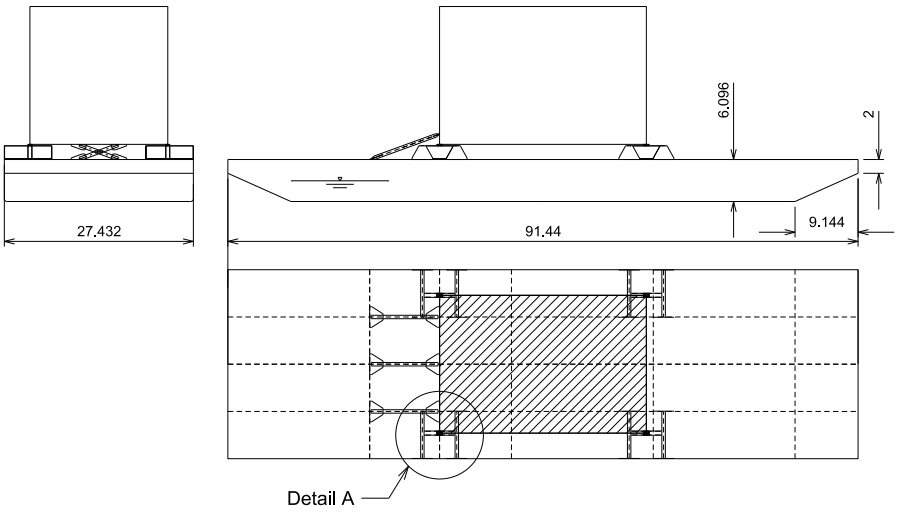

Figure B.2: Example of a barge with a transported object and grillage and seafastening. Detail A is shown in Fig. B.5, page 184

.

B.2.2 Barge geometry

Consider a standard North Sea Barge with a length of 91.4 m, width of 27.4 m and depth of 6.1 m (300 by 90 by 20 feet). An example of the

barge geometry is shown in Table B.1. The steel yield stress is typically $f_y = 235MPa$.

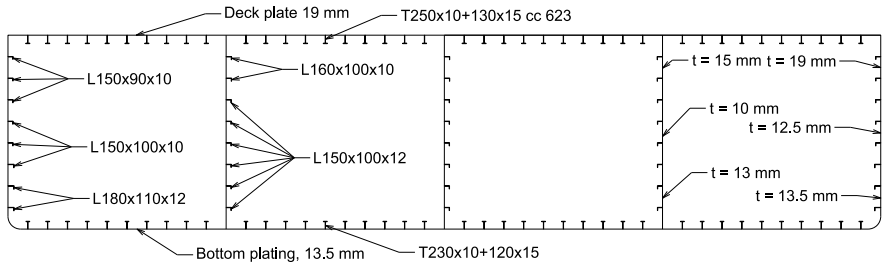

Figure B.3: Example of the cross section of a Standard North Sea Barge. The welds between the stiffeners (stringers) and the barge plates are typically fillet welds with a throat thickness equal to 4 mm.

B.2.3 Layout of the transported object

The transported object can have any shape and layout, but here, it is assumed to have a regular, box-shaped symmetric structure. There are typically vertical support points in each corner intended for the in-place condition. These supports are assumed to be used for the vertical support of the object during transport.

B.2.4 Grillage and seafastening

The grillage beams transfer the vertical loads from the transported object into the barge structure. They are welded to the barge as part of the preparations prior to load-out of the transported object. The grillage beams are shown in figure B.4. The seafastening consists of the following:

- roll stoppers to prevent sliding of the object in the transverse direction of the barge
- pitch stoppers to prevent sliding in the longitudinal direction of the barge
- if required, uplift stoppers to prevent lift-off of the transported object from the grillage in severe seas

Item	Plate th.	Stiffeners
Deck	19	T 250x10+130x15 cc 623.4, length 2286
Bottom plating	13.5	T 230x10+120x15 c/c 623.4
Longitudinal bulkhead	15	L160x100x10, 2 of
	10	L150x100x12, 3 of
	13	L150x100x12, 3 of
Transverse bulkhead	10	vert. T320x12.5+170x19 c/c 623.4
		Add. stiffs at top:
		vert. FB100x10 L=1200 mm, c/c 623.4
Side shell	19	L150x90x10, 3 of
	12.5	L150x100x12, 3 of
	13.5	L180x110x12, 2 of
Web frame section:		
Top girders (below deck)		1200x20 web, 300x20 FB
Bottom girders		800x12 web, 220x20 FB
Vertical girders		1250x25 web, 400x35 FB

Table B.1: Barge geometry, dimensions in mm

B.3 Structural capacity

B.3.1 Uncertainties in structural capacity

The statistical variation in the structural capacity is due to:

- geometric tolerances
- variations in the yield stress
- fabrication tolerances

The geometric tolerances, in particular the out-of-straightness, are mainly of interest with respect to buckling of structural members. For members in tension, the relevant geometric variations are the thickness variations or variations in the members' cross section.

B.3.2 Structural elements in the grillage and seafastening

The structural system for marine transports is a combination of conventional and unconventional components. Typical structural components are:

- grillage beams made by welded I-girders and box girders

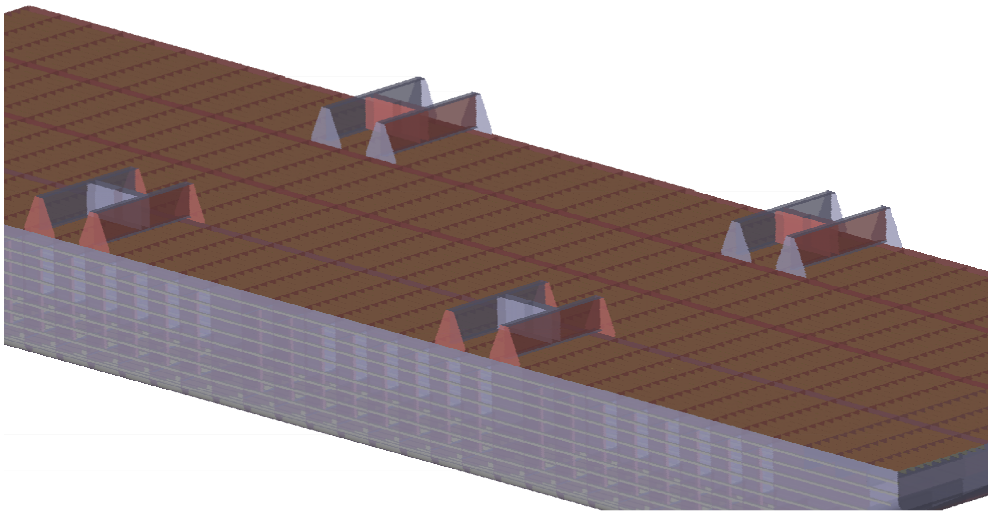

Figure B.4: Iso-view of grillage beams preinstalled on the barge deck

- the connection between the grillage beams and the barge, typically made from plates welded to the barge deck (wing plates) to distribute the load to the web frames and bulkheads
- tubular or rectangular hollow sections used as pitch and roll stoppers
- roll and pitch stoppers connected to the barge deck and the transported object by gusset plates
- concentrated vertical loads in the stiffened panels, i.e., bulkhead and web frames
- concentrated horizontal loads in the deck (horizontal component of the load in the roll and pitch stoppers)

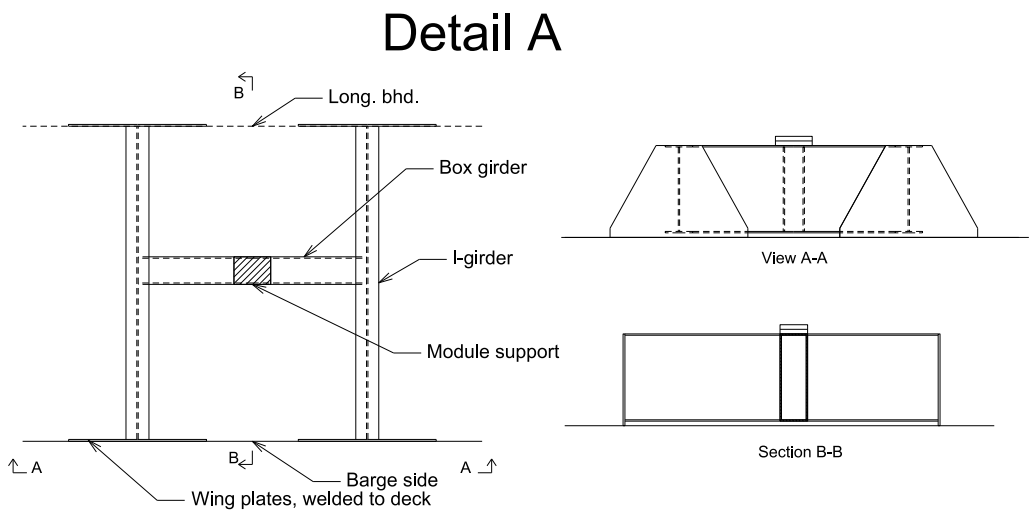

Figure B.5: Typical barge grillage, detail A from figure B.2. Box girders, e.g., with side plates 1900×30 *and top/bottom plates* 600×30*, and I-girders, e.g., with web plates* 1900×30 *and top/bottom flanges* 500×40*, and the stiffeners are typically fitted as required to prevent local buckling*

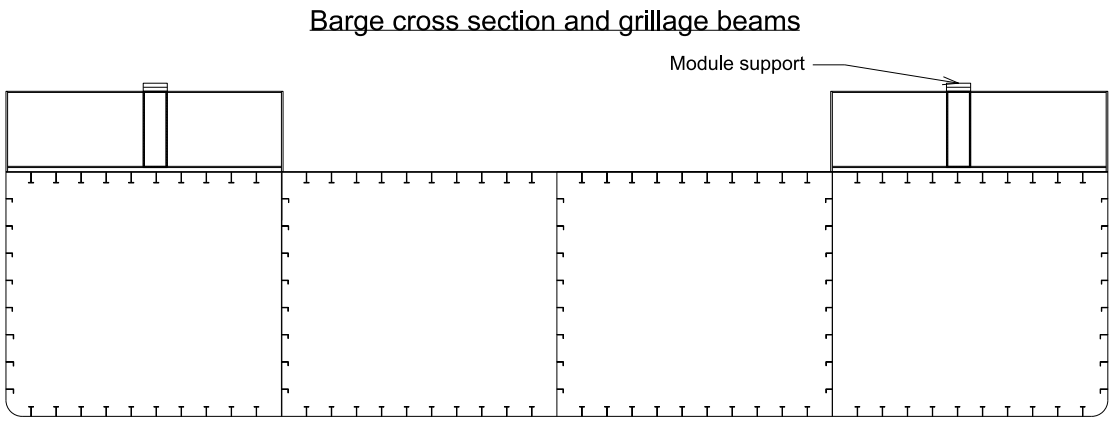

Figure B.6: Transverse cross section of the barge and grillage beams

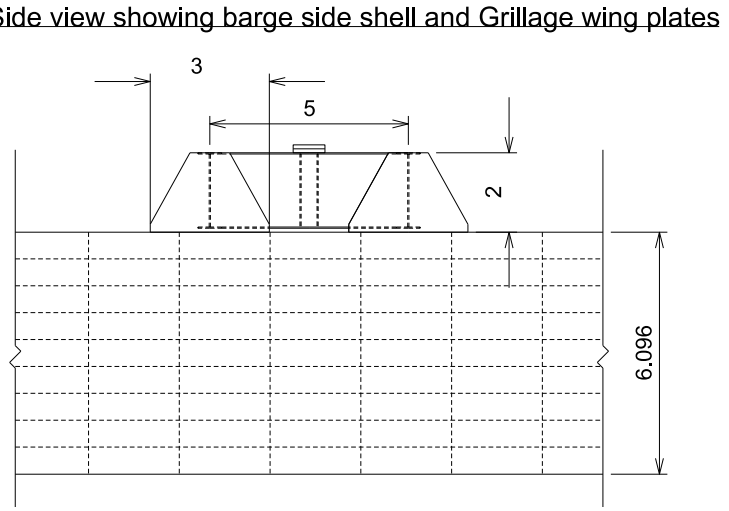

Figure B.7: Side view of the barge and grillage

Appendix C

Motion analysis of ships and barges

C.1 Simplified motion analyses

Simplified methods are given in standards and guide lines. A simplified criteria is given below [31]. The criteria in Tab. C.1, can normally be applied to barges with breadth at least 20 m and length at least 50 m.

Table C.1: Simplified barge rolling criteria [31] ($g = 9.81\ m/s^2$, the x-axis is in longitudinal direction, y-axis in transverse direction and z-axis upwards.

Acceleration / wind pressure	Unrestricted	$H_s = 6$ m	$H_s = 4$ m
a_y at waterline, g	0.50	0.37	0.26
a_y increase for each metre (z) above waterline, g/m	0.017	0.017	0.017
a_z at centre (C) barge, g	0.20	0.20	0.15
a_z incr. each metre from C , g/m	0.017	0.017	0.017
Wind pressure, kN/m^2	1.0	0.5	0.4

The horizontal acceleration in the CoG of the transported object is calculated as

$$a_{y,CoG} = a_{y,wl} + 0.017g/m \cdot z_{CoG} \tag{C.1}$$

The roll acceleration is calculated as

$$\ddot{\theta}_{roll} = 0.017g/m = 0.167rad/s^2 \tag{C.2}$$

The simplified accelerations for the Roll Case in Tab. C.1 are used in [107] to calculate the seafastening forces for a typical barge transport.

C.2 Linear analysis in frequency domain

The equation of motion for a floating vessel is expressed on complex form in the frequency domain as

$$[\boldsymbol{M} + \boldsymbol{A}(\omega)]\ddot{\boldsymbol{\eta}} + [\boldsymbol{B_1}(\omega) + \boldsymbol{B_{eq}}]\dot{\boldsymbol{\eta}} + \boldsymbol{C\eta} = \boldsymbol{F_0}(\omega)e^{i\omega t} \tag{C.3}$$

where

- ω is the angular frequency of the wave in rad/s
- $\boldsymbol{F_0}(\omega)$ is the amplitude of the wave load, given on complex form
- $\boldsymbol{M}$ is the mass matrix for the barge including the transported object
- $\boldsymbol{A}(\omega)$ is the hydrodynamic added mass matrix
- $\boldsymbol{B_1}(\omega)$ is the linear damping matrix from potential damping (due to wave radiation)
- $\boldsymbol{B_{eq}}$ is the equivalent linear damping representing the non-linear damping caused by vortex shedding at the bilges. This matrix has only one non-zero element; $B_{2,44}$ for roll
- $\boldsymbol{C}$ is the restoring matrix
- $\boldsymbol{\eta} = [\eta_1\ \eta_2\ \eta_3\ \eta_4\ \eta_5\ \eta_6]^T$ is the motion vector; index 1-6 means surge, sway, heave, roll, pitch and yaw, respectively

It is noted that even if the equation of motion is given on complex form, the solution of interest is the real part of the mathematical solution. The wave load, $\boldsymbol{F_0}(\omega)$, the added mass, $\boldsymbol{A}(\omega)$, and the potential damping matrix, $\boldsymbol{B_1}(\omega)$, are calculated from potential theory using the boundary element method, and is a function of the wave frequency, see e.g., [38]. The method is implemented in commercial software, e.g., Wadam [129].

The viscous damping is not calculated by potential theory, but it is estimated by empirical methods. The viscous damping is caused by vortex shedding at the bilges and is estimated as a quadratic damping term. The quadratic damping is replaced by an equivalent damping term $B_{2,44}$ when the equation of motion is solved in the frequency domain. More details are given in [120] and in [109].

When Eq. (C.3) is solved in the frequency domain, the transfer functions for the motion in six degrees of freedom is found as follows:

$$\boldsymbol{H_{\zeta\eta}}(\omega) = \left(-[\boldsymbol{M} + \boldsymbol{A}(\omega)]\omega^2 + [\boldsymbol{B_1}(\omega) + \boldsymbol{B_{eq}}]i\omega + \boldsymbol{C}\right)^{-1} \boldsymbol{F_0}(\omega) \quad \text{(C.4)}$$

The vessel motion no. j is calculated as follows:

$$\eta_j = H_{\zeta\eta,j}(\omega)e^{i\omega t} \quad \text{(C.5)}$$

Based on this transfer function and the power spectrum $S_\zeta(\omega)$ for the sea elevation, the power spectrum of the vessel motion can be calculated as follows [104]:

$$S_{\eta,j}(\omega) = H^2_{\zeta\eta,j}(\omega)S_\zeta(\omega) \quad \text{(C.6)}$$

The expected maximum response during N cycles is estimated under the assumption that the individual response maxima follow a Rayleigh distribution and is calaulated as follows:

$$\eta_{max} = \sigma_{\eta,j}\left(\sqrt{2\ln N} + \frac{0.577}{\sqrt{2\ln N}}\right) \quad \text{(C.7)}$$

where the variance of the response is calculated as $\sigma^2_{\eta,j} = \int_0^\infty S_{\eta,j}(\omega)\mathrm{d}\omega$.

C.3 Non-linear analysis in the time domain

The non-linearity can be included in many forms in the hydrodynamic analyses. From a slightly non-linear to a highly non-linear model. In this thesis, the non-linear analysis in time domain is based on the wave load, the added mass and the wave radiation damping from potential theory. The reason for running the analysis in the time domain is that the viscous damping do not have to be linearized, but can be kept on a quadratic form in the equation of motion.

Below, the equation of motion as defined in a ship fixed coordinate system is studied, as used on the time domain analyses. It is seen that some additional non-linear terms are included into the equation, terms that are negligible for small vessel motions, but will affect the solution for larger motions.

C.3.1 Coordinate systems

While the coordinate system used in the frequency domain analysis was earth fixed, e.g., in Wadam [129], a ship fixed coordinate system is used,

in accordance with Simo [131]. For large motions, the choice of coordinate system will affect the results, ref. Sec. 3.4. In order to describe the motion, several coordinate systems are used in Simo:

- A global coordinate system
- A local, body fixed, coordinate system
- A body related coordinate system

The body related coordinate system follows the body horizontal motion, and the xy-plane is parallel to the global xy-plane

C.3.2 Equations of motion

In the following, the equations of motions are solved in local (ship fixed) coordinates. Using a body fixed coordinate system in the time domain analysis introduce some additional terms in the equations of motions. For small waves and small ship motions, these terms are negligible, but in severe seas they will affect the solution. This topic was discussed in Paper 1, but not in much details. Therefore, the equitations are derived in more detail below to illustrate this interesting result of the choice of coordinate system.

The kinetics for the vessel is described by setting the time derivative of the momentum equal to the external forces:

$$\dot{\boldsymbol{P}}_B = \boldsymbol{F} \tag{C.8}$$

$$\dot{\boldsymbol{L}}_B = \boldsymbol{M} \tag{C.9}$$

where the linear momentum is given as

$$\boldsymbol{P}_B = m(\boldsymbol{u} + \boldsymbol{\Omega} \times \boldsymbol{r}_c) \tag{C.10}$$

and the angular momentum is given as

$$\boldsymbol{L}_B = \boldsymbol{I}\boldsymbol{\Omega} + m\boldsymbol{r}_c \times \boldsymbol{u} \tag{C.11}$$

where

$$\boldsymbol{I} = \begin{bmatrix} I_x & 0 & 0 \\ 0 & I_y & 0 \\ 0 & 0 & I_z \end{bmatrix}, \quad \boldsymbol{\Omega} = \begin{bmatrix} p \\ q \\ r \end{bmatrix}, \quad \boldsymbol{r}_c = \begin{bmatrix} x_c \\ y_c \\ z_c \end{bmatrix} \text{ and } \quad \boldsymbol{u} = \begin{bmatrix} u \\ v \\ w \end{bmatrix} \tag{C.12}$$

$\boldsymbol{I}$ is the rotational inertia, $\boldsymbol{\Omega}$ is the rotational velocity, $\boldsymbol{r}_c$ is the CoG-position and $\boldsymbol{u}$ is the translational velocity. When the vectors are defined in the

local coordinate system, the time derivative will have to account for the motion of the local system relative to the global system. As an example, the velocity is differentiated with respect to time. The velocity can be written as $\boldsymbol{u} = u\boldsymbol{e}_1 + v\boldsymbol{e}_2 + w\boldsymbol{e}_3$, where the unit vectors $\boldsymbol{e}_i$ are functions of time. The time derivative is then:

$$\dot{\boldsymbol{u}} = \frac{\partial \boldsymbol{u}}{\partial t} = \underbrace{\dot{u}\boldsymbol{e}_1 + \dot{v}\boldsymbol{e}_2 + \dot{w}\boldsymbol{e}_3}_{\equiv \dot{\boldsymbol{u}}^*} + \underbrace{u\dot{\boldsymbol{e}}_1 + v\dot{\boldsymbol{e}}_2 + w\dot{\boldsymbol{e}}_3}_{\equiv \boldsymbol{\Omega}\times\boldsymbol{u}} \tag{C.13}$$

A derivation of this expression is given by Faltinsen [39, page 422-423].

Equations (C.8) and (C.9) can now be expressed as

$$\dot{\boldsymbol{P}}_B^* + \boldsymbol{\Omega} \times \boldsymbol{P}_B = \boldsymbol{F} \tag{C.14}$$

$$\dot{\boldsymbol{L}}_B^* + \boldsymbol{\Omega} \times \boldsymbol{L}_B + \boldsymbol{u} \times \boldsymbol{P}_B = \boldsymbol{M} \tag{C.15}$$

Let us now consider beam sea exposure. Then $q = r = u = 0$. Further, it is assumed that the centre of gravity is located in the symmetry plane, such that $x_c = y_c = 0$.

The equations of motions will then be considerably simplified.

Let us write the vector cross products used above:

$$\boldsymbol{\Omega} \times \boldsymbol{r}_c = \begin{vmatrix} \boldsymbol{i} & \boldsymbol{j} & \boldsymbol{k} \\ p & 0 & 0 \\ 0 & 0 & z_c \end{vmatrix} = \begin{bmatrix} 0 \\ -z_c p \\ 0 \end{bmatrix} \tag{C.16}$$

The linear momentum is then:

$$\boldsymbol{P}_B = m \begin{bmatrix} 0 \\ v - z_c p \\ w \end{bmatrix} \tag{C.17}$$

Further,

$$\boldsymbol{r_c} \times \boldsymbol{u} = \begin{vmatrix} \boldsymbol{i} & \boldsymbol{j} & \boldsymbol{k} \\ 0 & 0 & z_c \\ 0 & v & w \end{vmatrix} = \begin{bmatrix} -z_c v \\ 0 \\ 0 \end{bmatrix} \tag{C.18}$$

The angular momentum is then:

$$\boldsymbol{L}_B = \begin{bmatrix} I_x p - m z_c v \\ 0 \\ 0 \end{bmatrix} \tag{C.19}$$

The cross product in the time derivative of the velocity is

$$\boldsymbol{\Omega} \times \boldsymbol{u} = \begin{bmatrix} 0 \\ -wp \\ vp \end{bmatrix} \tag{C.20}$$

The time derivative of the velocity is now:

$$\dot{v} = \dot{v}^* - wp \tag{C.21}$$

$$\dot{w} = \dot{w}^* + vp \tag{C.22}$$

Hence,

$$\boldsymbol{\Omega} \times \boldsymbol{P}_B = \begin{vmatrix} \boldsymbol{i} & \boldsymbol{j} & \boldsymbol{k} \\ p & 0 & 0 \\ mu & m(v - z_c p) & mw \end{vmatrix} = \begin{bmatrix} 0 \\ -mwp \\ m(v - z_c p)p \end{bmatrix} \tag{C.23}$$

$$\boldsymbol{\Omega} \times \boldsymbol{L}_B = \begin{vmatrix} \boldsymbol{i} & \boldsymbol{j} & \boldsymbol{k} \\ p & 0 & 0 \\ I_x p - m z_c v & 0 & 0 \end{vmatrix} = \boldsymbol{0} \tag{C.24}$$

$$\boldsymbol{u} \times \boldsymbol{P}_B = \begin{vmatrix} \boldsymbol{i} & \boldsymbol{j} & \boldsymbol{k} \\ 0 & v & w \\ 0 & m(v - z_c p) & mw \end{vmatrix} = \begin{bmatrix} m z_c w p \\ 0 \\ 0 \end{bmatrix} \tag{C.25}$$

Equations (C.14) and (C.15) can then be written as

$$m(\dot{v}^* - z_c \dot{p}^* - wp) = F_y \tag{C.26}$$

$$m(\dot{w}^* + vp - z_c p^2) = F_z \tag{C.27}$$

$$-m z_c \dot{v}^* + I_x \dot{p}^* + m z_c w p = M_x \tag{C.28}$$

It should be noted that while v and w follow eq. (C.21) and (C.22), the roll acceleration is expressed by $\dot{p}^* \equiv \dot{p}$ ($\dot{\Omega} = \dot{\Omega}^* + \underbrace{\Omega \times \Omega}_{=0} = \dot{\Omega}^*$)

In addition to the equillibrium for the body formulated in eq. (C.26) to (C.28), the added mass from water also need to be included.

The added mass matrix for a double symmetric vessel is written as

$$\boldsymbol{A} = \begin{bmatrix} A_{11} & A_{12} \\ A_{21} & A_{22} \end{bmatrix} = \begin{bmatrix} a_{11} & 0 & 0 & 0 & a_{15} & 0 \\ 0 & a_{22} & 0 & a_{24} & 0 & 0 \\ 0 & 0 & a_{33} & 0 & 0 & 0 \\ 0 & a_{42} & 0 & a_{44} & 0 & 0 \\ a_{51} & 0 & 0 & 0 & a_{55} & 0 \\ 0 & 0 & 0 & 0 & 0 & a_{66} \end{bmatrix} \tag{C.29}$$

The momentum is expressed as:

$$\boldsymbol{P}_A = \boldsymbol{A}_{11}\boldsymbol{u} + \boldsymbol{A}_{12}\boldsymbol{\Omega} = \begin{bmatrix} 0 \\ a_{22}v + a_{24}p \\ a_{33}w \end{bmatrix} \tag{C.30}$$

$$\boldsymbol{L}_A = \boldsymbol{A}_{21}\boldsymbol{u} + \boldsymbol{A}_{22}\boldsymbol{\Omega} = \begin{bmatrix} a_{42}v + a_{44}p \\ 0 \\ 0 \end{bmatrix} \tag{C.31}$$

Equations (C.8) and (C.9) can now be expressed for added mass as

$$\dot{\boldsymbol{P}}_A^* + \boldsymbol{\Omega} \times \boldsymbol{P}_A = -\boldsymbol{F}_A \tag{C.32}$$

$$\dot{\boldsymbol{L}}_A^* + \boldsymbol{\Omega} \times \boldsymbol{L}_A + \boldsymbol{u} \times \boldsymbol{P}_A = -\boldsymbol{M}_A \tag{C.33}$$

$$\boldsymbol{\Omega} \times \boldsymbol{P}_A = \begin{vmatrix} \boldsymbol{i} & \boldsymbol{j} & \boldsymbol{k} \\ p & 0 & 0 \\ 0 & a_{22}v + a_{24}p & a_{33}w \end{vmatrix} = \begin{bmatrix} 0 \\ -a_{33}wp \\ (a_{22}v + a_{24}p)p \end{bmatrix} \tag{C.34}$$

$$\boldsymbol{\Omega} \times \boldsymbol{L}_A = \begin{vmatrix} \boldsymbol{i} & \boldsymbol{j} & \boldsymbol{k} \\ p & 0 & 0 \\ a_{42}v + a_{44}p & 0 & 0 \end{vmatrix} = \boldsymbol{0} \tag{C.35}$$

$$\boldsymbol{u} \times \boldsymbol{P}_a = \begin{vmatrix} \boldsymbol{i} & \boldsymbol{j} & \boldsymbol{k} \\ 0 & v & w \\ 0 & a_{22}v + a_{24}p & a_{33}w \end{vmatrix} = \begin{bmatrix} (a_{33} - a_{22})vw - a_{24}wp \\ 0 \\ 0 \end{bmatrix} \tag{C.36}$$

the equilibrium equations for added mass (eq. (C.32) and (C.33)) can be written:

$$a_{22}\dot{v}^* + a_{24}\dot{p} - a_{33}wp = -F_{Ay} \tag{C.37}$$

$$a_{33}\dot{w}^* + a_{22}vp + a_{24}p^2 = -F_{Az} \tag{C.38}$$

$$a_{42}\dot{v}^* + a_{44}\dot{p} + \underbrace{(a_{33} - a_{22})vw - a_{24}wp}_{\boldsymbol{u}\times\boldsymbol{P}_B} = -M_{Ax} \tag{C.39}$$

By adding equations (C.26)-(C.28) and (C.37)-(C.39), it is found that

$$(m+a_{22})\dot{v}^* + (-mz_c+a_{24})\dot{p} - (m+a_{33})wp = \underbrace{F_y - F_{Ay}}_{=F_{I,y}} \tag{C.40}$$

$$(m+a_{33})\dot{w}^* + (m+a_{22})vp + (-mz_c+a_{24})p^2 = \underbrace{F_z - F_{Az}}_{=F_{I,z}} \tag{C.41}$$

$$(-mz_c+a_{42})\dot{v}^* + (I_x+a_{44})\dot{p} + (a_{33}-a_{22})vw + mz_cvp - a_{24}wp = \underbrace{M_x - M_{Ax}}_{=M_{I,x}} \tag{C.42}$$

By use of Eqs. (C.21) and (C.22) the sway acceleration may be written as $\dot{v}^* = \dot{v} + wp$ and the heave acceleration written as $\dot{w}^* = \dot{w} - vp$, hence the equations of motions related to a fixed coordinate system is

$$(m+a_{22})\dot{v} + (-mz_c+a_{24})\dot{p} + (a_{22}-a_{33})wp = F_{I,y} \tag{C.43}$$

$$(m+a_{33})\dot{w} + (a_{22}-a_{33})vp + (-mz_c+a_{24})p^2 = F_{I,z} \tag{C.44}$$

$$(-mz_c+a_{42})\dot{v} + (I_x+a_{44})\dot{p} + (a_{33}-a_{22})vw + mz_cvp + (-mz_c+a_{42}-a_{24})wp = M_{I,x} \tag{C.45}$$

On matrix form, it may be written as

$$\boldsymbol{N}\begin{bmatrix}\dot{v}\\ \dot{w}\\ \dot{p}\end{bmatrix} + (p\boldsymbol{O}+v\boldsymbol{P})\begin{bmatrix}v\\ w\\ p\end{bmatrix} = \boldsymbol{Q} \tag{C.46}$$

where

$$\boldsymbol{N} = \begin{bmatrix} m+a_{22} & 0 & -mz_c+a_{24} \\ 0 & m+a_{33} & 0 \\ -mz_c+a_{42} & 0 & I_x+a_{44} \end{bmatrix} \tag{C.47}$$

$$\boldsymbol{O} = \begin{bmatrix} 0 & a_{22}-a_{33} & 0 \\ a_{22}-a_{33} & 0 & -mz_c+a_{24} \\ mz_c & -mz_c+a_{42}-a_{24} & 0 \end{bmatrix} \tag{C.48}$$

$$\boldsymbol{P} = \begin{bmatrix} 0 & 0 & 0 \\ 0 & 0 & 0 \\ 0 & a_{33}-a_{22} & 0 \end{bmatrix} \tag{C.49}$$

$$\boldsymbol{Q} = \begin{bmatrix} F_{I,y} \\ F_{I,z} \\ M_{I,x} \end{bmatrix} \tag{C.50}$$

The accelerations may then be found as

$$\begin{bmatrix} \dot{v} \\ \dot{w} \\ \dot{p} \end{bmatrix} = \boldsymbol{N}^{-1}\{\boldsymbol{Q} - (p\boldsymbol{O} + v\boldsymbol{P}) \begin{bmatrix} v \\ w \\ p \end{bmatrix}\} \tag{C.51}$$

The loadvector $\boldsymbol{Q}$ is formulated as:

$$\boldsymbol{Q} = \begin{bmatrix} F_{I,y} \\ F_{I,z} \\ M_{I,x} \end{bmatrix} = \boldsymbol{F}_{wave} - mg \begin{bmatrix} \sin\phi \\ \cos\phi \\ 0 \end{bmatrix} - \boldsymbol{B}(\omega) \begin{bmatrix} v \\ w \\ p \end{bmatrix} - \boldsymbol{C} \begin{bmatrix} y \\ z \\ \phi \end{bmatrix} \tag{C.52}$$

where y and z are the coordinates for the position of the vessel in global coordinates, and ϕ is the roll angle.

The purpose of this exercise is to illustrate the difference between the earth fixed and the ship fixed local coordinates for a double symmetric barge exposed to beam seas. The non-linear terms can be seen in Eqs. (C.43)-(C.45), where the terms vp, wp and p^2 are included. For other wave directions and/or a non-symmetric vessel, several terms would have occured, but the principle is illustrated in the above. For small velocities, these non-linear terms are negligible, but for large velocities, these terms will affect the solution.

Since the added mass and damping depends on the excitation frequency, the matrices $\boldsymbol{N}$, $\boldsymbol{O}$ and $\boldsymbol{P}$ are also functions of the frequency. This must be transformed into a convolution term before the equation of motion can be solved in the time domain. That is not discussed further here, but it is discussed in Paper 1.

Appendix D

Model tests

D.1 Introduction

The experiments were performed using the equipment and model tanks at NTNU and Sintef Ocean[1]. A brief description of the model tests is given in Sec. 3.4. The model tests are described in more detail below. The barge with the cargo secured to the deck of the barge is shown in Fig. D.1. Two model tanks were used for the experiments: the MC-lab (Marine

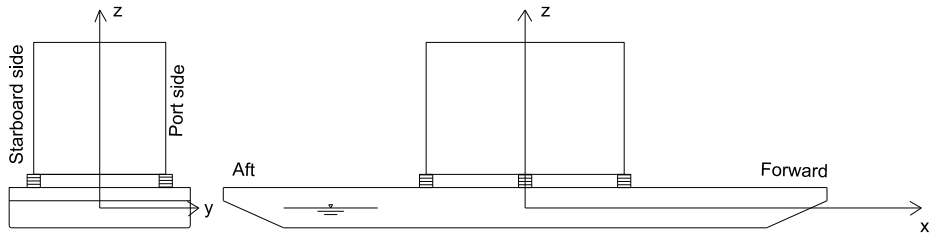

Figure D.1: Barge with a transported object, global axes shown

Cybernetics Laboratory) and the Towing tank. The model tests included free decay and forced roll tests, as well as the free floating barge model exposed to regular and irregular waves. In the forced roll tests, the model was rolled about the water line, while in the free decay tests, the model rolled about the center of gravity (i.e. about an axis parallel to the x-axis close to the center of gravity), see figure D.2.

[1]The part of Sintef Ocean referred to here operated under the name Marintek until 2017-01-01.

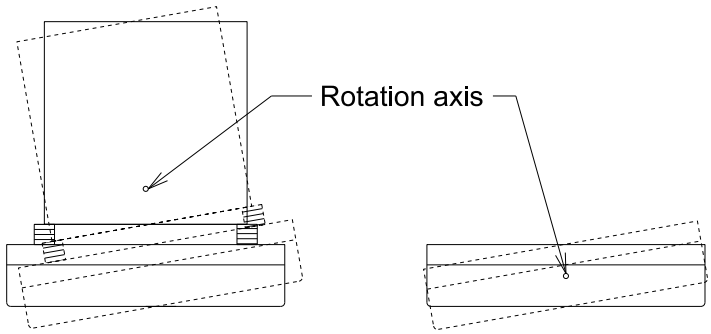

Figure D.2: Rotation axes (roll centers) for the free decay (left) and forced roll tests

Both two-dimensional and three-dimensional model tanks were available. In a two-dimensional test, only a section of the barge would have been tested, and end effects at the bow and stern would not be included. Moreover, for large model motions, it could be difficult to prevent contact with the tank walls. Therefore, a full model of the barge was tested.

D.2 Model test tanks

The MC-laboratory [116] and the Towing tank (actually a part of the Towing tank) [132] were used. The MC-Lab has a single-flap wave maker in one end and a parabolic beach in the other end. It is 40 m long (including the beach), 6.45 m wide and 1.5 m deep. The model was located in the center of the tank, half way between the wave maker and the beach. There was approximately a 2.3 m distance from the model to the tank walls (for the 1.8 m long model in a 6.45 m wide tank).

The Towing tank is 260 m long. It can be divided into two parts, and one part was used for the barge model tests. The tank has a double-flap wave maker in one end and a beach in the other end. The tank is then 85 m long (including the beach), 10.5 m wide and 10 m deep. The model was located near the center of the tank, approximately half way between the wave maker and the beach. There was a 4.35 m distance from the model to the tank walls at each side.

Forced roll and free decay tests were performed in the MC-Lab, and irregular wave tests were performed in the Towing Tank. Regular wave tests were performed in both tanks.

Table D.1: Key figures for the test facilities used for the model tests. Tank 1 is the MC-lab at NTNU [116], Tank 2 is the extension of the Towing tank at Sintef Ocean [132].

	Tank 1	Tank 2
Length	40 m	85 m
Width	6.5 m	10.5 m
Depth	1.5 m	10 m
Wavemaker	Single flap	Double flap
Maximum wave height	0.3 m	0.9 m
Wave period range	0.3-3 s	0.8-5 s

Key figures for the two model tanks are shown in Table D.1.

D.3 Model scaling

Froude scaling [137] was used in the experiments. The scale was 1:50. The bilge radius was 0.55 m at the full scale and 11 mm at the model scale.

The geometry of the model and wave elevations are then scaled by λ, the time and velocity are scaled by $\sqrt{\lambda}$, where $\lambda = 50$. The accelerations and roll angles are the same at the model scale and full scale. Linear roll damping, $B_{44,1}$ is scaled by $\lambda^{4.5}$, and quadratic roll damping, $B_{44,2}$, is scaled by λ^5.

The model was moored by soft springs to prevent drift. The natural sway period was approximately one minute in the full scale, and the mooring lines are neglected for the motion of the barge in waves.

D.4 Barge model

The model was made by Divinycell foam with a density of 60 kg/m^3 and reinforced with plywood plates in strategic areas. The model was coated with glass-fibre reinforced polyester and painted to achieve a smooth surface. The model was produced by Sintef Ocean.

A model of the barge at a scale of 1:50 was used. The barge model had a displacement of approximately 50 kg for a draught of 60 mm, corresponding to a full-scale displacement of 6250 tonnes.

Ballast compartments in the model allowed steel plates to be fitted to achieve the correct center of gravity and radius of gyration. The steel plates and the cargo were fastened by means of screws.

The model could be fitted with either a bilge radius or a sharp corner, see Fig. D.3. The model had a slot with dimensions of 11 by 11 mm at the bilges. Rails with a radius of 11 mm or sharp corners could be fitted with screws, enabling the same model to be used for testing the full-scale bilge radius and a sharp corner.

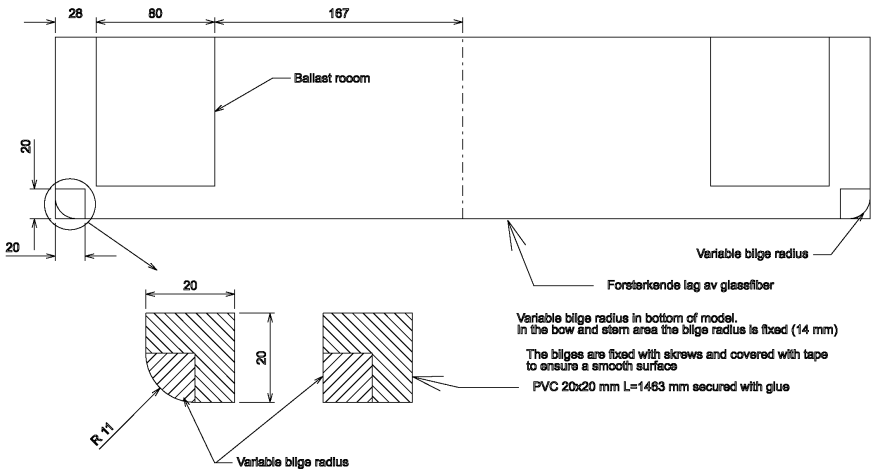

Figure D.3: Barge model cross section with bilge radius 11 mm and sharp corner

D.5 Monitoring

The following information was collected during the regular and irregular wave tests and the free decay tests:

- barge motions in six degrees of freedom
- sway, heave and roll accelerations
- wave elevations in several positions in the basin
- some test runs were filmed by a high-speed camera

The barge motions in six degrees of freedom were directly measured by the real-time positioning system. The barge model accelerations were monitored by three accelerometers fitted on the barge deck at the mid ship port and starboard side and in the centerline at the stern. The accelerometers measured the acceleration in the x-, y- and z-directions. Hence, the barge accelerations could be calculated and integrated twice to obtain the barge displacements for comparison with the real-time positioning system. During the forced roll tests, the exciting force and the roll angle of the barge were monitored, and several wave elevations were observed.

The monitoring equipment was provided by Sintef Ocean and was calibrated and used according to their procedures with assistance from Sintef Ocean personnel.

D.6 Free decay roll tests

The barge model was given an initial roll angle and then released. The motions and accelerations were monitored. A ship model can be given an roll angle simply by pushing it. The barge model, on the other hand, is quite stiff in roll (a large metacentric height, GM), and the setup shown in Figures D.4 and D.5 was used for the free decay tests.

The barge model was tested in free decay during rolling to estimate the damping. The equilibrium equation during rolling is written as:

$$(I_m + A_{44})\ddot{\theta} + B_1\dot{\theta} + B_2|\dot{\theta}|\dot{\theta} + C\theta = 0 \tag{D.1}$$

where
θ is the roll angle,
I_m is the rotational moment of inertia for the barge including the transported object and
A_{44} is the hydrodynamic added mass in rolling.
The linear and quadratic damping B_1 and B_2 are replaced by an equivalent linear damping B_{eq}, and based on energy considerations, the equivalent damping is described as

$$B_{eq} = B_1 + \frac{8}{3\pi}\omega_d\theta_i B_2 \tag{D.2}$$

and hence the rolling equation is

$$(I_m + A_{44})\ddot{\theta} + B_{eq}\dot{\theta} + C\theta = 0 \tag{D.3}$$

The solution to this equation can be written as

$$\theta(t) = Ae^{-\xi\omega_0 t}\cos(\omega_d t + \phi) \tag{D.4}$$

where A and ϕ are determined by the initial conditions. However, the concern here is the damping, represented by the damping ratio

$$\xi = \frac{B_{eq}}{2(I_m + A_{44})\omega_0} \tag{D.5}$$

The relationship between the damping ratio and the logarithmic decrement $\Lambda = \ln(\frac{\theta_{i-1}}{\theta_{i+1}})$ is

$$\Lambda = \xi\omega_0 T_d = \frac{2\pi\xi}{\sqrt{1-\xi^2}} \tag{D.6}$$

when the time between θ_{i-1} and θ_{i+1} is T_d. By combining Eq. (D.5) and (D.6), the equivalent damping is written as

$$B_{eq} = 2(I_m + A_{44})\omega_0\xi = \frac{2(I_m + A_{44})\omega_0\Lambda}{\sqrt{(2\pi)^2 + \Lambda^2}} \approx \underline{\frac{(I_m + A_{44})\omega_0\Lambda}{\pi}} \tag{D.7}$$

Λ is found from the model tests by plotting $\frac{8}{3\pi}\omega_d\theta_i$ on the abscissa and B_{eq} on the ordinate and fitting a straight line through the points. Then, by Eq. (D.2), B_1 and B_2 are read directly from the plot.

D.7 Forced roll tests

The forced roll tests were performed with the barge model in a rig and by use of hydraulic actuators, as shown schematically in Figures D.6 and D.7. A photo of the model in the forced roll rig is shown in Fig. D.8. The exiting force was monitored and used to calculate the applied roll moment. The actuators have the following characteristics: maximum stroke of 0.5 m, maximum speed of 1 m/s, and maximum acceleration of 2 m/s^2. The barge rotates about a point in the water line and was supported by a pivot (hinged support) at each end.

The damping is calculated based on the results from the model tests [106].

D.8 Tests with wave-induced motions

The model was equipped with soft mooring lines to prevent drift. The mooring lines were connected to support points on the barge at the water surface. The natural period of the mooring system was high relative to the wave periods, and the effect of the mooring lines on the motion was assumed to be negligible for the wave periodic barge motions. The barge was exposed

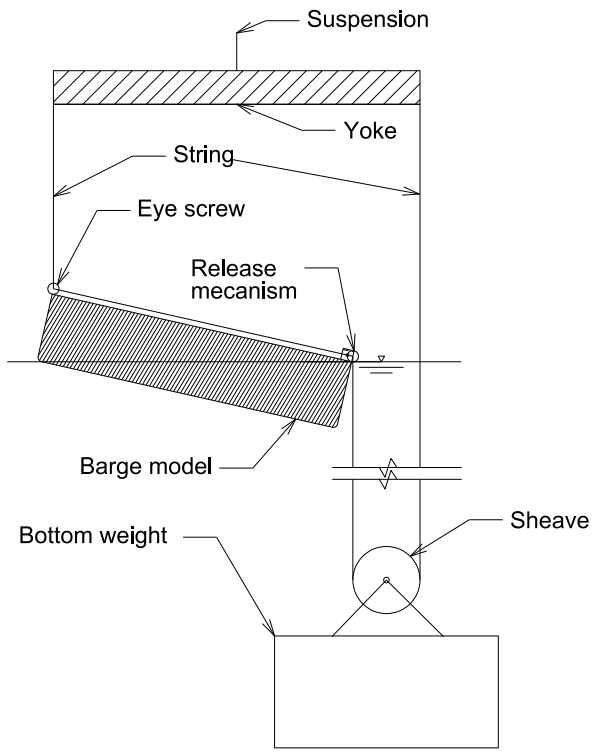

Figure D.4: Barge cross section with the arrangement for the free decay test in rolling (designed to give pure roll motion)

to waves from 90 ° (beam sea). The setup in the MC-lab is indicated in Fig. D.9.

In the regular wave tests, the purpose was to study the barge motion as a function of the wave height and wave period. For a given wave height, a range of periods were included. The minimum wave periods (maximum wave steepness) were calculated based on recommendations given in the *DNV Rules for Planning and Execution of Marine Operations*. Deep water was assumed. In the irregular wave tests, three-hour simulations of several sea states were tested, as described in Paper 1 [109].

Figure D.5: Barge model with the arrangement for the free decay test in rolling

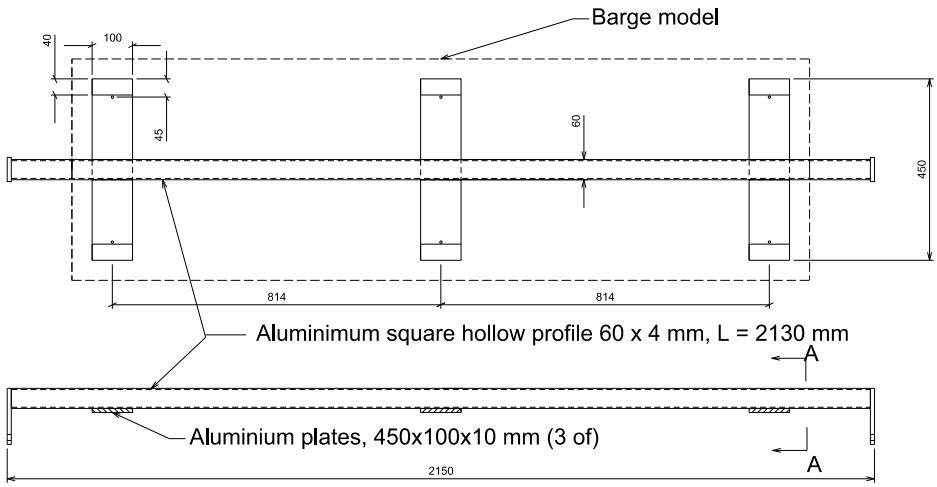

Figure D.6: Plan view (upper) and front elevation (lower) of the jig used during the forced roll test. The outline of the barge model is indicated on the plan view. View A-A is shown in figure D.7.

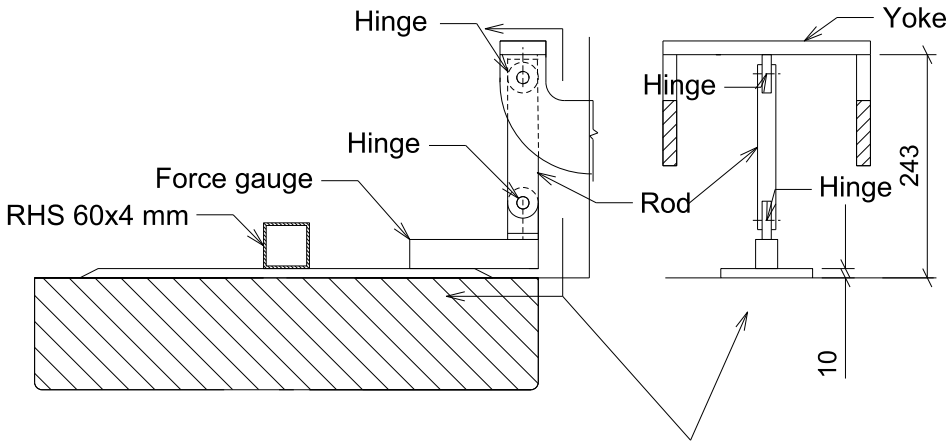

Figure D.7: View A-A from figure D.6: The barge model with the jig (RHS 60x4) and the arrangement for the forced roll test. The roll motion was induced by the yoke being moved up and down by electric actuators fitted on the carriage in the model tank. See Fig. D.8 for an overview of the barge model.

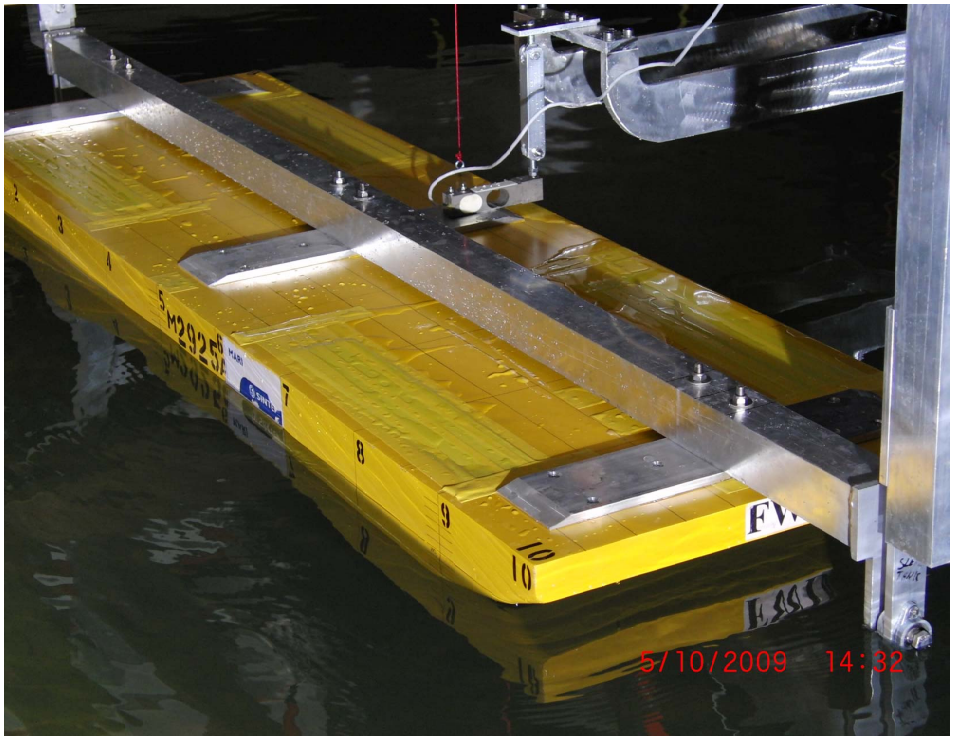

Figure D.8: Barge model fitted in the forced roll jig. The barge model was rolled about hinges in the water line.

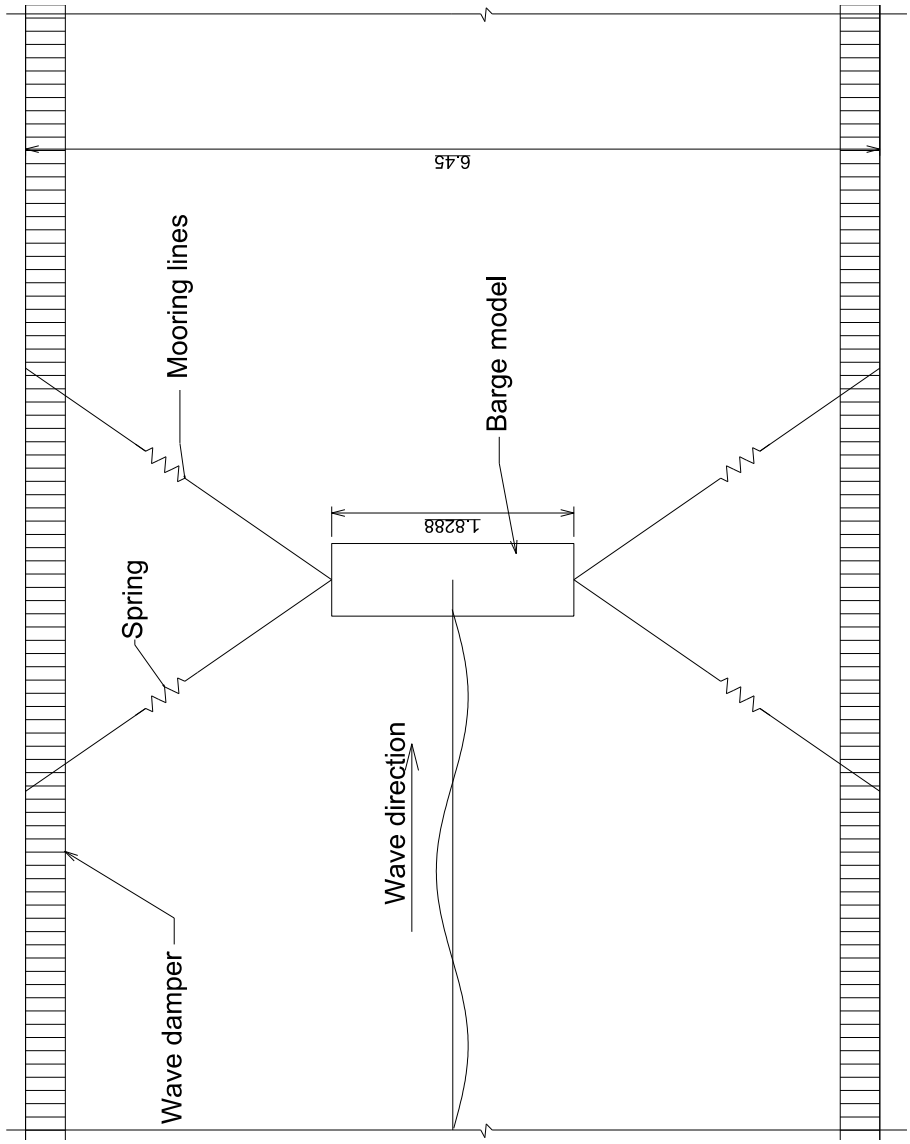

Figure D.9: Barge model with the arrangement for mooring in the MC-Lab

Appendix E

List of previous PhD theses at Dept. of Marine Tech.

Previous PhD theses published at the Department of Marine Technology
(earlier: Faculty of Marine Technology)
NORWEGIAN UNIVERSITY OF SCIENCE AND TECHNOLOGY

Report No.	Author	Title
	Kavlie, Dag	Optimization of Plane Elastic Grillages, 1967
	Hansen, Hans R.	Man-Machine Communication and Data-Storage Methods in Ship Structural Design, 1971
	Gisvold, Kaare M.	A Method for non-linear mixed-integer programming and its Application to Design Problems, 1971
	Lund, Sverre	Tanker Frame Optimalization by means of SUMT-Transformation and Behaviour Models, 1971
	Vinje, Tor	On Vibration of Spherical Shells Interacting with Fluid, 1972
	Lorentz, Jan D.	Tank Arrangement for Crude Oil Carriers in Accordance with the new Anti-Pollution Regulations, 1975
	Carlsen, Carl A.	Computer-Aided Design of Tanker Structures, 1975
	Larsen, Carl M.	Static and Dynamic Analysis of Offshore Pipelines during Installation, 1976
UR-79-01	Brigt Hatlestad, MK	The finite element method used in a fatigue evaluation of fixed offshore platforms. (Dr.Ing. Thesis)
UR-79-02	Erik Pettersen, MK	Analysis and design of cellular structures. (Dr.Ing. Thesis)
UR-79-03	Sverre Valsgård, MK	Finite difference and finite element methods applied to nonlinear analysis of plated structures. (Dr.Ing. Thesis)
UR-79-04	Nils T. Nordsve, MK	Finite element collapse analysis of structural members considering imperfections and stresses due to fabrication. (Dr.Ing. Thesis)
UR-79-05	Ivar J. Fylling, MK	Analysis of towline forces in ocean towing systems. (Dr.Ing. Thesis)
UR-80-06	Nils Sandsmark, MM	Analysis of Stationary and Transient Heat Conduction by the Use of the Finite Element Method. (Dr.Ing. Thesis)
UR-80-09	Sverre Haver, MK	Analysis of uncertainties related to the stochastic modeling of ocean waves. (Dr.Ing. Thesis)
UR-81-15	Odland, Jonas	On the Strength of welded Ring stiffened cylindrical Shells primarily subjected to axial Compression
UR-82-17	Engesvik, Knut	Analysis of Uncertainties in the fatigue Capacity of Welded Joints

Report No.	Author	Title
UR-82-18	Rye, Henrik	Ocean wave groups
UR-83-30	Eide, Oddvar Inge	On Cumulative Fatigue Damage in Steel Welded Joints
UR-83-33	Mo, Olav	Stochastic Time Domain Analysis of Slender Offshore Structures
UR-83-34	Amdahl, Jørgen	Energy absorption in Ship-platform impacts
UR-84-37	Mørch, Morten	Motions and mooring forces of semi submersibles as determined by full-scale measurements and theoretical analysis
UR-84-38	Soares, C. Guedes	Probabilistic models for load effects in ship structures
UR-84-39	Aarsnes, Jan V.	Current forces on ships
UR-84-40	Czujko, Jerzy	Collapse Analysis of Plates subjected to Biaxial Compression and Lateral Load
UR-85-46	Alf G. Engseth, MK	Finite element collapse analysis of tubular steel offshore structures. (Dr.Ing. Thesis)
UR-86-47	Dengody Sheshappa, MP	A Computer Design Model for Optimizing Fishing Vessel Designs Based on Techno-Economic Analysis. (Dr.Ing. Thesis)
UR-86-48	Vidar Aanesland, MH	A Theoretical and Numerical Study of Ship Wave Resistance. (Dr.Ing. Thesis)
UR-86-49	Heinz-Joachim Wessel, MK	Fracture Mechanics Analysis of Crack Growth in Plate Girders. (Dr.Ing. Thesis)
UR-86-50	Jon Taby, MK	Ultimate and Post-ultimate Strength of Dented Tubular Members. (Dr.Ing. Thesis)
UR-86-51	Walter Lian, MH	A Numerical Study of Two-Dimensional Separated Flow Past Bluff Bodies at Moderate KC-Numbers. (Dr.Ing. Thesis)
UR-86-52	Bjørn Sortland, MH	Force Measurements in Oscillating Flow on Ship Sections and Circular Cylinders in a U-Tube Water Tank. (Dr.Ing. Thesis)
UR-86-53	Kurt Strand, MM	A System Dynamic Approach to One-dimensional Fluid Flow. (Dr.Ing. Thesis)
UR-86-54	Arne Edvin Løken, MH	Three Dimensional Second Order Hydrodynamic Effects on Ocean Structures in Waves. (Dr.Ing. Thesis)
UR-86-55	Sigurd Falch, MH	A Numerical Study of Slamming of Two-Dimensional Bodies. (Dr.Ing. Thesis)
UR-87-56	Arne Braathen, MH	Application of a Vortex Tracking Method to the Prediction of Roll Damping of a Two-Dimension Floating Body. (Dr.Ing. Thesis)
UR-87-57	Bernt Leira, MK	Gaussian Vector Processes for Reliability Analysis involving Wave-Induced Load Effects. (Dr.Ing. Thesis)
UR-87-58	Magnus Småvik, MM	Thermal Load and Process Characteristics in a Two-Stroke Diesel Engine with Thermal Barriers (in Norwegian). (Dr.Ing. Thesis)

Report No.	Author	Title
MTA-88-59	Bernt Arild Bremdal, MP	An Investigation of Marine Installation Processes – A Knowledge-Based Planning Approach. (Dr.Ing. Thesis)
MTA-88-60	Xu Jun, MK	Non-linear Dynamic Analysis of Space-framed Offshore Structures. (Dr.Ing. Thesis)
MTA-89-61	Gang Miao, MH	Hydrodynamic Forces and Dynamic Responses of Circular Cylinders in Wave Zones. (Dr.Ing. Thesis)
MTA-89-62	Martin Greenhow, MH	Linear and Non-Linear Studies of Waves and Floating Bodies. Part I and Part II. (Dr.Techn. Thesis)
MTA-89-63	Chang Li, MH	Force Coefficients of Spheres and Cubes in Oscillatory Flow with and without Current. (Dr.Ing. Thesis
MTA-89-64	Hu Ying, MP	A Study of Marketing and Design in Development of Marine Transport Systems. (Dr.Ing. Thesis)
MTA-89-65	Arild Jæger, MH	Seakeeping, Dynamic Stability and Performance of a Wedge Shaped Planing Hull. (Dr.Ing. Thesis)
MTA-89-66	Chan Siu Hung, MM	The dynamic characteristics of tilting-pad bearings
MTA-89-67	Kim Wikstrøm, MP	Analysis av projekteringen for ett offshore projekt. (Licenciat-avhandling)
MTA-89-68	Jiao Guoyang, MK	Reliability Analysis of Crack Growth under Random Loading, considering Model Updating. (Dr.Ing. Thesis)
MTA-89-69	Arnt Olufsen, MK	Uncertainty and Reliability Analysis of Fixed Offshore Structures. (Dr.Ing. Thesis)
MTA-89-70	Wu Yu-Lin, MR	System Reliability Analyses of Offshore Structures using improved Truss and Beam Models. (Dr.Ing. Thesis)
MTA-90-71	Jan Roger Hoff, MH	Three-dimensional Green function of a vessel with forward speed in waves. (Dr.Ing. Thesis)
MTA-90-72	Rong Zhao, MH	Slow-Drift Motions of a Moored Two-Dimensional Body in Irregular Waves. (Dr.Ing. Thesis)
MTA-90-73	Atle Minsaas, MP	Economical Risk Analysis. (Dr.Ing. Thesis)
MTA-90-74	Knut-Ariel Farnes, MK	Long-term Statistics of Response in Non-linear Marine Structures. (Dr.Ing. Thesis)
MTA-90-75	Torbjørn Sotberg, MK	Application of Reliability Methods for Safety Assessment of Submarine Pipelines. (Dr.Ing. Thesis)
MTA-90-76	Zeuthen, Steffen, MP	SEAMAID. A computational model of the design process in a constraint-based logic programming environment. An example from the offshore domain. (Dr.Ing. Thesis)

Report No.	Author	Title
MTA-91-77	Haagensen, Sven, MM	Fuel Dependant Cyclic Variability in a Spark Ignition Engine – An Optical Approach. (Dr.Ing. Thesis)
MTA-91-78	Løland, Geir, MH	Current forces on and flow through fish farms. (Dr.Ing. Thesis)
MTA-91-79	Hoen, Christopher, MK	System Identification of Structures Excited by Stochastic Load Processes. (Dr.Ing. Thesis)
MTA-91-80	Haugen, Stein, MK	Probabilistic Evaluation of Frequency of Collision between Ships and Offshore Platforms. (Dr.Ing. Thesis)
MTA-91-81	Sødahl, Nils, MK	Methods for Design and Analysis of Flexible Risers. (Dr.Ing. Thesis)
MTA-91-82	Ormberg, Harald, MK	Non-linear Response Analysis of Floating Fish Farm Systems. (Dr.Ing. Thesis)
MTA-91-83	Marley, Mark J., MK	Time Variant Reliability under Fatigue Degradation. (Dr.Ing. Thesis)
MTA-91-84	Krokstad, Jørgen R., MH	Second-order Loads in Multidirectional Seas. (Dr.Ing. Thesis)
MTA-91-85	Molteberg, Gunnar A., MM	The Application of System Identification Techniques to Performance Monitoring of Four Stroke Turbocharged Diesel Engines. (Dr.Ing. Thesis)
MTA-92-86	Mørch, Hans Jørgen Bjelke, MH	Aspects of Hydrofoil Design: with Emphasis on Hydrofoil Interaction in Calm Water. (Dr.Ing. Thesis)
MTA-92-87	Chan Siu Hung, MM	Nonlinear Analysis of Rotordynamic Instabilities in Highspeed Turbomachinery. (Dr.Ing. Thesis)
MTA-92-88	Bessason, Bjarni, MK	Assessment of Earthquake Loading and Response of Seismically Isolated Bridges. (Dr.Ing. Thesis)
MTA-92-89	Langli, Geir, MP	Improving Operational Safety through exploitation of Design Knowledge – an investigation of offshore platform safety. (Dr.Ing. Thesis)
MTA-92-90	Sævik, Svein, MK	On Stresses and Fatigue in Flexible Pipes. (Dr.Ing. Thesis)
MTA-92-91	Ask, Tor Ø., MM	Ignition and Flame Growth in Lean Gas-Air Mixtures. An Experimental Study with a Schlieren System. (Dr.Ing. Thesis)
MTA-86-92	Hessen, Gunnar, MK	Fracture Mechanics Analysis of Stiffened Tubular Members. (Dr.Ing. Thesis)
MTA-93-93	Steinebach, Christian, MM	Knowledge Based Systems for Diagnosis of Rotating Machinery. (Dr.Ing. Thesis)
MTA-93-94	Dalane, Jan Inge, MK	System Reliability in Design and Maintenance of Fixed Offshore Structures. (Dr.Ing. Thesis)
MTA-93-95	Steen, Sverre, MH	Cobblestone Effect on SES. (Dr.Ing. Thesis)

Report No.	Author	Title
MTA-93-96	Karunakaran, Daniel, MK	Nonlinear Dynamic Response and Reliability Analysis of Drag-dominated Offshore Platforms. (Dr.Ing. Thesis)
MTA-93-97	Hagen, Arnulf, MP	The Framework of a Design Process Language. (Dr.Ing. Thesis)
MTA-93-98	Nordrik, Rune, MM	Investigation of Spark Ignition and Autoignition in Methane and Air Using Computational Fluid Dynamics and Chemical Reaction Kinetics. A Numerical Study of Ignition Processes in Internal Combustion Engines. (Dr.Ing. Thesis)
MTA-94-99	Passano, Elizabeth, MK	Efficient Analysis of Nonlinear Slender Marine Structures. (Dr.Ing. Thesis)
MTA-94-100	Kvålsvold, Jan, MH	Hydroelastic Modelling of Wetdeck Slamming on Multihull Vessels. (Dr.Ing. Thesis)
MTA-94-102	Bech, Sidsel M., MK	Experimental and Numerical Determination of Stiffness and Strength of GRP/PVC Sandwich Structures. (Dr.Ing. Thesis)
MTA-95-103	Paulsen, Hallvard, MM	A Study of Transient Jet and Spray using a Schlieren Method and Digital Image Processing. (Dr.Ing. Thesis)
MTA-95-104	Hovde, Geir Olav, MK	Fatigue and Overload Reliability of Offshore Structural Systems, Considering the Effect of Inspection and Repair. (Dr.Ing. Thesis)
MTA-95-105	Wang, Xiaozhi, MK	Reliability Analysis of Production Ships with Emphasis on Load Combination and Ultimate Strength. (Dr.Ing. Thesis)
MTA-95-106	Ulstein, Tore, MH	Nonlinear Effects of a Flexible Stern Seal Bag on Cobblestone Oscillations of an SES. (Dr.Ing. Thesis)
MTA-95-107	Solaas, Frøydis, MH	Analytical and Numerical Studies of Sloshing in Tanks. (Dr.Ing. Thesis)
MTA-95-108	Hellan, Øyvind, MK	Nonlinear Pushover and Cyclic Analyses in Ultimate Limit State Design and Reassessment of Tubular Steel Offshore Structures. (Dr.Ing. Thesis)
MTA-95-109	Hermundstad, Ole A., MK	Theoretical and Experimental Hydroelastic Analysis of High Speed Vessels. (Dr.Ing. Thesis)
MTA-96-110	Bratland, Anne K., MH	Wave-Current Interaction Effects on Large-Volume Bodies in Water of Finite Depth. (Dr.Ing. Thesis)
MTA-96-111	Herfjord, Kjell, MH	A Study of Two-dimensional Separated Flow by a Combination of the Finite Element Method and Navier-Stokes Equations. (Dr.Ing. Thesis)
MTA-96-112	AEsøy, Vilmar, MM	Hot Surface Assisted Compression Ignition in a Direct Injection Natural Gas Engine. (Dr.Ing. Thesis)

Report No.	Author	Title
MTA-96-113	Eknes, Monika L., MK	Escalation Scenarios Initiated by Gas Explosions on Offshore Installations. (Dr.Ing. Thesis)
MTA-96-114	Erikstad, Stein O., MP	A Decision Support Model for Preliminary Ship Design. (Dr.Ing. Thesis)
MTA-96-115	Pedersen, Egil, MH	A Nautical Study of Towed Marine Seismic Streamer Cable Configurations. (Dr.Ing. Thesis)
MTA-97-116	Moksnes, Paul O., MM	Modelling Two-Phase Thermo-Fluid Systems Using Bond Graphs. (Dr.Ing. Thesis)
MTA-97-117	Halse, Karl H., MK	On Vortex Shedding and Prediction of Vortex-Induced Vibrations of Circular Cylinders. (Dr.Ing. Thesis)
MTA-97-118	Igland, Ragnar T., MK	Reliability Analysis of Pipelines during Laying, considering Ultimate Strength under Combined Loads. (Dr.Ing. Thesis)
MTA-97-119	Pedersen, Hans-P., MP	Levendefiskteknologi for fiskefartøy. (Dr.Ing. Thesis)
MTA-98-120	Vikestad, Kyrre, MK	Multi-Frequency Response of a Cylinder Subjected to Vortex Shedding and Support Motions. (Dr.Ing. Thesis)
MTA-98-121	Azadi, Mohammad R. E., MK	Analysis of Static and Dynamic Pile-Soil-Jacket Behaviour. (Dr.Ing. Thesis)
MTA-98-122	Ulltang, Terje, MP	A Communication Model for Product Information. (Dr.Ing. Thesis)
MTA-98-123	Torbergsen, Erik, MM	Impeller/Diffuser Interaction Forces in Centrifugal Pumps. (Dr.Ing. Thesis)
MTA-98-124	Hansen, Edmond, MH	A Discrete Element Model to Study Marginal Ice Zone Dynamics and the Behaviour of Vessels Moored in Broken Ice. (Dr.Ing. Thesis)
MTA-98-125	Videiro, Paulo M., MK	Reliability Based Design of Marine Structures. (Dr.Ing. Thesis)
MTA-99-126	Mainçon, Philippe, MK	Fatigue Reliability of Long Welds Application to Titanium Risers. (Dr.Ing. Thesis)
MTA-99-127	Haugen, Elin M., MH	Hydroelastic Analysis of Slamming on Stiffened Plates with Application to Catamaran Wetdecks. (Dr.Ing. Thesis)
MTA-99-128	Langhelle, Nina K., MK	Experimental Validation and Calibration of Nonlinear Finite Element Models for Use in Design of Aluminium Structures Exposed to Fire. (Dr.Ing. Thesis)
MTA-99-129	Berstad, Are J., MK	Calculation of Fatigue Damage in Ship Structures. (Dr.Ing. Thesis)
MTA-99-130	Andersen, Trond M., MM	Short Term Maintenance Planning. (Dr.Ing. Thesis)
MTA-99-131	Tveiten, Bård Wathne, MK	Fatigue Assessment of Welded Aluminium Ship Details. (Dr.Ing. Thesis)

Report No.	Author	Title
MTA-99-132	Søreide, Fredrik, MP	Applications of underwater technology in deep water archaeology. Principles and practice. (Dr.Ing. Thesis)
MTA-99-133	Tønnessen, Rune, MH	A Finite Element Method Applied to Unsteady Viscous Flow Around 2D Blunt Bodies With Sharp Corners. (Dr.Ing. Thesis)
MTA-99-134	Elvekrok, Dag R., MP	Engineering Integration in Field Development Projects in the Norwegian Oil and Gas Industry. The Supplier Management of Norne. (Dr.Ing. Thesis)
MTA-99-135	Fagerholt, Kjetil, MP	Optimeringsbaserte Metoder for Ruteplanlegging innen skipsfart. (Dr.Ing. Thesis)
MTA-99-136	Bysveen, Marie, MM	Visualization in Two Directions on a Dynamic Combustion Rig for Studies of Fuel Quality. (Dr.Ing. Thesis)
MTA-2000-137	Storteig, Eskild, MM	Dynamic characteristics and leakage performance of liquid annular seals in centrifugal pumps. (Dr.Ing. Thesis)
MTA-2000-138	Sagli, Gro, MK	Model uncertainty and simplified estimates of long term extremes of hull girder loads in ships. (Dr.Ing. Thesis)
MTA-2000-139	Tronstad, Harald, MK	Nonlinear analysis and design of cable net structures like fishing gear based on the finite element method. (Dr.Ing. Thesis)
MTA-2000-140	Kroneberg, André, MP	Innovation in shipping by using scenarios. (Dr.Ing. Thesis)
MTA-2000-141	Haslum, Herbjørn Alf, MH	Simplified methods applied to nonlinear motion of spar platforms. (Dr.Ing. Thesis)
MTA-2001-142	Samdal, Ole Johan, MM	Modelling of Degradation Mechanisms and Stressor Interaction on Static Mechanical Equipment Residual Lifetime. (Dr.Ing. Thesis)
MTA-2001-143	Baarholm, Rolf Jarle, MH	Theoretical and experimental studies of wave impact underneath decks of offshore platforms. (Dr.Ing. Thesis)
MTA-2001-144	Wang, Lihua, MK	Probabilistic Analysis of Nonlinear Wave-induced Loads on Ships. (Dr.Ing. Thesis)
MTA-2001-145	Kristensen, Odd H. Holt, MK	Ultimate Capacity of Aluminium Plates under Multiple Loads, Considering HAZ Properties. (Dr.Ing. Thesis)
MTA-2001-146	Greco, Marilena, MH	A Two-Dimensional Study of Green-Water Loading. (Dr.Ing. Thesis)
MTA-2001-147	Heggelund, Svein E., MK	Calculation of Global Design Loads and Load Effects in Large High Speed Catamarans. (Dr.Ing. Thesis)
MTA-2001-148	Babalola, Olusegun T., MK	Fatigue Strength of Titanium Risers – Defect Sensitivity. (Dr.Ing. Thesis)
MTA-2001-149	Mohammed, Abuu K., MK	Nonlinear Shell Finite Elements for Ultimate Strength and Collapse Analysis of Ship Structures. (Dr.Ing. Thesis)

Report No.	Author	Title
MTA-2002-150	Holmedal, Lars E., MH	Wave-current interactions in the vicinity of the sea bed. (Dr.Ing. Thesis)
MTA-2002-151	Rognebakke, Olav F., MH	Sloshing in rectangular tanks and interaction with ship motions. (Dr.Ing. Thesis)
MTA-2002-152	Lader, Pål Furset, MH	Geometry and Kinematics of Breaking Waves. (Dr.Ing. Thesis)
MTA-2002-153	Yang, Qinzheng, MH	Wash and wave resistance of ships in finite water depth. (Dr.Ing. Thesis)
MTA-2002-154	Melhus, Øyvin, MM	Utilization of VOC in Diesel Engines. Ignition and combustion of VOC released by crude oil tankers. (Dr.Ing. Thesis)
MTA-2002-155	Ronæss, Marit, MH	Wave Induced Motions of Two Ships Advancing on Parallel Course. (Dr.Ing. Thesis)
MTA-2002-156	Økland, Ole D., MK	Numerical and experimental investigation of whipping in twin hull vessels exposed to severe wet deck slamming. (Dr.Ing. Thesis)
MTA-2002-157	Ge, Chunhua, MK	Global Hydroelastic Response of Catamarans due to Wet Deck Slamming. (Dr.Ing. Thesis)
MTA-2002-158	Byklum, Eirik, MK	Nonlinear Shell Finite Elements for Ultimate Strength and Collapse Analysis of Ship Structures. (Dr.Ing. Thesis)
IMT-2003-1	Chen, Haibo, MK	Probabilistic Evaluation of FPSO-Tanker Collision in Tandem Offloading Operation. (Dr.Ing. Thesis)
IMT-2003-2	Skaugset, Kjetil Bjørn, MK	On the Suppression of Vortex Induced Vibrations of Circular Cylinders by Radial Water Jets. (Dr.Ing. Thesis)
IMT-2003-3	Chezhian, Muthu	Three-Dimensional Analysis of Slamming. (Dr.Ing. Thesis)
IMT-2003-4	Buhaug, Øyvind	Deposit Formation on Cylinder Liner Surfaces in Medium Speed Engines. (Dr.Ing. Thesis)
IMT-2003-5	Tregde, Vidar	Aspects of Ship Design: Optimization of Aft Hull with Inverse Geometry Design. (Dr.Ing. Thesis)
IMT-2003-6	Wist, Hanne Therese	Statistical Properties of Successive Ocean Wave Parameters. (Dr.Ing. Thesis)
IMT-2004-7	Ransau, Samuel	Numerical Methods for Flows with Evolving Interfaces. (Dr.Ing. Thesis)
IMT-2004-8	Soma, Torkel	Blue-Chip or Sub-Standard. A data interrogation approach of identity safety characteristics of shipping organization. (Dr.Ing. Thesis)
IMT-2004-9	Ersdal, Svein	An experimental study of hydrodynamic forces on cylinders and cables in near axial flow. (Dr.Ing. Thesis)
IMT-2005-10	Brodtkorb, Per Andreas	The Probability of Occurrence of Dangerous Wave Situations at Sea. (Dr.Ing. Thesis)
IMT-2005-11	Yttervik, Rune	Ocean current variability in relation to offshore engineering. (Dr.Ing. Thesis)

Report No.	Author	Title
IMT-2005-12	Fredheim, Arne	Current Forces on Net-Structures. (Dr.Ing. Thesis)
IMT-2005-13	Heggernes, Kjetil	Flow around marine structures. (Dr.Ing. Thesis
IMT-2005-14	Fouques, Sebastien	Lagrangian Modelling of Ocean Surface Waves and Synthetic Aperture Radar Wave Measurements. (Dr.Ing. Thesis)
IMT-2006-15	Holm, Håvard	Numerical calculation of viscous free surface flow around marine structures. (Dr.Ing. Thesis)
IMT-2006-16	Bjørheim, Lars G.	Failure Assessment of Long Through Thickness Fatigue Cracks in Ship Hulls. (Dr.Ing. Thesis)
IMT-2006-17	Hansson, Lisbeth	Safety Management for Prevention of Occupational Accidents. (Dr.Ing. Thesis)
IMT-2006-18	Zhu, Xinying	Application of the CIP Method to Strongly Nonlinear Wave-Body Interaction Problems. (Dr.Ing. Thesis)
IMT-2006-19	Reite, Karl Johan	Modelling and Control of Trawl Systems. (Dr.Ing. Thesis)
IMT-2006-20	Smogeli, Øyvind Notland	Control of Marine Propellers. From Normal to Extreme Conditions. (Dr.Ing. Thesis)
IMT-2007-21	Storhaug, Gaute	Experimental Investigation of Wave Induced Vibrations and Their Effect on the Fatigue Loading of Ships. (Dr.Ing. Thesis)
IMT-2007-22	Sun, Hui	A Boundary Element Method Applied to Strongly Nonlinear Wave-Body Interaction Problems. (PhD Thesis, CeSOS)
IMT-2007-23	Rustad, Anne Marthine	Modelling and Control of Top Tensioned Risers. (PhD Thesis, CeSOS)
IMT-2007-24	Johansen, Vegar	Modelling flexible slender system for real-time simulations and control applications
IMT-2007-25	Wroldsen, Anders Sunde	Modelling and control of tensegrity structures. (PhD Thesis, CeSOS)
IMT-2007-26	Aronsen, Kristoffer Høye	An experimental investigation of in-line and combined inline and cross flow vortex induced vibrations. (Dr. avhandling, IMT)
IMT-2007-27	Gao, Zhen	Stochastic Response Analysis of Mooring Systems with Emphasis on Frequency-domain Analysis of Fatigue due to Wide-band Response Processes (PhD Thesis, CeSOS)
IMT-2007-28	Thorstensen, Tom Anders	Lifetime Profit Modelling of Ageing Systems Utilizing Information about Technical Condition. (Dr.ing. thesis, IMT)
IMT-2008-29	Berntsen, Per Ivar B.	Structural Reliability Based Position Mooring. (PhD-Thesis, IMT)
IMT-2008-30	Ye, Naiquan	Fatigue Assessment of Aluminium Welded Box-stiffener Joints in Ships (Dr.ing. thesis, IMT)
IMT-2008-31	Radan, Damir	Integrated Control of Marine Electrical Power Systems. (PhD-Thesis, IMT)

Report No.	Author	Title
IMT-2008-32	Thomassen, Paul	Methods for Dynamic Response Analysis and Fatigue Life Estimation of Floating Fish Cages. (Dr.ing. thesis, IMT)
IMT-2008-33	Pákozdi, Csaba	A Smoothed Particle Hydrodynamics Study of Two-dimensional Nonlinear Sloshing in Rectangular Tanks. (Dr.ing.thesis, IMT/ CeSOS)
IMT-2008-34	Grytøyr, Guttorm	A Higher-Order Boundary Element Method and Applications to Marine Hydrodynamics. (Dr.ing.thesis, IMT)
IMT-2008-35	Drummen, Ingo	Experimental and Numerical Investigation of Nonlinear Wave-Induced Load Effects in Containerships considering Hydroelasticity. (PhD thesis, CeSOS)
IMT-2008-36	Skejic, Renato	Maneuvering and Seakeeping of a Singel Ship and of Two Ships in Interaction. (PhD-Thesis, CeSOS)
IMT-2008-37	Harlem, Alf	An Age-Based Replacement Model for Repairable Systems with Attention to High-Speed Marine Diesel Engines. (PhD-Thesis, IMT)
IMT-2008-38	Alsos, Hagbart S.	Ship Grounding. Analysis of Ductile Fracture, Bottom Damage and Hull Girder Response. (PhD-thesis, IMT)
IMT-2008-39	Graczyk, Mateusz	Experimental Investigation of Sloshing Loading and Load Effects in Membrane LNG Tanks Subjected to Random Excitation. (PhD-thesis, CeSOS)
IMT-2008-40	Taghipour, Reza	Efficient Prediction of Dynamic Response for Flexible amd Multi-body Marine Structures. (PhD-thesis, CeSOS)
IMT-2008-41	Ruth, Eivind	Propulsion control and thrust allocation on marine vessels. (PhD thesis, CeSOS)
IMT-2008-42	Nystad, Bent Helge	Technical Condition Indexes and Remaining Useful Life of Aggregated Systems. PhD thesis, IMT
IMT-2008-43	Soni, Prashant Kumar	Hydrodynamic Coefficients for Vortex Induced Vibrations of Flexible Beams. PhD thesis, CeSOS
IMT-2009-43	Amlashi, Hadi K.K.	Ultimate Strength and Reliability-based Design of Ship Hulls with Emphasis on Combined Global and Local Loads. PhD Thesis, IMT
IMT-2009-44	Pedersen, Tom Arne	Bond Graph Modelling of Marine Power Systems. PhD Thesis, IMT
IMT-2009-45	Kristiansen, Trygve	Two-Dimensional Numerical and Experimental Studies of Piston-Mode Resonance. PhD thesis, CeSOS
IMT-2009-46	Ong, Muk Chen	Applications of a Standard High Reynolds Number Model and a Stochastic Scour Prediction Model for Marine Structures. PhD-thesis, IMT

Report No.	Author	Title
IMT-2009-47	Hong, Lin	Simplified Analysis and Design of Ships subjected to Collision and Grounding. PhD-thesis, IMT
IMT-2009-48	Koushan, Kamran	Vortex Induced Vibrations of Free Span Pipelines, PhD thesis, IMT
IMT-2009-49	Korsvik, Jarl Eirik	Heuristic Methods for Ship Routing and Scheduling. PhD-thesis, IMT
IMT-2009-50	Lee, Jihoon	Experimental Investigation and Numerical in Analyzing the Ocean Current Displacement of Longlines. Ph.d.-Thesis, IMT.
IMT-2009-51	Vestbøstad, Tone Gran	A Numerical Study of Wave-in-Deck Impact usin a Two-Dimensional Constrained Interpolation Profile Method, Ph.d.thesis, CeSOS.
IMT-2009-52	Bruun, Kristine	Bond Graph Modelling of Fuel Cells for Marine Power Plants. Ph.d.-thesis, IMT
IMT-2009-53	Holstad, Anders	Numerical Investigation of Turbulence in a Sekwed Three-Dimensional Channel Flow, Ph.d.-thesis, IMT.
IMT-2009-54	Ayala-Uraga, Efren	Reliability-Based Assessment of Deteriorating Ship-shaped Offshore Structures, Ph.d.-thesis, IMT
IMT-2009-55	Kong, Xiangjun	A Numerical Study of a Damaged Ship in Beam Sea Waves. Ph.d.-thesis, IMT/CeSOS.
IMT-2010-56	Kristiansen, David	Wave Induced Effects on Floaters of Aquaculture Plants, Ph.d.-thesis, CeSOS.
IMT-2010-57	Ludvigsen, Martin	An ROV-Toolbox for Optical and Acoustic Scientific Seabed Investigation. Ph.d.-thesis IMT.
IMT-2010-58	Hals, Jørgen	Modelling and Phase Control of Wave-Energy Converters. Ph.d.thesis, CeSOS.
IMT-2010-59	Shu, Zhi	Uncertainty Assessment of Wave Loads and Ultimate Strength of Tankers and Bulk Carriers in a Reliability Framework. Ph.d. Thesis, IMT/ CeSOS
IMT-2010-60	Shao, Yanlin	Numerical Potential-Flow Studies on Weakly-Nonlinear Wave-Body Interactions with/without Small Forward Speed, Ph.d.thesis, CeSOS.
IMT-2010-61	Califano, Andrea	Dynamic Loads on Marine Propellers due to Intermittent Ventilation. Ph.d.thesis, IMT.
IMT-2010-62	El Khoury, George	Numerical Simulations of Massively Separated Turbulent Flows, Ph.d.-thesis, IMT
IMT-2010-63	Seim, Knut Sponheim	Mixing Process in Dense Overflows with Emphasis on the Faroe Bank Channel Overflow. Ph.d.thesis, IMT
IMT-2010-64	Jia, Huirong	Structural Analysis of Intect and Damaged Ships in a Collission Risk Analysis Perspective. Ph.d.thesis CeSoS.
IMT-2010-65	Jiao, Linlin	Wave-Induced Effects on a Pontoon-type Very Large Floating Structures (VLFS). Ph.D.-thesis, CeSOS.

Report No.	Author	Title
IMT-2010-66	Abrahamsen, Bjørn Christian	Sloshing Induced Tank Roof with Entrapped Air Pocket. Ph.d.thesis, CeSOS.
IMT-2011-67	Karimirad, Madjid	Stochastic Dynamic Response Analysis of Spar-Type Wind Turbines with Catenary or Taut Mooring Systems. Ph.d.-thesis, CeSOS.
IMT-2011-68	Erlend Meland	Condition Monitoring of Safety Critical Valves. Ph.d.-thesis, IMT.
IMT-2011-69	Yang, Limin	Stochastic Dynamic System Analysis of Wave Energy Converter with Hydraulic Power Take-Off, with Particular Reference to Wear Damage Analysis, Ph.d. Thesis, CeSOS.
IMT-2011-70	Visscher, Jan	Application of Particla Image Velocimetry on Turbulent Marine Flows, Ph.d.Thesis, IMT.
IMT-2011-71	Su, Biao	Numerical Predictions of Global and Local Ice Loads on Ships. Ph.d.Thesis, CeSOS.
IMT-2011-72	Liu, Zhenhui	Analytical and Numerical Analysis of Iceberg Collision with Ship Structures. Ph.d.Thesis, IMT.
IMT-2011-73	Aarsæther, Karl Gunnar	Modeling and Analysis of Ship Traffic by Observation and Numerical Simulation. Ph.d.Thesis, IMT.
IMT-2011-74	Wu, Jie	Hydrodynamic Force Identification from Stochastic Vortex Induced Vibration Experiments with Slender Beams. Ph.d.Thesis, IMT.
IMT-2011-75	Amini, Hamid	Azimuth Propulsors in Off-design Conditions. Ph.d.Thesis, IMT.
IMT-2011-76	Nguyen, Tan-Hoi	Toward a System of Real-Time Prediction and Monitoring of Bottom Damage Conditions During Ship Grounding. Ph.d.thesis, IMT.
IMT-2011-77	Tavakoli, Mohammad T.	Assessment of Oil Spill in Ship Collision and Grounding, Ph.d.thesis, IMT.
IMT-2011-78	Guo, Bingjie	Numerical and Experimental Investigation of Added Resistance in Waves. Ph.d.Thesis, IMT.
IMT-2011-79	Chen, Qiaofeng	Ultimate Strength of Aluminium Panels, considering HAZ Effects, IMT
IMT-2012-80	Kota, Ravikiran S.	Wave Loads on Decks of Offshore Structures in Random Seas, CeSOS.
IMT-2012-81	Sten, Ronny	Dynamic Simulation of Deep Water Drilling Risers with Heave Compensating System, IMT.
IMT-2012-82	Berle, Øyvind	Risk and resilience in global maritime supply chains, IMT.
IMT-2012-83	Fang, Shaoji	Fault Tolerant Position Mooring Control Based on Structural Reliability, CeSOS.
IMT-2012-84	You, Jikun	Numerical studies on wave forces and moored ship motions in intermediate and shallow water, CeSOS.
IMT-2012-85	Xiang, Xu	Maneuvering of two interacting ships in waves, CeSOS

Report No.	Author	Title
IMT-2012-86	Dong, Wenbin	Time-domain fatigue response and reliability analysis of offshore wind turbines with emphasis on welded tubular joints and gear components, CeSOS
IMT-2012-87	Zhu, Suji	Investigation of Wave-Induced Nonlinear Load Effects in Open Ships considering Hull Girder Vibrations in Bending and Torsion, CeSOS
IMT-2012-88	Zhou, Li	Numerical and Experimental Investigation of Station-keeping in Level Ice, CeSOS
IMT-2012-90	Ushakov, Sergey	Particulate matter emission characteristics from diesel enignes operating on conventional and alternative marine fuels, IMT
IMT-2013-1	Yin, Decao	Experimental and Numerical Analysis of Combined In-line and Cross-flow Vortex Induced Vibrations, CeSOS
IMT-2013-2	Kurniawan, Adi	Modelling and geometry optimisation of wave energy converters, CeSOS
IMT-2013-3	Al Ryati, Nabil	Technical condition indexes doe auxiliary marine diesel engines, IMT
IMT-2013-4	Firoozkoohi, Reza	Experimental, numerical and analytical investigation of the effect of screens on sloshing, CeSOS
IMT-2013-5	Ommani, Babak	Potential-Flow Predictions of a Semi-Displacement Vessel Including Applications to Calm Water Broaching, CeSOS
IMT-2013-6	Xing, Yihan	Modelling and analysis of the gearbox in a floating spar-type wind turbine, CeSOS
IMT-7-2013	Balland, Océane	Optimization models for reducing air emissions from ships, IMT
IMT-8-2013	Yang, Dan	Transitional wake flow behind an inclined flat plate – Computation and analysis, IMT
IMT-9-2013	Abdillah, Suyuthi	Prediction of Extreme Loads and Fatigue Damage for a Ship Hull due to Ice Action, IMT
IMT-10-2013	Ramìrez, Pedro Agustìn Pèrez	Ageing management and life extension of technical systems. Concepts and methods applied to oil and gas facilities, IMT
IMT-11-2013	Chuang, Zhenju	Experimental and Numerical Investigation of Speed Loss due to Seakeeping and Maneuvering. IMT
IMT-12-2013	Etemaddar, Mahmoud	Load and Response Analysis of Wind Turbines under Atmospheric Icing and Controller System Faults with Emphasis on Spar Type Floating Wind Turbines, IMT
IMT-13-2013	Lindstad, Haakon	Strategies and measures for reducing maritime CO2 emissons, IMT
IMT-14-2013	Haris, Sabril	Damage interaction analysis of ship collisions, IMT

Report No.	Author	Title
IMT-15-2013	Shainee, Mohamed	Conceptual Design, Numerical and Experimental Investigation of a SPM Cage Concept for Offshore Mariculture, IMT
IMT-16-2013	Gansel, Lars	Flow past porous cylinders and effects of biofouling and fish behavior on the flow in and around Atlantic salmon net cages, IMT
IMT-17-2013	Gaspar, Henrique	Handling Aspects of Complexity in Conceptual Ship Design, IMT
IMT-18-2013	Thys, Maxime	Theoretical and Experimental Investigation of a Free Running Fishing Vessel at Small Frequency of Encounter, CeSOS
IMT-19-2013	Aglen, Ida	VIV in Free Spanning Pipelines, CeSOS
IMT-1-2014	Song, An	Theoretical and experimental studies of wave diffraction and radiation loads on a horizontally submerged perforated plate, CeSOS
IMT-2-2014	Rogne, Øyvind Ygre	Numerical and Experimental Investigation of a Hinged 5-body Wave Energy Converter, CeSOS
IMT-3-2014	Dai, Lijuan	Safe and efficient operation and maintenance of offshore wind farms, IMT
IMT-4-2014	Bachynski, Erin Elizabeth	Design and Dynamic Analysis of Tension Leg Platform Wind Turbines, CeSOS
IMT-5-2014	Wang, Jingbo	Water Entry of Freefall Wedged – Wedge motions and Cavity Dynamics, CeSOS
IMT-6-2014	Kim, Ekaterina	Experimental and numerical studies related to the coupled behavior of ice mass and steel structures during accidental collisions, IMT
IMT-7-2014	Tan, Xiang	Numerical investigation of ship's continuous-mode icebreaking in leverl ice, CeSOS
IMT-8-2014	Muliawan, Made Jaya	Design and Analysis of Combined Floating Wave and Wind Power Facilities, with Emphasis on Extreme Load Effects of the Mooring System, CeSOS
IMT-9-2014	Jiang, Zhiyu	Long-term response analysis of wind turbines with an emphasis on fault and shutdown conditions, IMT
IMT-10-2014	Dukan, Fredrik	ROV Motion Control Systems, IMT
IMT-11-2014	Grimsmo, Nils I.	Dynamic simulations of hydraulic cylinder for heave compensation of deep water drilling risers, IMT
IMT-12-2014	Kvittem, Marit I.	Modelling and response analysis for fatigue design of a semisubmersible wind turbine, CeSOS
IMT-13-2014	Akhtar, Juned	The Effects of Human Fatigue on Risk at Sea, IMT
IMT-14-2014	Syahroni, Nur	Fatigue Assessment of Welded Joints Taking into Account Effects of Residual Stress, IMT
IMT-1-2015	Bøckmann, Eirik	Wave Propulsion of ships, IMT

Report No.	Author	Title
IMT-2-2015	Wang, Kai	Modelling and dynamic analysis of a semi-submersible floating vertical axis wind turbine, CeSOS
IMT-3-2015	Fredriksen, Arnt Gunvald	A numerical and experimental study of a two-dimensional body with moonpool in waves and current, CeSOS
IMT-4-2015	Jose Patricio Gallardo Canabes	Numerical studies of viscous flow around bluff bodies, IMT
IMT-5-2015	Vegard Longva	Formulation and application of finite element techniques for slender marine structures subjected to contact interactions, IMT
IMT-6-2015	Jacobus De Vaal	Aerodynamic modelling of floating wind turbines, CeSOS
IMT-7-2015	Fachri Nasution	Fatigue Performance of Copper Power Conductors, IMT
IMT-8-2015	Oleh Karpa	Development of bivariate extreme value distributions for applications in marine technology, CeSOS
IMT-9-2015	Daniel de Almeida Fernandes	An output feedback motion control system for ROVs, CeSOS/AMOS
IMT-10-2015	Bo Zhao	Particle Filter for Fault Diagnosis: Application to Dynamic Positioning Vessel and Underwater Robotics, CeSOS
IMT-11-2015	Wenting Zhu	Impact of emission allocation in maritime transportation, IMT
IMT-12-2015	Amir Rasekhi Nejad	Dynamic Analysis and Design of Gearboxes in Offshore Wind Turbines in a Structural Reliability Perspective, CeSOS
IMT-13-2015	Arturo Jesùs Ortega Malca	Dynamic Response of Flexibles Risers due to Unsteady Slug Flow, CeSOS
IMT-14-2015	Dagfinn Husjord	Guidance and decision-support system for safe navigation of ships operating in close proximity, IMT
IMT-15-2015	Anirban Bhattacharyya	Ducted Propellers: Behaviour in Waves and Scale Effects, IMT
IMT-16-2015	Qin Zhang	Image Processing for Ice Parameter Identification in Ice Management, IMT
IMT-1-2016	Vincentius Rumawas	Human Factors in Ship Design and Operation: An Experiential Learning, IMT
IMT-2-2016	Martin Storheim	Structural response in ship-platform and ship-ice collisions, IMT
IMT-3-2016	Mia Abrahamsen Prsic	Numerical Simulations of the Flow around single and Tandem Circular Cylinders Close to a Plane Wall, IMT
IMT-4-2016	Tufan Arslan	Large-eddy simulations of cross-flow around ship sections, IMT
IMT-5-2016	Pierre Yves-Henry	Parametrisation of aquatic vegetation in hydraulic and coastal research,IMT

Report No.	Author	Title
IMT-6-2016	Lin Li	Dynamic Analysis of the Instalation of Monopiles for Offshore Wind Turbines, CeSOS
IMT-7-2016	Øivind Kåre Kjerstad	Dynamic Positioning of Marine Vessels in Ice, IMT
IMT-8-2016	Xiaopeng Wu	Numerical Analysis of Anchor Handling and Fish Trawling Operations in a Safety Perspective, CeSOS
IMT-9-2016	Zhengshun Cheng	Integrated Dynamic Analysis of Floating Vertical Axis Wind Turbines, CeSOS
IMT-10-2016	Ling Wan	Experimental and Numerical Study of a Combined Offshore Wind and Wave Energy Converter Concept
IMT-11-2016	Wei Chai	Stochastic dynamic analysis and reliability evaluation of the roll motion for ships in random seas, CeSOS
IMT-12-2016	Øyvind Selnes Patricksson	Decision support for conceptual ship design with focus on a changing life cycle and future uncertainty, IMT
IMT-13-2016	Mats Jørgen Thorsen	Time domain analysis of vortex-induced vibrations, IMT
IMT-14-2016	Edgar McGuinness	Safety in the Norwegian Fishing Fleet - Analysis and measures for improvement, IMT
IMT-15-2016	Sepideh Jafarzadeh	Energy effiency and emission abatement in the fishing fleet, IMT
IMT-16-2016	Wilson Ivan Guachamin Acero	Assessment of marine operations for offshore wind turbine installation with emphasis on response-based operational limits, IMT
IMT-17-2016	Mauro Candeloro	Tools and Methods for Autonomous Operations on Seabed and Water Coumn using Underwater Vehicles, IMT
IMT-18-2016	Valentin Chabaud	Real-Time Hybrid Model Testing of Floating Wind Tubines, IMT
IMT-1-2017	Mohammad Saud Afzal	Three-dimensional streaming in a sea bed boundary layer
IMT-2-2017	Peng Li	A Theoretical and Experimental Study of Wave-induced Hydroelastic Response of a Circular Floating Collar
IMT-3-2017	Martin Bergström	A simulation-based design method for arctic maritime transport systems
IMT-4-2017	Bhushan Taskar	The effect of waves on marine propellers and propulsion
IMT-5-2017	Mohsen Bardestani	A two-dimensional numerical and experimental study of a floater with net and sinker tube in waves and current
IMT-6-2017	Fatemeh Hoseini Dadmarzi	Direct Numerical Simualtion of turbulent wakes behind different plate configurations
IMT-7-2017	Michel R. Miyazaki	Modeling and control of hybrid marine power plants

Report No.	Author	Title
IMT-8-2017	Giri Rajasekhar Gunnu	Safety and effiency enhancement of anchor handling operations with particular emphasis on the stability of anchor handling vessels
IMT-9-2017	Kevin Koosup Yum	Transient Performance and Emissions of a Turbocharged Diesel Engine for Marine Power Plants
IMT-10-2017	Zhaolong Yu	Hydrodynamic and structural aspects of ship collisions
IMT-11-2017	Martin Hassel	Risk Analysis and Modelling of Allisions between Passing Vessels and Offshore Installations
IMT-12-2017	Astrid H. Brodtkorb	Hybrid Control of Marine Vessels - Dynamic Positioning in Varying Conditions
IMT-13-2017	Kjersti Bruserud	Simultaneous stochastic model of waves and current for prediction of structural design loads
IMT-14-2017	Finn-Idar Grøtta Giske	Long-Term Extreme Response Analysis of Marine Structures Using Inverse Reliability Methods
IMT-15-2017	Stian Skjong	Modeling and Simulation of Maritime Systems and Operations for Virtual Prototyping using co-Simulations
IMT-1-2018	Yingguang Chu	Virtual Prototyping for Marine Crane Design and Operations
IMT-2-2018	Sergey Gavrilin	Validation of ship manoeuvring simulation models
IMT-3-2018	Jeevith Hegde	Tools and methods to manage risk in autonomous subsea inspection,maintenance and repair operations
IMT-4-2018	Ida M. Strand	Sea Loads on Closed Flexible Fish Cages
IMT-5-2018	Erlend Kvinge Jørgensen	Navigation and Control of Underwater Robotic Vehicles
IMT-6-2018	Bård Stovner	Aided Intertial Navigation of Underwater Vehicles
IMT-7-2018	Erlend Liavåg Grotle	Thermodynamic Response Enhanced by Sloshing in Marine LNG Fuel Tanks
IMT-8-2018	Børge Rokseth	Safety and Verification of Advanced Maritime Vessels
IMT-9-2018	Jan Vidar Ulveseter	Advances in Semi-Empirical Time Domain Modelling of Vortex-Induced Vibrations
IMT-10-2018	Chenyu Luan	Design and analysis for a steel braceless semi-submersible hull for supporting a 5-MW horizontal axis wind turbine
IMT-11-2018	Carl Fredrik Rehn	Ship Design under Uncertainty
IMT-12-2018	Øyvind Ødegård	Towards Autonomous Operations and Systems in Marine Archaeology
IMT-13- 2018	Stein Melvær Nornes	Guidance and Control of Marine Robotics for Ocean Mapping and Monitoring

Report No.	Author	Title
IMT-14-2018	Petter Norgren	Autonomous Underwater Vehicles in Arctic Marine Operations: Arctic marine research and ice monitoring
IMT-15-2018	Minjoo Choi	Modular Adaptable Ship Design for Handling Uncertainty in the Future Operating Context
MT-16-2018	Ole Alexander Eidsvik	Dynamics of Remotely Operated Underwater Vehicle Systems
IMT-17-2018	Mahdi Ghane	Fault Diagnosis of Floating Wind Turbine Drivetrain- Methodologies and Applications
IMT-18-2018	Christoph Alexander Thieme	Risk Analysis and Modelling of Autonomous Marine Systems
IMT-19-2018	Yugao Shen	Operational limits for floating-collar fish farms in waves and current, without and with well-boat presence
IMT-20-2018	Tianjiao Dai	Investigations of Shear Interaction and Stresses in Flexible Pipes and Umbilicals
IMT-21-2018	Sigurd Solheim Pettersen	Resilience by Latent Capabilities in Marine Systems
IMT-22-2018	Thomas Sauder	Fidelity of Cyber-physical Empirical Methods. Application to the Active Truncation of Slender Marine Structures
IMT-23-2018	Jan-Tore Horn	Statistical and Modelling Uncertainties in the Design of Offshore Wind Turbines
IMT-24-2018	Anna Swider	Data Mining Methods for the Analysis of Power Systems of Vessels
IMT-1-2019	Zhao He	Hydrodynamic study of a moored fish farming cage with fish influence
IMT-2-2019	Isar Ghamari	Numerical and Experimental Study on the Ship Parametric Roll Resonance and the Effect of Anti-Roll Tank
IMT-3-2019	Håkon Strandenes	Turbulent Flow Simulations at Higher Reynolds Numbers
IMT-4-2019	Siri Mariane Holen	Safety in Norwegian Fish Farming - Concepts and Methods for Improvement
IMT-5-2019	Ping Fu	Reliability Analysis of Wake-Induced Riser Collision
IMT-6-2019	Vladimir Krivopolianskii	Experimental Investigation of Injection and Combustion Processes in Marine Gas Engines using Constant Volume Rig
IMT-7-2019	Anna Maria Kozlowska	Hydrodynamic Loads on Marine Propellers Subject to Ventilation and out of Water Condition.
IMT-8-2019	Hans-Martin Heyn	Motion Sensing on Vessels Operating in Sea Ice: A Local Ice Monitoring System for Transit and Stationkeeping Operations under the Influence of Sea Ice

Report No.	Author	Title
IMT-9-2019	Stefan Vilsen	Method for Real-Time Hybrid Model Testing of Ocean Structures - Case on Slender Marine Systems
IMT-10-2019	Finn-Christian W. Hanssen	Non-Linear Wave-Body Interaction in Severe Waves
IMT-11-2019	Trygve Olav Fossum	Adaptive Sampling for Marine Robotics
IMT-12-2019	Jørgen Bremnes Nielsen	Modeling and Simulation for Design Evaluation
IMT-13-2019	Yuna Zhao	Numerical modelling and dyncamic analysis of offshore wind turbine blade installation
IMT-14-2019	Daniela Myland	Experimental and Theoretical Investigations on the Ship Resistance in Level Ice
IMT-15-2019	Zhengru Ren	Advanced control algorithms to support automated offshore wind turbine installation
IMT-16-2019	Drazen Polic	Ice-propeller impact analysis using an inverse propulsion machinery simulation approach
IMT-17-2019	Endre Sandvik	Sea passage scenario simulation for ship system performance evaluation
IMT-18-2019	Loup Suja-Thauvin	Response of Monopile Wind Turbines to Higher Order Wave Loads
IMT-19-2019	Emil Smilden	Structural control of offshore wind turbines - Increasing the role of control design in offshore wind farm development
IMT-20-2019	Aleksandar-Sasa Milakovic	On equivalent ice thickness and machine learning in ship ice transit simulations
IMT-1-2020	Amrit Shankar Verma	Modelling, Analysis and Response-based Operability Assessment of Offshore Wind Turbine Blade Installation with Emphasis on Impact Damages
IMT-2-2020	Bent Oddvar Arnesen Haugaløkken	Autonomous Technology for Inspection, Maintenance and Repair Operations in the Norwegian Aquaculture
IMT-3-2020	Seongpil Cho	Model-based fault detection and diagnosis of a blade pitch system in floating wind turbines
IMT-4-2020	Jose Jorge Garcia Agis	Effectiveness in Decision-Making in Ship Design under Uncertainty
IMT-5-2020	Thomas H. Viuff	Uncertainty Assessment of Wave-and Current-induced Global Response of Floating Bridges
IMT-6-2020	Fredrik Mentzoni	Hydrodynamic Loads on Complex Structures in the Wave Zone
IMT-7-2020	Senthuran Ravinthrakumar	Numerical and Experimental Studies of Resonant Flow in Moonpools in Operational Conditions
IMT-8-2020	Stian Skaalvik Sandøy	Acoustic-based Probabilistic Localization and Mapping using Unmanned Underwater Vehicles for Aquaculture Operations

Report No.	Author	Title
IMT-9-2020	Kun Xu	Design and Analysis of Mooring System for Semi-submersible Floating Wind Turbine in Shallow Water
IMT-10-2020	Jianxun Zhu	Cavity Flows and Wake Behind an Elliptic Cylinder Translating Above the Wall
IMT-11-2020	Sandra Hogenboom	Decision-making within Dynamic Positioning Operations in the Offshore Industry - A Human Factors based Approach
IMT-12-2020	Woongshik Nam	Structural Resistance of Ship and Offshore Structures Exposed to the Risk of Brittle Failure
IMT-13-2020	Svenn Are Tutturen Værnø	Transient Performance in Dynamic Positioning of Ships: Investigation of Residual Load Models and Control Methods for Effective Compensation
IMT-14-2020	Mohd Atif Siddiqui	Experimental and Numerical Hydrodynamics Analysis of a Damaged Ship in Waves
IMT-15-2020	John Marius Hegseth	Efficient Modelling and Design Optimization of Large Floating Wind Turbines
IMT-16-2020	Asle Natskår	Reliability-based Assessment of Marine Operations with Emphasis on Sea Transport on Barges